INVESTIGATION OF FATIGUE BEHAVIOR OF A HIGH STRENGTH LOWER BAINITIC STRUCTURE IN 60SIMN5 STEEL VIA A MODIFIED TESTING METHOD

A THESIS SUBMITTED TO
THE GRADUATE SCHOOL OF NATURAL AND APPLIED SCIENCES
OF
MIDDLE EAST TECHNICAL UNIVERSITY

BY

EMİRHAN ULUĞ

IN PARTIAL FULFILLMENT OF THE REQUIREMENTS
FOR
THE DEGREE OF MASTER OF SCIENCE
IN
METALLURGICAL AND MATERIALS ENGINEERING

DECEMBER 2019

Approval of the thesis:

INVESTIGATION OF FATIGUE BEHAVIOR OF A HIGH STRENGTH LOWER BAINITIC STRUCTURE IN 60SIMN5 STEEL VIA A MODIFIED TESTING METHOD

submitted by **EMİRHAN ULUĞ** in partial fulfillment of the requirements for the degree of **Master of Science in Metallurgical and Materials Engineering Department, Middle East Technical University** by,

Prof. Dr. Halil Kalıpçılar
Dean, Graduate School of **Natural and Applied Sciences** _____

Prof. Dr. Cemil Hakan Gür
Head of Department, **Metallurgical and Materials Engineering** _____

Prof. Dr. Bilgehan Ögel
Supervisor, **Metallurgical and Materials Engineering, METU** _____

Prof. Dr. Rıza Gürbüz
Co-Supervisor, **Met. and Mat. Eng., METU** _____

Examining Committee Members:

Prof. Dr. Ali Kalkanlı
Metallurgical and Materials Engineering, METU _____

Prof. Dr. Bilgehan Ögel
Metallurgical and Materials Engineering, METU _____

Prof. Dr. Rıza Gürbüz
Metallurgical and Materials Engineering, METU _____

Assoc. Prof. Dr. Mert Efe
Metallurgical and Materials Engineering, METU _____

Prof. Dr. Nuri Durlu
Mechanical Engineering, TOBB ETU _____

Date: 06.12.2019

I hereby declare that all information in this document has been obtained and presented in accordance with academic rules and ethical conduct. I also declare that, as required by these rules and conduct, I have fully cited and referenced all material and results that are not original to this work.

Name, Surname: Emirhan Uluğ

Signature:

ABSTRACT

INVESTIGATION OF FATIGUE BEHAVIOR OF A HIGH STRENGTH LOWER BAINITIC STRUCTURE IN 60SIMN5 STEEL VIA A MODIFIED TESTING METHOD

Uluğ, Emirhan
Master of Science, Metallurgical and Materials Engineering
Supervisor: Prof. Dr. Bilgehan Ögel
Co-Supervisor: Prof. Dr. Rıza Gürbüz

December 2019, 128 pages

A steel with high silicon content can yield carbide-free bainite after an isothermal bainitic transformation. In this thesis study, fatigue behavior of a high strength carbide-free lower bainitic structure, which was produced from 60SiMn5 steel, was investigated. The fatigue tests of the same steel with tempered martensitic microstructure were also carried out for comparison purposes. Before fatigue testing, the mechanical properties of the specimens were also determined, which include hardness, yield strength, tensile strength and modulus of elasticity. The fatigue tests were performed on the fatigue specimens, which have rectangular cross sections, under single amplitude loading (stress ratio, R = 0) using bending fatigue mechanism. In accordance with this purpose, a new fatigue test machine and a new type fatigue specimen were designed. The design of the fatigue specimen was based on ASTM B 593 – 96 Standard, and the design of Krouse-type fatigue specimen in the standard was revised via numerical analyses according to the mechanical properties of the specimens to be tested. S-N curves and fractographic investigations of the fatigue specimens were used while comparing fatigue behaviors of the structures. It has been observed that there is no clear difference between the fatigue lives and endurance limits of lower bainitic and tempered martensitic fatigue specimens as most commonly

observed for high strength bainitic and martensitic structures in literature. It has been demonstrated that bending fatigue application, in ASTM B 593 – 96 Standard, is also applicable to high strength steels by revising Krouse-type specimen specified in the standard.

Keywords: 60SiMn5 Steel, High Strength Lower Bainite, High Strength Tempered Martensite, High Cycle Fatigue, Bending Fatigue Test

ÖZ

60SİMN5 ÇELİĞİNDE YÜKSEK MUKAVEMETLİ ALT BEYNİTİK BİR YAPININ YORULMA DAVRANIŞININ DEĞİŞKİN BİR TEST YÖNTEMİ VASITASIYLA İNCELENMESİ

Uluğ, Emirhan
Yüksek Lisans, Metalurji ve Malzeme Mühendisliği
Tez Danışmanı: Prof. Dr. Bilgehan Ögel
Ortak Tez Danışmanı: Prof. Dr. Rıza Gürbüz

Aralık 2019, 128 sayfa

Yüksek silisyum içerikli bir çelik, eşısıl bir beynitik dönüşümden sonra karbürsüz beynit oluşturabilir. Bu tez çalışmasında, 60SiMn5 çeliğinden üretilmiş yüksek mukavemetli karbürsüz alt beynitik bir yapının yorulma davranışı incelenmiştir. Karşılaştırma amaçları ile, aynı çeliğin temperlenmiş martenzitik mikroyapılı hâline de yorulma testleri uygulanmıştır. Ayrıca yorulma testlerinden önce, numunelerin sertlik, akma mukavemeti, çekme mukavemeti ve elastisite modülünü içeren mekanik özellikleri de belirlenmiştir. Yorulma testleri, dikdörtgen enkesitlere sahip yorulma numuneleri üstünde tekil genlik yüklemesi (gerilme oranı, R = 0) altında eğilme yorulması mekanizması kullanılarak gerçekleştirilmiştir. Bu amaç doğrultusunda yeni bir yorulma testi makinası ve yeni bir tip yorulma numunesi tasarlanmıştır. Yorulma numunesi tasarımında ASTM B 593 – 96 Standardı baz alınmış ve standarttaki Krouse tipi yorulma numunesinin tasarımı nümerik analizler vasıtasıyla test edilecek numunelerin mekanik özelliklerine göre yenilenmiştir. Yapıların yorulma davranışları kıyaslanırken, yorulma numunelerinin S-N eğrileri ve kırılma incelemeleri kullanılmıştır. Alt beynitik ve temperlenmiş martenzitik yorulma numunelerinin yorulma ömürleri ve yorulma dayanımları arasında, literatürde yüksek mukavemetli beynitik ve martenzitik yapılar için de yaygınca görüldüğü üzere belirgin bir fark

gözlenmemiştir. Ayrıca, ASTM B 593 – 96 Standardı'ndaki eğilme yorulması uygulamasının, standartta belirtilen Krouse tipi numunesinin yenilenerek yüksek mukavemetli çelikler için de uygulanabilir olduğu gösterilmiştir.

Anahtar Kelimeler: 60SiMn5 Çeliği, Yüksek Mukavemetli Alt Beynit, Yüksek Mukavemetli Menevişlenmiş Martenzit, Yüksek Çevrimli Yorulma, Eğilme Yorulması Testi

To the memory of my beloved mom…

ACKNOWLEDGEMENTS

First of all, I would like to express my sincere appreciation to my supervisor Prof. Dr. Bilgehan Ögel for his guidance, patience and endless support throughout my graduate study. I would also like to express my sincere gratitude to my co-supervisor Prof. Dr. Rıza Gürbüz for his guidance and precious support throughout my thesis study.

I want to express my gratitude to Tanatar Kalıp and in particular to Uğur Kuyucu for contribution to the production process of the test set-up which i used throughout this study. I am also deeply indebted to my friends in Arçelik Compressor Plant for their priceless contribution to the completion of this thesis.

I would like to express my gratitude to Esmikron Taşlama and in particular to Adnan Tunç for his precious effort in the production process of the test specimens. I must also express my special thanks to Saşa Makine and Asil Çelik for their invaluable supports to this process.

I want to express my special thanks to Servet Şehirli, from METU Mechanical Engineering Department, for his invaluable contribution to the testing process of the specimens in this thesis; and i also owe sincere thanks to Aslan Makina for their contribution to this process.

I am so much thankful to my friends and all laboratory personnel, from METU Metallurgical and Materials Engineering Department, for their invaluable supports to me in the completion of my graduate study.

Finally, I would like to express my deepest appreciation to my mom Meryem Uluğ whom I still feel being with me, my dad Selahattin Uluğ, my little nephew Bulut Bilge Evren, my sister Merve Evren and my brother-in-law Vedat Evren and to my big family for their motivations, moral supports in the completion of this thesis and for always being there for me.

That’s all folks!

TABLE OF CONTENTS

LIST OF TABLES

TABLES

LIST OF FIGURES

FIGURES

LIST OF ABBREVIATIONS

ABBREVIATIONS

3D : Three-Dimensional

ASTM : American Society for Testing and Materials

BLDC : Brushless Direct Current

CNC : Computer Numerical Control

CPU : Central Process Unit

FEM : Finite Element Method

LED : Light Emitting Diode

LDR : Light Dependent Resistor

Nat Geo^{TM} : National Geographic Channel

PSB: : Persistent Slip Band

PWM : Pulse with Modulation

SEM : Scanning Electron Microscope

SMS : Short Message Service

TEM : Transmission Electron Microscope

UTS : Ultimate Tensile Strength

LB : Lower Bainite

TM : Tempered Martensite

min : Minimum

max : Maximum

wt% : Weight Percent

min : Minute(s)

h : Hour(s)

kg : Kilogram

kgf : Kilogram-force

N : Newton

MPa : Mega Pascal

GPa : Giga Pascal

mm : Millimeter

m : Meter

in. : Inch

rpm : Revolution per Minute

log : Logarithm with Base 10

Hz : Hertz

e.g. : For Example

vs. : Versus

LIST OF SYMBOLS

SYMBOLS

σ_{max}	: Maximum Bending Stress
σ_{min}	: Minimum Bending Stress
σ_a	: Stress Amplitude
S_a	: Stress Amplitude
$S_{a,50\%}$	: Half of Stress Amplitude
S_e	: Endurance Limit
S'_e	: Endurance Limit (for rotating beam)
S_{ut}	: Tensile Strength
K_t	: Stress Concentration Factor
σ_y	: Yield Strength
ε	: Strain
$\mu\varepsilon$	: Micro Strain
R	: Radius
Φ	: Diameter
^{o}	: Degree
%	: Percent
$\approx$	: Approximately Equal
&	: And
®	: Registered Trademark

$\#$: Number

^{o}C : Centigrade Degree

R : Stress Ratio

h : Height between Axes of Eccentric & Main Shafts

d : An Equally Divided Stress Interval

ρ : Density

v : Poisson's Ratio

E : Modulus of Elasticity (Young's Modulus)

J : Impact Toughness

M_s : Martensite Start Temperature

M_f : Martensite Finish Temperature

T : Temperature

S : Stress

N : Number of Cycles

F : Force

L : Length

w : Width

t : Thickness

α : Ferrite Phase

γ : Retained Austenite Phase

α' : Martensitic Structure

α_b : Bainitic Structure

CHAPTER 1

INTRODUCTION

Fatigue, in material science, is a damage of a structure which is constantly exposed to a cyclic loading. Normally, a material which is exposed to a gradual increasing load faces permanent deformation after a limit called a yield strength, and starts to break off after a limit called ultimate tensile strength. However, the material can suddenly face rupture in brittle manner if it's worked over a stress value which is defined as endurance limit even if it is exposed to cyclic loading under yield point. This is because of fatigue phenomena. An example to a fatigue fracture is as seen in Figure 1.1; the dark region shows fatigue fracture while the bright region shows fast fracture zone which is due to overloading after fatigue fracture.

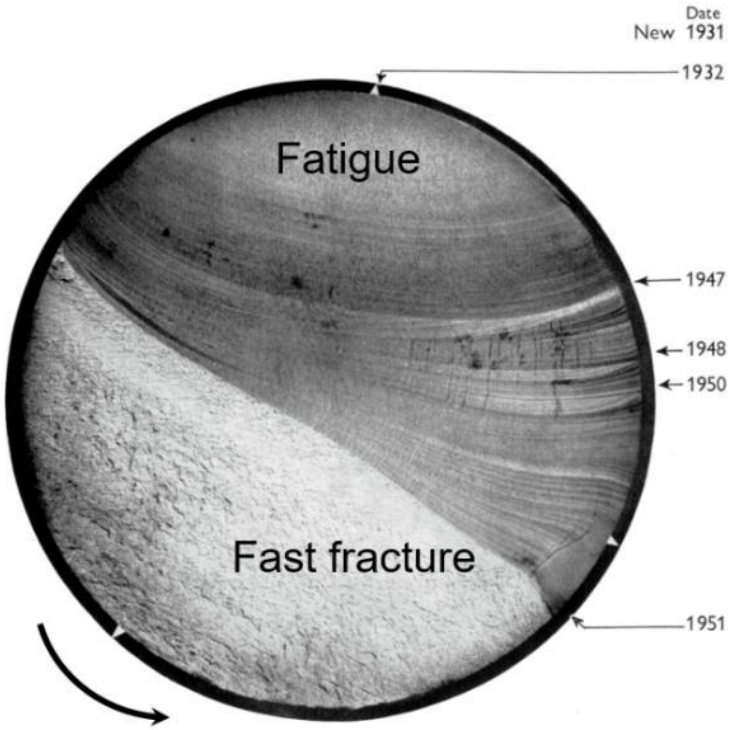

Figure 1.1. Macroscopic View of Fatigue Fracture of a Steel Shaft[1]

Fatigue phonemena does not make sign in such a way that can be observed from outside, because it does not make a significant deformation to the material. Therefore, failures due to fatigue are sudden and unexpected, so it could create catastropic consequences. For this reason, it is important that the devices which are to be exposed to cyclic loading should be designed according to fatigue failure criteria. This type of fracture phonemena can be encountered on steel bridges, cars which goes on rough roads and aircrafts' wings and this can make bad outcomes. For example, the aircraft which belonged to China Airlines Flight 611 had an accident and caused 225 people's death in 25th May 2002 because of a fatigue failure on the rear body of the aircraft[2] (See Figure 1.2). Therefore, it is very important to take precautions regarding fatigue phenomena.

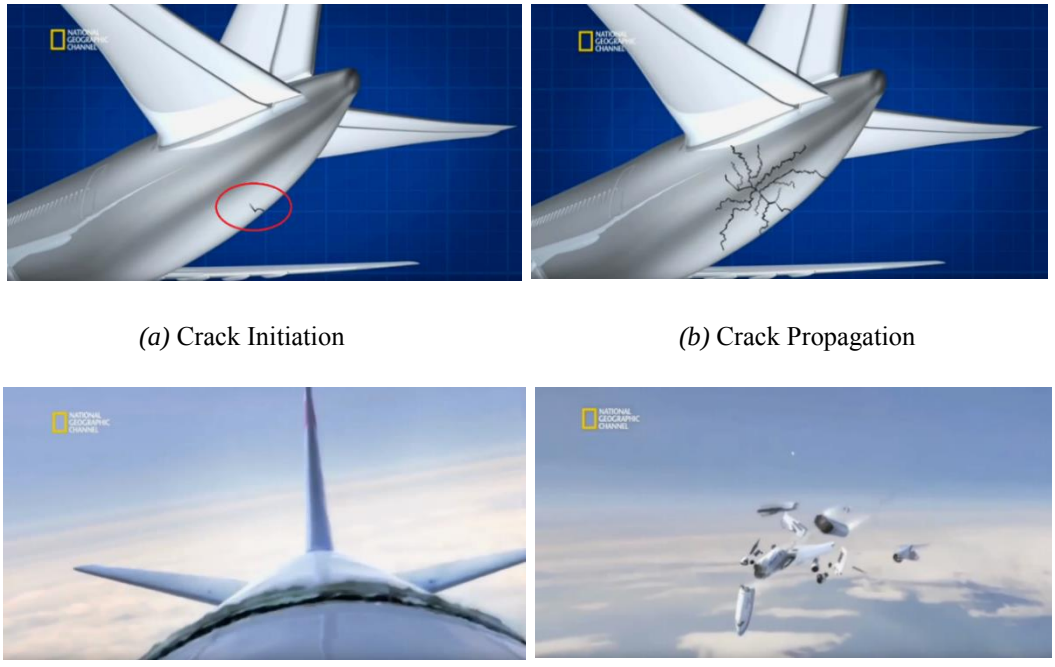

(a) Crack Initiation

(b) Crack Propagation

(c) Rupture of Rear Body

(d) Complete Breakup

Figure 1.2. Illustration [by Nat Geo^{TM}] of Fatigue Failure of the Aircraft which belonged to China Airlines Flight 611

In this thesis study, fatigue behavior of a high strength carbide-free lower bainitic structure, which was produced from 60SiMn5 steel, was investigated. Steels with high silicon content can form carbon-free bainite after isothermal bainitic transformations[3]. These steels can form carbide-free lower bainite or nanobainitic structures according to their silicon and carbon content and how heat treatment processes they undergo. These structures are expected to be more durable (UTS > 2000 MPa) than conventional bainitic structures. A number of studies have been carried out in the literature on fatigue life of such bainitic structures, conventional bainitic structures and other microstructures with similar mechanical properties. Data by Mayer et al. (2009) show that bainitic structures are more successful in terms of fatigue life than martensitic structures[4]. However, it is seen that there is no significant difference between the bainitic and martensitic states when data from many different sources [Sakai et al. (2002), Baudry et al. (2004), Bathias (2010), Almaraz (2008)] are merged, at conventional or ultrasonic test frequencies[5]. R. Rementeria tried to compare fatigue lives of different nanobainitic structures to each other in itself but did not clearly reveal the effect of bainite block size on fatigue strength[6]. Sourmail et al also examined the fatigue life of nanobainitic structures according to conventional lower bainite or quenched and tempered materials, but did not show particular advantages on the fatigue life of these structures[7].

While the fatigue life of conventional bainitic structures cannot be clearly differentiated from the fatigue life of other microstructures in the literature, it is quite insufficient to compare fatigue behavior of such bainitic structures with other microstructures having similar strength values. In addition, there is probably no literature with an example comparing the fatigue behavior of microstructures that have exactly the same element content but are completely different in character. In this thesis, fatigue behavior of a high strength carbide-free lower bainitic structure was investigated by comparing it with fatigue behavior of a sample (a high strength tempered martensitic structure) with similar mechanical properties but completely different in microstructure using 60SiMn5 steel. In this study, it is aimed to clearly

understand the fatigue behaviour difference of a carbide-free bainitic structure which is formed in 60SiMn5 steel when compared to a structure which has different microstructure (tempered martensite) which is formed in 60SiMn5 steel.

CHAPTER 2

THEORY & LITERATURE REVIEW

2.1. Fatigue Theory

2.1.1. Fatigue Formation & Endurance Limit

Fatigue is an important design criteria while designing machines. However, only yield strength values are regarded in general because avoiding plastic deformation is the main field of interest. However, one of the major reasons of the failure of the working machines is fatigue. Moving parts such as shafts, connecting rods, gears, etc. can be shown as example to the parts which may be broken due to fatigue.

Fatigue occurs when a material is exposed constantly to loading and discharge. If the load are upper than a limit which is called endurance limit, microscopic cracks start to form on the surface of material depending upon slip band formation. This formation of persistent slip bands (PSB), where crack initiates, which is induced by dislocation motion due to cyclic loading is as illustrated in Figure 2.1. In time, this crack reaches a critical size, and there would be cleavage and rupture in the structure. This causes the working part to be break and become nonfunctional.

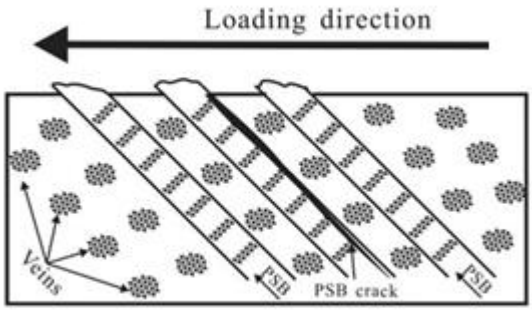

Figure 2.1. Illustration of Formation of Persistent Slip Bands[8]

Surface cracks may also occur on machine elements operating below the endurance limit due to slip band formation, and this is usual. However, cracks under this stress value do not propagate or propagate much slower. The endurance limit is actually a hypothetical stress value that can be defined as the maximum stress value required not to propagate the crack caused by fatigue on the surface. This value is determined by the service life of the machine element; and in the literature, it is generally assumed that fatigue cracks that may occur on the surface of a machine element which do not break up to a million cycle will never propagate. That is, the endurance limit is determined according to this number of cycles; and a machine element that has worked without breaking until this cycle value is considered to have infinite life. In Figure 2.2, it is illustrated on "stress vs. number of cycles" curve that, the time intervals in which fatigue crack initiates, crack propagates and failure occurs according to the stress value applied. Correspondingly, effect of the structure shape were found to be related to time of fatigue, because it has influence on stress distribution on the surface of the structure. Because of that, round holes, blended corners and smooth surfaces are preferred rather than square holes, sharp corners and rough surfaces as precauiton against fatigue while designing structures.

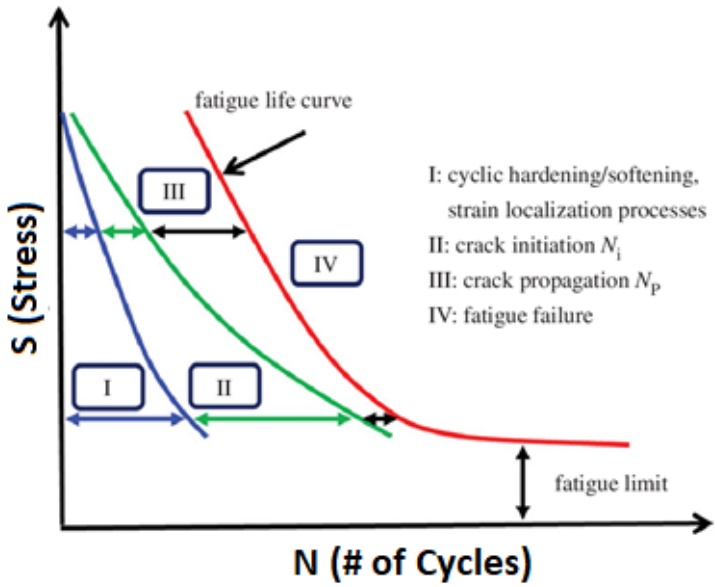

Figure 2.2. Four Stages of Fatigue[9]

Endurance limit increases with UTS. The endurance limit is considered to be between 0.4 and 0.6 times the UTS values of the iron or steel samples. However, after a certain value of UTS (> 1400 MPa), the endurance limit value does not increase and is assumed to be fixed at a certain value (700 MPa). The reason why it is considered such that is presence of the inclusions in the microstructure of a steel starts to play a negative role at high strength values. The graph showing the endurance limit value data according to their UTS value data, which were collected from actual test results for a large number of wrought iron and steels in the condition of R = -1, is seen in Figure 2.3. In Figure 2.3, ratios of S'_e/S_{ut} of 0.60, 0.50 and 0.40 are shown by the solid and dashed lines, and the endurance limit value for high UTS values is shown by horizontal dashed line at S'_e = 735 MPa with a standard deviation of 95 MPa. The prime mark on S'_e in this formulation refers to the rotating beam specimen itself. Data of the graph in Figure 2.3 are also formulated as in Table 2.1, in brief.

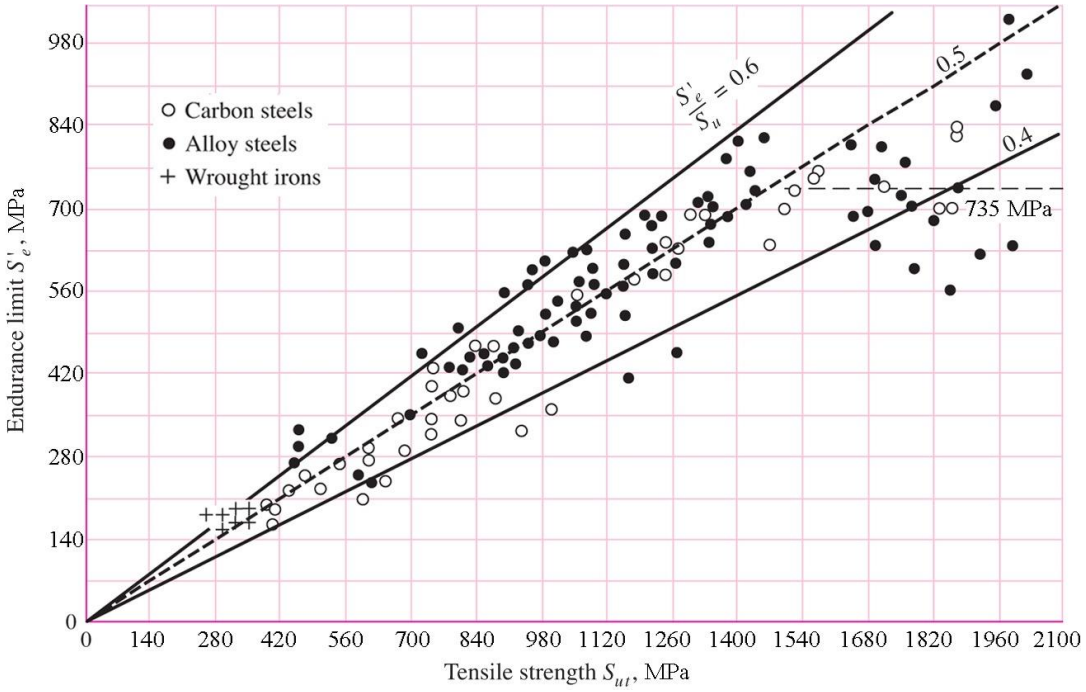

Figure 2.3. Graph of Endurance Limit versus Tensile Strength[10]

Table 2.1. *Simply Estimation of Endurance Limit versus Tensile Strength*[11]

	Endurance Limit, S'_e
$S_{ut} \leq 1400$ MPa	0,5 S_{ut}
$S_{ut} > 1400$ MPa	700 MPa

2.1.2. S-N Curve

S-N curve means "stress vs. number of cycles" graph. That is, this is a graph showing the fatigue life of samples according to the stress value of cyclic loading. The fatigue life data obtained from the tests performed at different stress values are placed on a curve and the S-N curve is created. This curve is important for defining the fatigue behavior of the materials. The fatigue life data of the samples tested at different stress values and the S-N curve created according to these data are as shown in Figure 2.4 as an example.

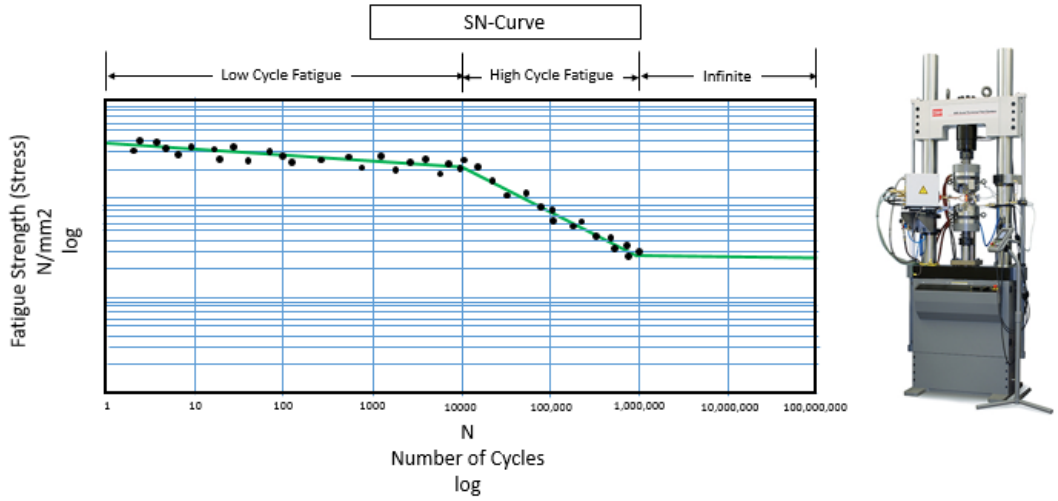

Figure 2.4. An S-N Curve[12]

In steels, if the maximum stress value of the cyclic loading to which the sample is exposed is between UTS and σ_y, the sample is likely to break at a cycle value of less than 10^3 to 10^4 cycles. On the S-N curve, this region is defined as low cycle fatigue region. If the maximum stress value of the cyclic loading to which the sample is exposed is between σ_y and the endurance limit, the sample is likely to break in a cycle range between greater than 10^3 to 10^4 cycles and less than 10^6 cycles. On the S-N curve, this region is defined as high cycle fatigue region. If the maximum stress value of the cyclic loading to which the sample is exposed is a stress value below the endurance limit, it is accepted in the literature that that sample will never break up and have an infinite life. For a more accurate determination of the endurance limit, it is recommended to continue the test for a longer period (e.g. 10^7 cycles), even if the sample did not break up until 10^6 cycles in the test. It is illustrated in Figure 2.5 that the stress values to which samples are exposed corresponds how much fatigue life of the samples. However, to note that, the fatigue lives mentioned in this context are valid for conventional operating speeds of the machines (e.g. 1000 rpm); if fatigue tests are performed at ultrasonic speeds (> 20000 Hz), longer fatigue lives are mentioned[13] but it is out of the scope of this thesis.

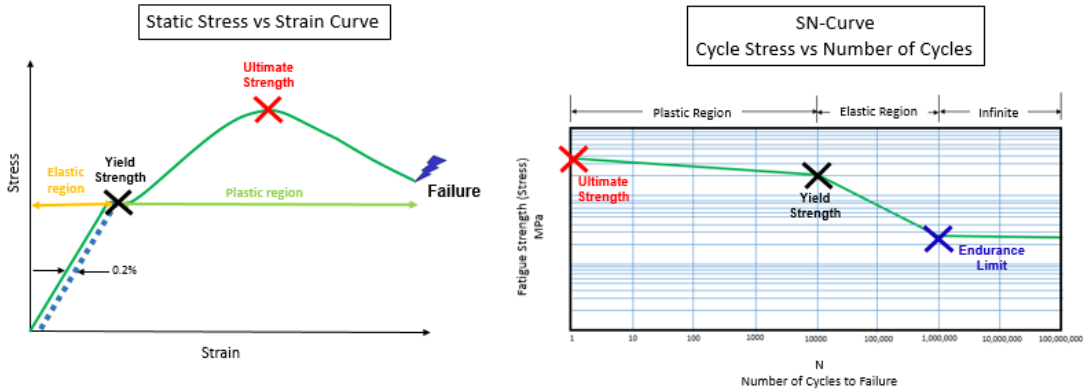

Figure 2.5. Correspondence of Strain vs. Stress Curve on S-N Curve[14]

One of the most common methods for determining the endurance limit is the staircase method. In this method, the stress zone where the endurance limit is expected to be is divided into equal stress ranges and samples are tested at these stress values (See Figure 2.6). First, the sample is subjected to fatigue test at a specified stress value. If the sample breaks at the end of the test, the test is repeated at a lower stress value because endurance limit is predicted to have a lower stress value. If the sample breaks again, the test is repeated at a lower stress value and these tests are repeated until that the stress value at which the sample is not broken is found. After the stress value at which the sample is not broken, the test is repeated with the new sample at a higher stress value. If the sample is not broken again, the test is repeated at an upper stress value and these tests are repeated until that the stress value at which the sample is broken is found. This test process is expected to continue with zigzags on the graph. At the end of several tests, a stress value at which the samples are never broken and a stress value at which all samples are broken are obtained. The range, where the endurance limit is, is between these two values, and the endurance limit value can be assumed as the average of these two stress values for the S-N curve. The difference between the average and these two stress values gives probably the amount of deviation from the endurance limit. It is inferred that the probability of fracture of the samples increases to the top and decreases to the bottom in the range obtained in graph.

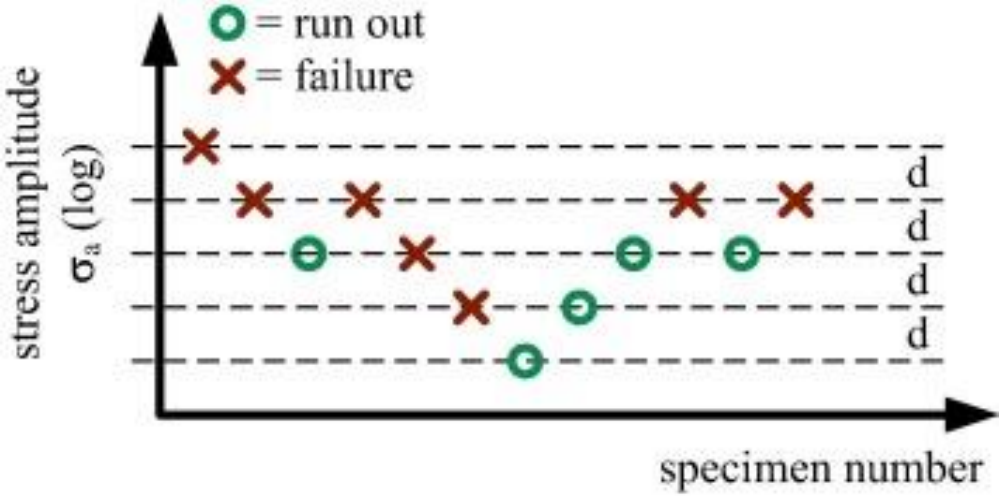

Figure 2.6. Staircase Method[15]

2.2. Standard & Design of Fatigue Specimen

2.2.1. Standard of Fatigue Specimen

In accordance with Krouse-type fatigue specimen (See Figure 2.7) which is planned to be used in the thesis, it is considered appropriate to use ASTM B 593 – 96 Standard which is utilized for bending fatigue testing. ASTM B 593 – 96 Standard is named as standard test method for bending fatigue testing for copper-alloy spring materials. This test method describes procedures for the determination of the reversed or repeated bending fatigue properties of copper alloy flat-sheet or strip-spring materials by fixed cantilever, constant amplitude of displacement-type testing machines. This method is limited to flat stock ranging in thickness from 0.005 to 0.062 in. (0.13 to 1.57 mm), to a fatigue-life range of 10^5 to 10^8 cycles, and to conditions where no significant change in stress-strain relations occurs during the test[16]. Considering the scope of the method, it is seen that ASTM B 593 – 96 Standard is suitable for the study to be carried out in this thesis.

Figure 2.7. A 316L Krouse-type Fatigue Specimen with Characteristic Crack just before Final Fracture[17]

For this purpose, there are basically two types of fatigue specimen and fatigue testing machine in the standard: Bell Telephone Laboratories Type and Krouse Type. Bell Telephone Laboratories Types are two types in itself according to the thickness of the specimen to be tested. The drawing dimensions (in inch unit) of these specimen types and the sketches of the fatigue test machines operating these specimens are as shown in Figure 2.8 and Figure 2.9, respectively.

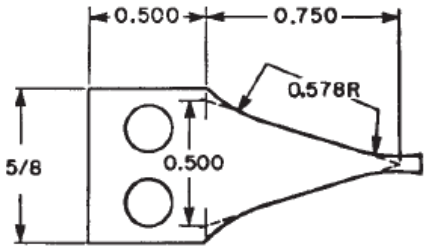

(a) Bell Telephone Laboratories Type for Thickness Ranging from 0.005 to 0.015 in. (0.127 to 0.381 mm)

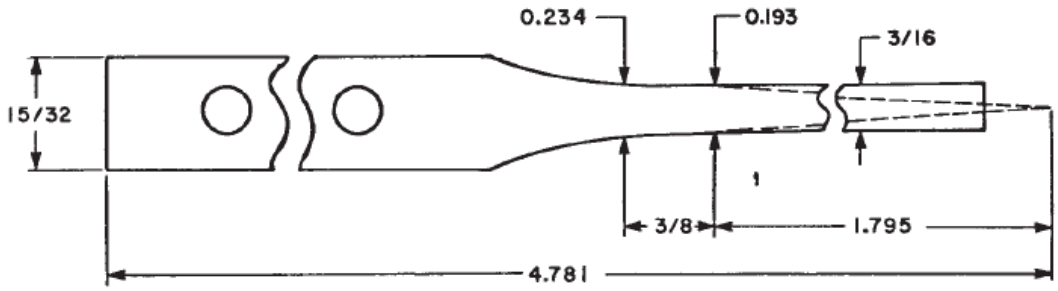

(b) Bell Telephone Laboratories Type for Thickness Ranging from 0.015 to 0.062 in. (0.381 to 1.575 mm)

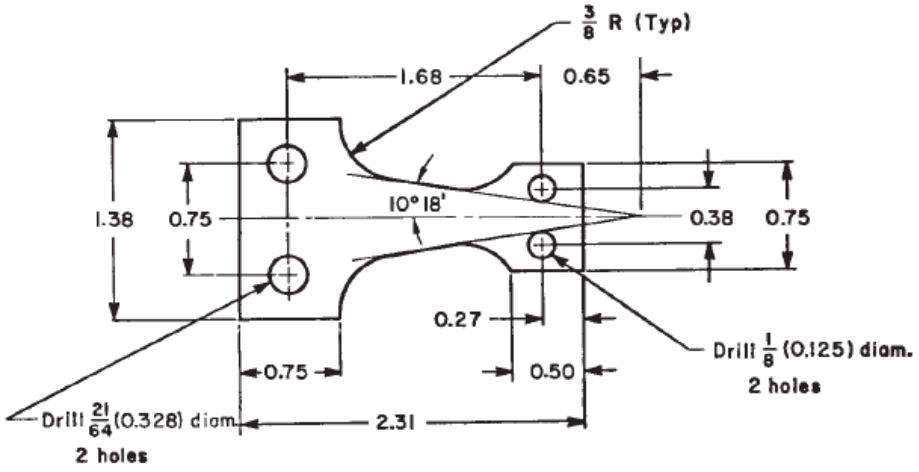

(c) Krouse Type for Thickness Ranging from 0.008 to 0.031 in. (0.203 to 0.787 mm)

Figure 2.8. Sheet or Strip Bending Fatigue Test Specimen Types on ASTM B 593 – 96 Standard[18]

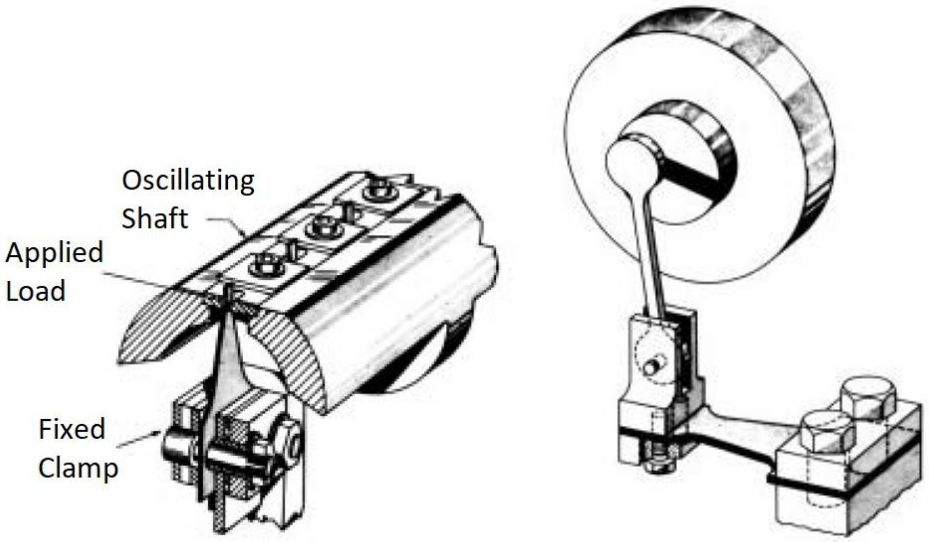

(a) Bell Laboratories Type *(b)* Krouse Type

Figure 2.9. Bending Fatigue Machine Types on ASTM B 593 – 96 Standard[19]

As seen from the specimen design at the standard, the bending region of the sample has a triangular design. The fatigue test machine creates an oscillating stress on the triangular region and tries to fatigue the specimen on this region. The purpose of the triangular design of the fatigue zone is to ensure that the maximum stress is distributed homogeneously over a given region rather than aggregate at a single point. This works for searching fatigue in a wider area. The maximum bending stress in the fatigue zone is calculated using the simple beam equation[20].

$$\sigma_{max} = \frac{6 \cdot F.L}{w.t^2}$$

where

σ_{max} = desired maximum bending stress, MPa,

F = applied load at the connecting pin (apex of triangle), N,

L = distance between the connecting pin and the point of stress, mm,

w = specimen width at length L from point of load application, mm, and

t = specimen thickness, mm.

The homogeneous distribution of stress in the bending region is due to the similarity of the triangle. Because “L/w” ratio in the simple beam equation is constant anywhere in the bending region. The maximum stress is therefore constant anywhere in the bending region. The positioning of the connecting pin of the fatigue test machine according to the triangular design in the bending region of a revised bending fatigue specimen is illustrated in Figure 2.10.

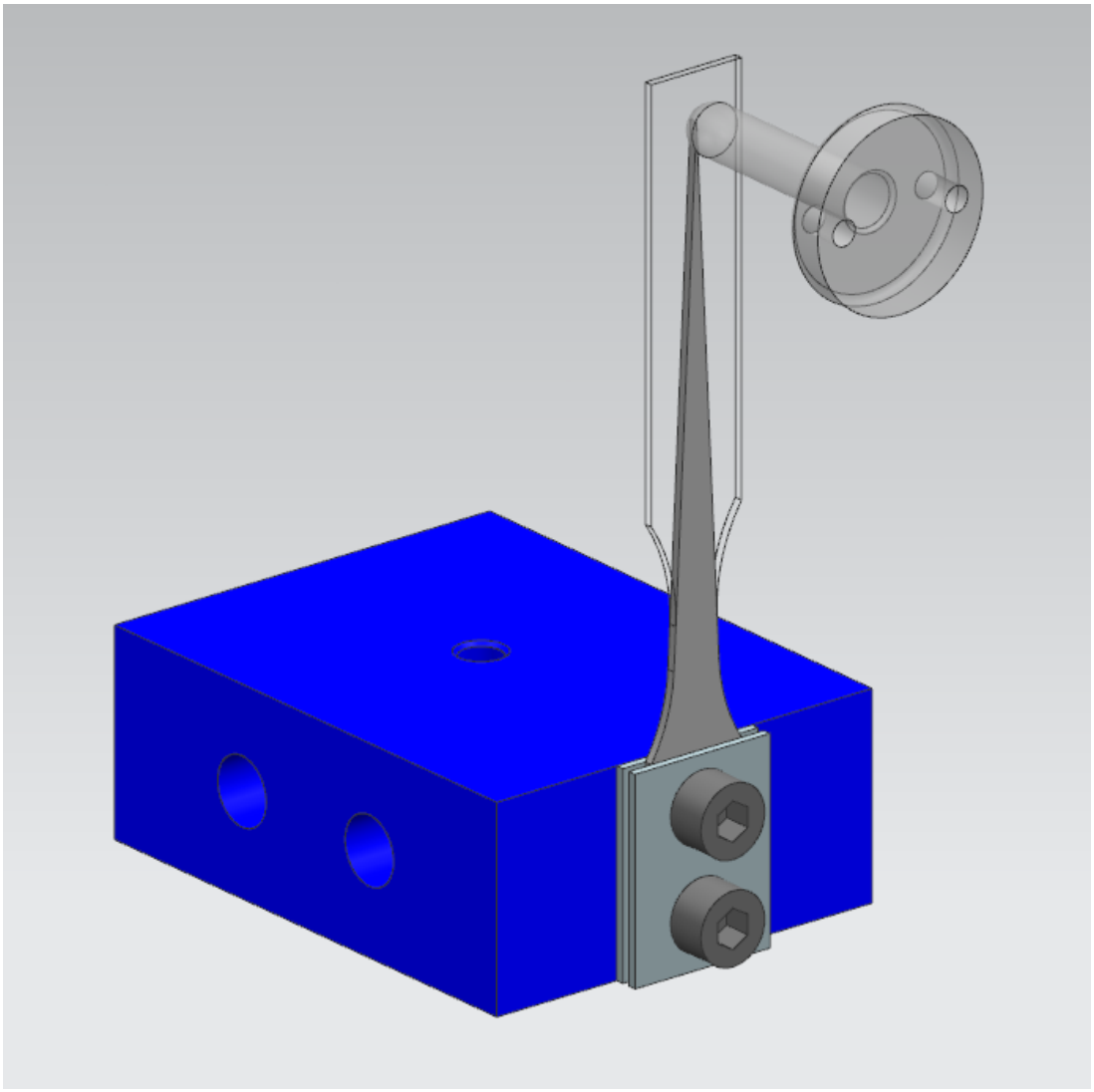

Figure 2.10. Positioning of Connecting Pin on Fatigue Specimen

2.2.1. Design of Fatigue Specimen

As it is seen from the different studies in the literature, it is seen that the measurements given in ASTM B 593 – 96 standard can be modified in accordance with the desired study[21]. The specimen to be modified in this thesis study can be described as the hybrid model of Bell Telephone Laboratories Type and Krouse Type (See Figure 2.11). Bending stress is applied as zero to tension (R = 0) instead of compression to tension (R = -1). In this way, the dynamic load to be applied to the specimen was planned to be single amplitude load at 1000 rpm (See Figure 2.12). Although the standard is slightly out of the way, the revised fatigue specimen in this thesis study has been called Krouse-type for ease of discourse.

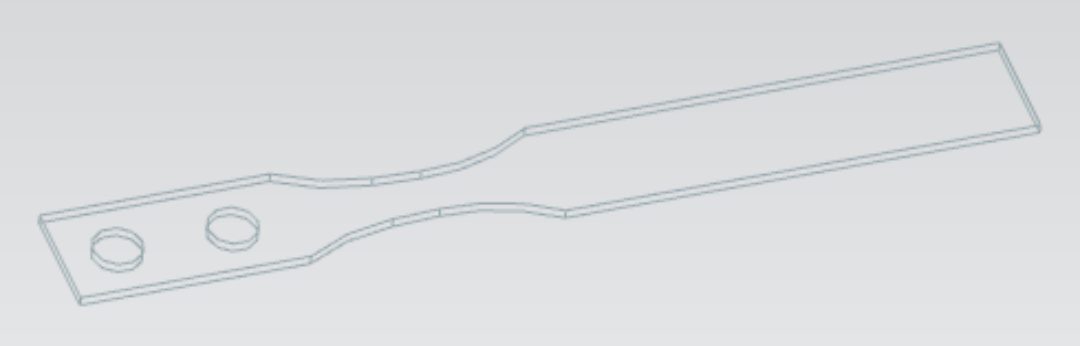

Figure 2.11. Hybride Model of Bell Telephone Laboratories Type and Krouse-type Fatigue Specimen

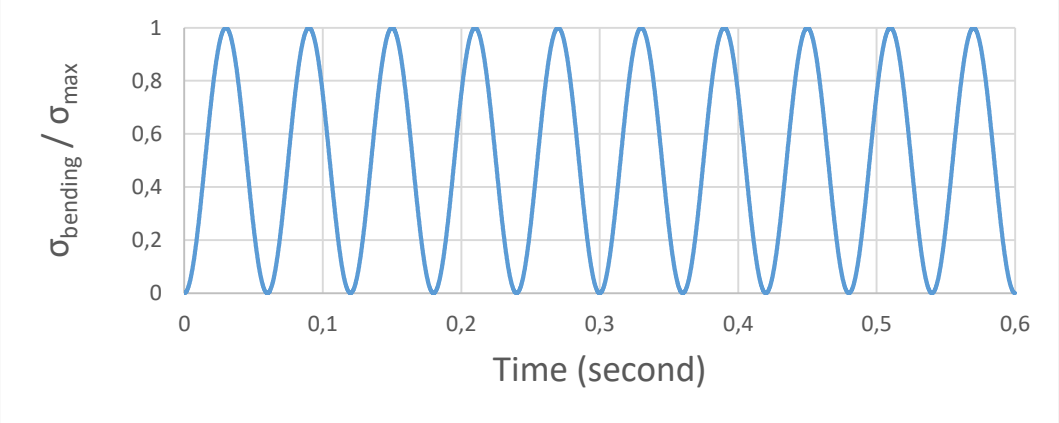

Figure 2.12. Load versus Time on the Fatigue Specimen at 1000 rpm

When modifying dimensions in the standard, numerical stress analyses are performed to obtain the desired stress values and stress distribution on the fatigue specimen. Numerical stress analyses are performed by means of a CAD program and the specimen is optimized for the displacement range in which the fatigue test machine can operate. The desired stress values on the fatigue specimen are optimized in order to scan the high cycle fatigue region and determine the endurance limit (See Figure 2.13). That is, the maximum displacement of the fatigue test machine creates a maximum bending stress slightly below the yield strength value on the specimen. This yield strength value is obtained from tensile test results. On the other hand, the minimum displacement of the fatigue test machine creates a maximum bending stress on the specimen slightly below the endurance limit value. Since the specimen is expected to exceed the UTS value of 1400 MPA in the study, this endurance limit value is considered as 700 MPa. In this way, it was planned to create a specimen model that works in the range in which the S-N curve in Figure 2.13 for stress ratio of -1.

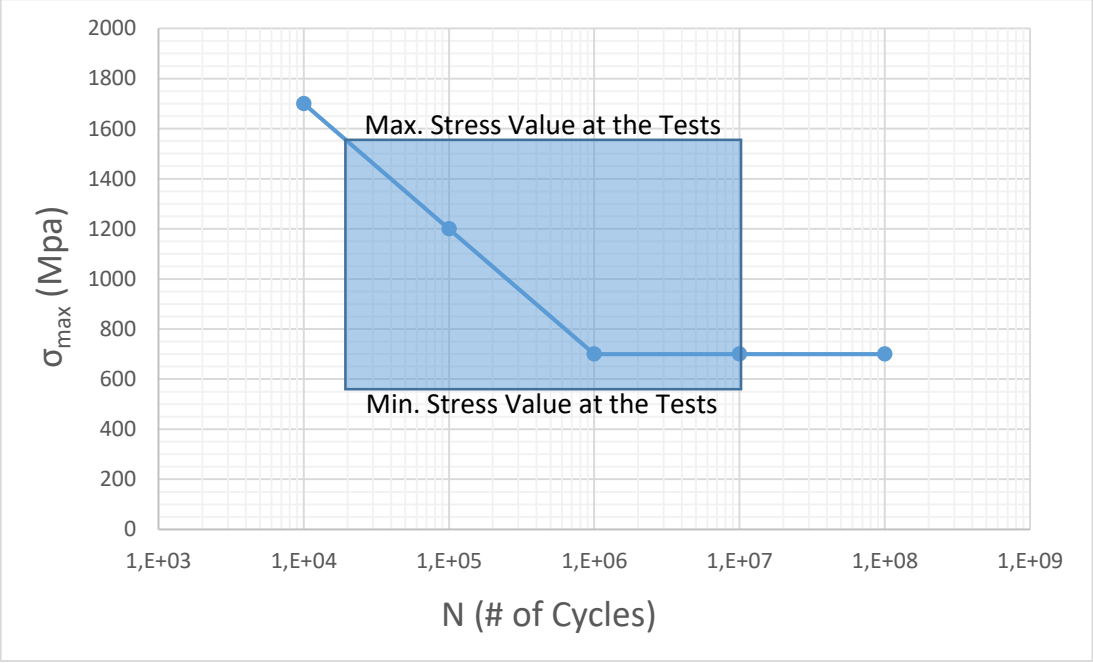

Figure 2.13. Test Region of Fatigue Specimens on Foreseen S-N Curve

Normally, the stress amplitude value is written to the stress axis in an S-N curve, and the endurance limit is expected to decrease as the stress ratio (R) value increases for the same stress amplitude value. It is a well-known information from literature. An example, which shows the variation of the endurance limit according to stress ratio and supports this information, is as seen in Figure 2.14. In this thesis study, although R = 0, the foreseen S-N curve was drawn based on R = -1 for ease of design of fatigue specimen. In other words, in the sample design criterion, the stress amplitude value was accepted as the maximum bending stress value and the endurance limit value was assumed as 700 MPa in the literature. In this thesis study, since R = 0, the stress amplitude value is actually half the maximum bending stress value and the endurance limit is expected to be slightly lower than 700 MPa. Therefore, the S-N curve calculated according to the maximum bending stress values needs to be revised according to the stress amplitude values at the end of the fatigue tests.

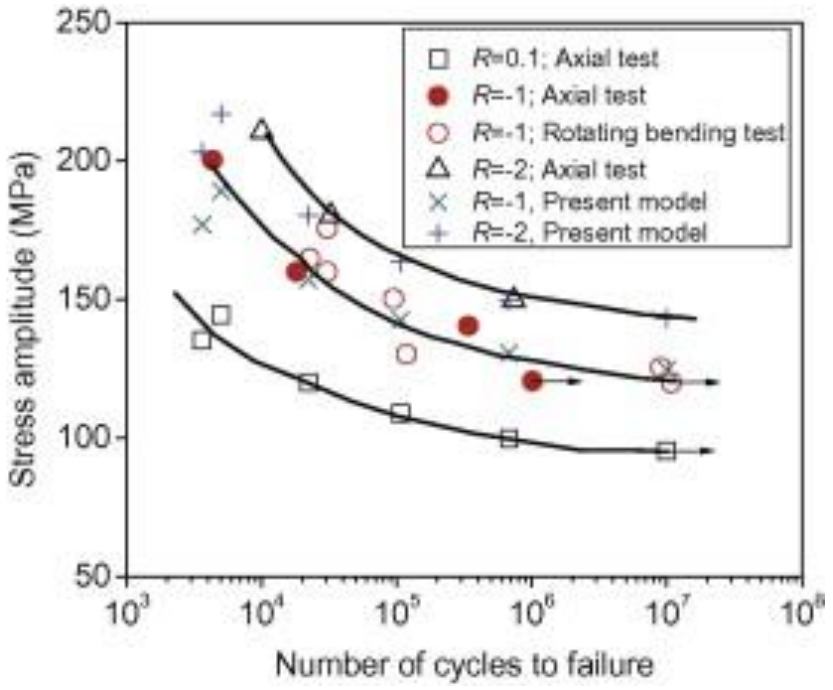

Figure 2.14. Effect of Stress Ratio (R) on Endurance Limit[22]

In the numerical analysis program, two types of stress values, elemental stress and nodal stress, are obtained for each stress analysis and there is some difference between these stress values. This difference comes from the difference in the method of solving Elemental FEM and Nodal FEM. When the mesh size in the model becomes smaller, this difference starts to shrink because the analysis of low mesh size is considered numerically more accurate. For this reason, it is recommended to make a nominal stress value assumption for the stress analysis by taking the average of these two stress values.

When optimizing the model, it is important that distributing the stress distribution homogeneously over the fracture zone. Therefore, instead of sharp transitions in the bending region, larger radii are preferred.

After the stress analyses of the specimen, structural modal analysis is also applied to the specimen to check resonance frequency of the specimen to see that the optimized specimen model works correctly on the fatigue test machine. The 1st mode value of the specimen is ought to be much greater than the operating frequency of the fatigue test machine. If the 1st mode value is close to the operating frequency, the specimen probably resonates; or if it is smaller than the operating frequency, the springback of the specimen is slower than the speed of the pin of fatigue fatigue test machine. These situations cause the specimen to run by hitting the pin and the test is not be able to produce the desired result.

2.3. Material

2.3.1. Carbide-Free Lower Bainite

Steels with high silicon content form carbide-free bainitic structures after isothermal bainitic transformations. For the formation of carbide-free bainite, relatively low temperatures (< 300 °C) are required during the heat treatment process after austenization. Normally, a low temperature (< 400 °C) bainitization process leads to the formation of a lower bainitic microstructure, that is, thin carbide plates are formed in the ferrite grains. However, when silicon is present in the structure, the carbides that must remain in the ferrite grains are deposited between the bainite shaves as retained austenite. This results in higher strength (UTS > 2000 MPa) steel formation[23].

For this study, 60SiMn5 type rolled steel is used. In order to obtain the desired carbide-free lower bainitic structure in the samples, after the samples are austenized at 900 ºC, they undergo to heat treatment process in a salt bath at 250 ºC. In the salt bath, the start time of bainitization is expected to be 5 minutes and the end time of bainitization is between 3-6 hours[24]. Therefore, it is recommended to continue the heat treatment process in the salt bath for at least 4 hours to obtain 100% lower bainite. 60SiMn5 steels are generally austenitized at 850 ºC in industrial applications[25]. However, since the uniform microstructure with 100% lower bainite content is targeted in this study, it is preferable that the austenitizing temperature is slightly higher, because larger grains are needed at the end of austenization.

If there is sufficient carbon content (> 1%) in silicon-containing steels, it is expected to obtain nanobainite[26]. Nanobainites are similar in structure to carbide-free lower bainites, but are smaller in size (See Figure 2.15). The smaller size is due to that high carbon content enable bainitic transformation above martensite start temperature even in relatively lower temperatures. Because high carbon content shift martensite start temperature to lower temperatures (See Figure 2.16). In this manner, the transformation is made above the martensite start temperature, and thus smaller (nano-

sized) bainitic structures are able to be obtained at relatively lower temperatures[27]. In addition, because of the high carbon content in its structure, more retained austenite forms among the bainite shaves with presence of high silicon content. More retained austenite and smaller bainite provide more strength and more ductility to the structure than carbide-free lower bainite has[28].

Considering the heat treatment conditions and 0.6% carbon content of the material to be used in the study, the samples are expected to be in a microstructure between nanobainite and carbide-free lower bainite. Therefore, the samples will be referred to as carbide-free lower bainite in this study instead of nanobainite.

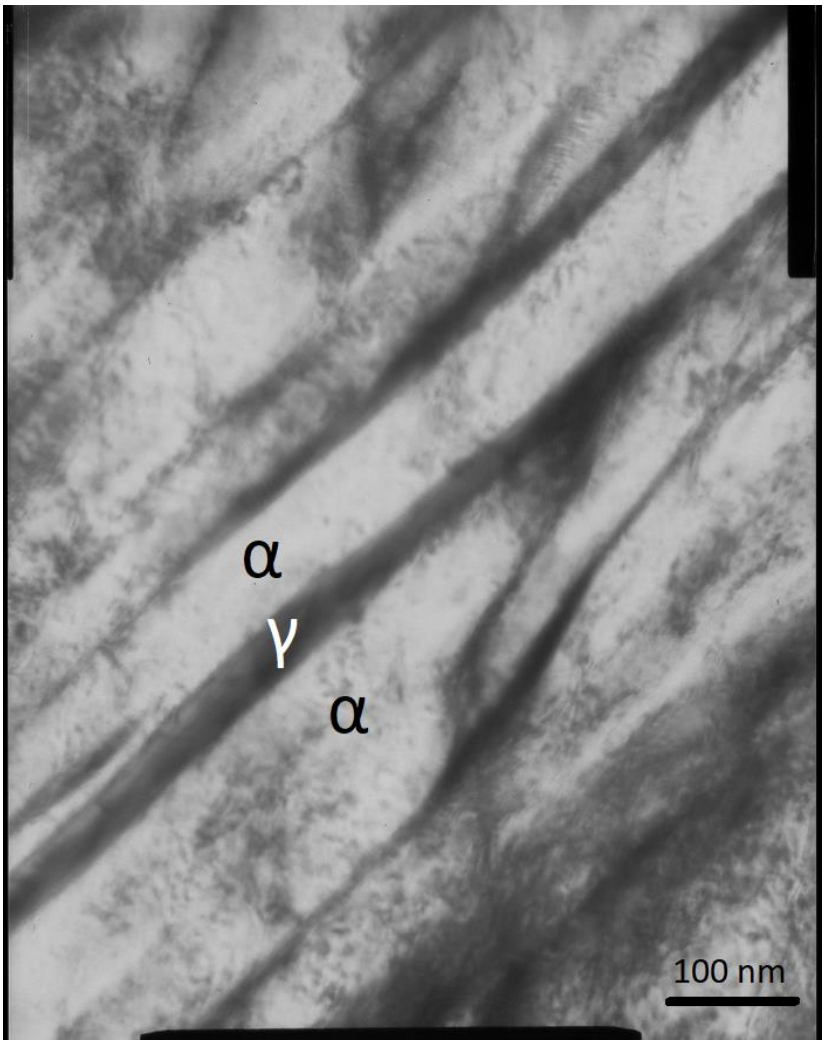

Figure 2.15. TEM Image of a Nanobainite Structure[29]

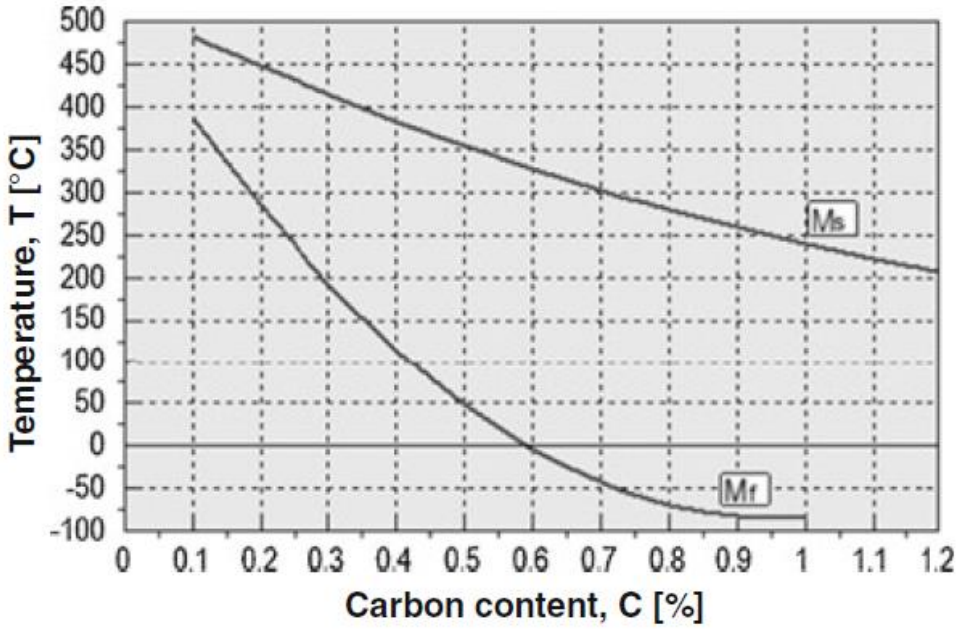

Figure 2.16. Effect of Carbon Content on Martensite Start & Finish Temperature[30]

2.3.2. Tempered Martensite

Since 60SiMn5 steel is spring steel, it is widely-used as martensitic structure in industrial use[31]. Because of this and because of its high strength, it is preferred that the structure to be compared with carbide-free lower bainitic structure in this study is tempered martensitic. It is important for the purpose of the thesis that the martensitic microstructure to be obtained is identical in whole microstructure of the samples; therefore, it is recommended the hardenability of the raw material in the study be high. 60SiMn5 steel is expected to have high hardenability due to its Silicon and Manganese alloying element contents, which makes it suitable for this study.

Samples are austenized at 900 ^{o}C in order to both austenize at the same temperature as lower bainite's and to obtain uniformity in the microstructure with 100% martensite. It is recommended that quenching be done in oil to prevent cracking of microstructure during quenching. In order to obtain similar mechanical properties with lower bainite's, the hardness examination is the first thing which is needed to check

in tempered martensite samples. To obtain a similar hardness value to lower bainite's, samples are produced under different tempering conditions, and the tempered martensite sample which is close to the hardness of the lower bainite sample is selected to compare with the lower bainite obtained.

The tempering temperatures of the martensitic structures were determined in the range of 400 – 550 ºC in the thesis study. At higher tempering temperatures, tempered martensites are obtained with larger grain sizes and are expected to have a lower hardness values than the obtained lower bainite. For this reason, it recommended that hardness tests be performed from 550 ºC to 400 ºC until to reach same hardness level as the lower bainite's. Below 400 ºC is not preferred due to temper embrittlement problem. Because, although the hardness of the samples, which are tempered below 400 ºC, increases, a drastic decrease in toughness occurs (See Figure 2.17). This means that the samples become very brittle, therefore tempering below 400 ºC is not recommended to apply since the correct mechanical properties are not be mentioned.

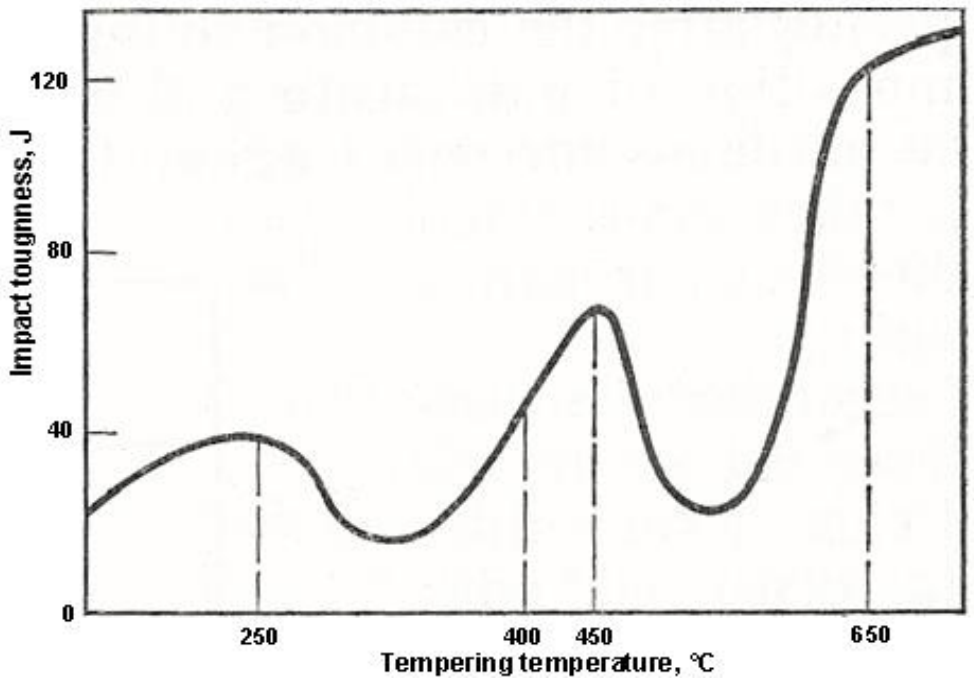

Figure 2.17. Effect of Tempering Temperature on Impact Toughness of a Martensitic Structure[32]

2.4. Literature Review

A study seen in Figure 2.18 shows data where the ratio of minimum to maximum stress is −1, for a classical bearing steel in two microstructural states. As seen, there is no significant difference between the bainitic and martensitic states when data from many different sources [Data from Sakai et al. (2002), Baudry et al. (2004), Bathias (2010), Almaraz (2008)] are merged, at conventional or ultrasonic test frequencies[33]. On the other hand, data by Mayer et al. (2009) indicate that bainitic bearing steels outperform martensitic microstructures in ultrasonic fatigue tests due to their greater ductility[34]. It is difficult therefore to reach generic conclusions about the performance of the different microstructures in ultrasonic fatigue tests.

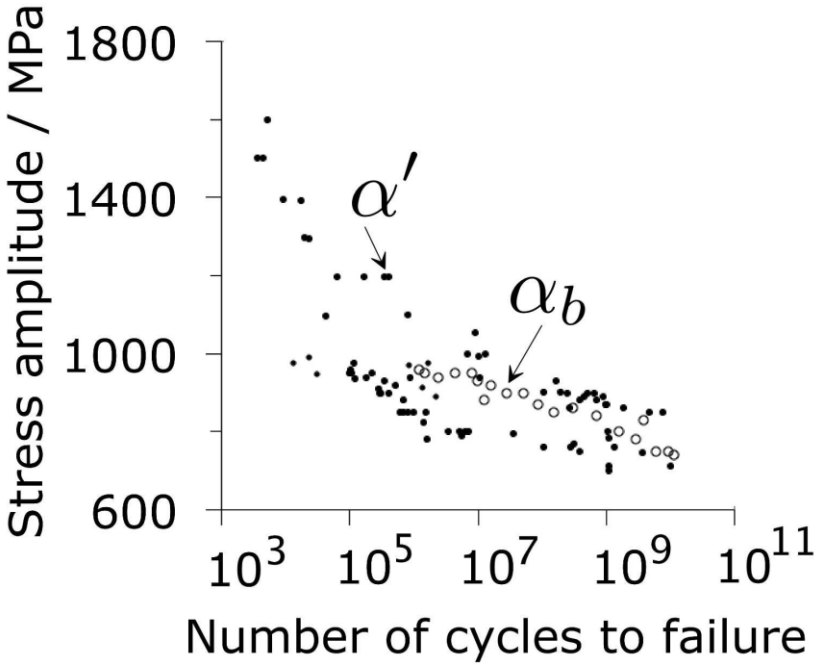

Figure 2.18. Fatigue Lives of a 1C-1.5Cr Bearing-steel Heat-treated to Bainitic and Martensitic States

On another study, R. Rementeria et al analyzed[35] the fatigue crack propagation in nanostructured bainitic steels on the basis of its deflection due to the crystallographic orientation and boundary distribution. The main goal is to understand the role of both ferrite and austenite crystals on crack transmission and deflection across boundaries,

and how this finally has an effect on fatigue life. They used three types of nanostructured bainitic steels named as 0.6CV/250, 0.6CV/270 and 1CSi/250:

- 0.6CV/250 means obtained at 250 ºC during 10 hours,
- 0.6CV/270 means obtained at 270 ºC during 7 hours,
- 1CSi/250 means obtained at 250 ºC during 16 hours in subsequent isothermal treatment.

The chemical compositions of the alloys investigated are 0.67C–1.67Si–1.31Mn–0.20Ni–1.73Cr–0.15Mo–0.18Cu–0.03Al–0.12V and 0.99C–2.47Si–0.74Mn–0.12Ni–0.97Cr–0.03Mo–0.17Cu–0.02Al wt%, encoded as 0.6CV and 1CSi, respectively. The S-N graphs which describes their fatigue behaviors are shown in Figure 2.19.

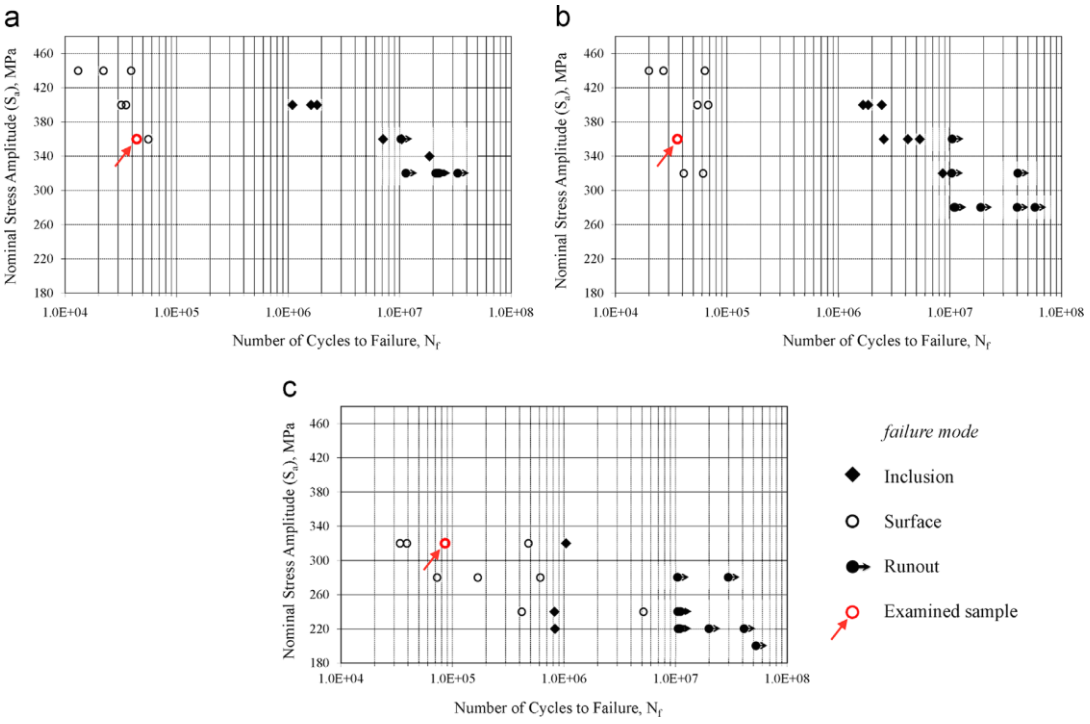

Figure 2.19. Wöhler (S–N) Curves of the Specimens (a) 0.6CV/250 (b) 0.6CV/270 (c) 1CSi/250

The fatigue behavior of these three different nano-bainitic structures has also been analyzed (See Figure 2.20), because macroscopic monotonic mechanical properties fail to explain it.

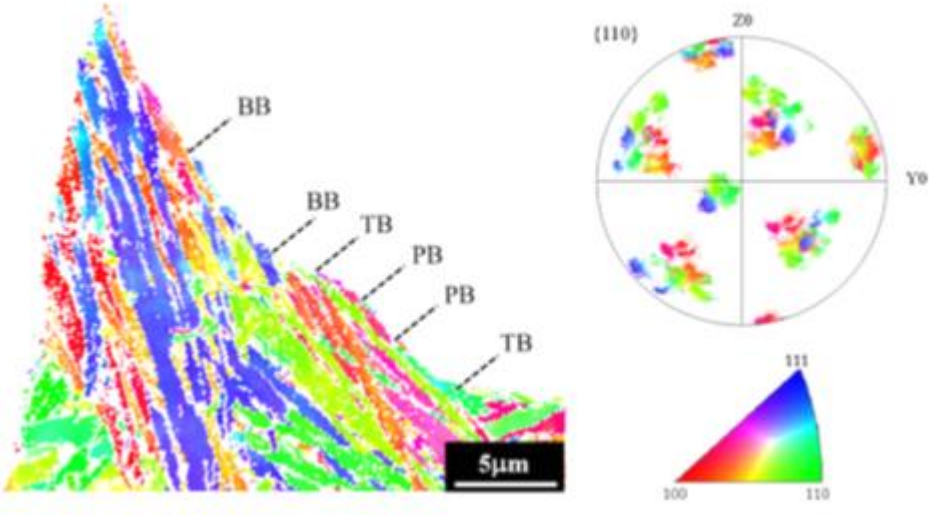

(a) Ferrite Inverse Pole Figure (IPF) map showing crystallographic boundaries and corresponding Pole Figure (PF), where BB stands for Block Boundary, TB stands for Twin Boundary and PB stands for Packet Boundary.

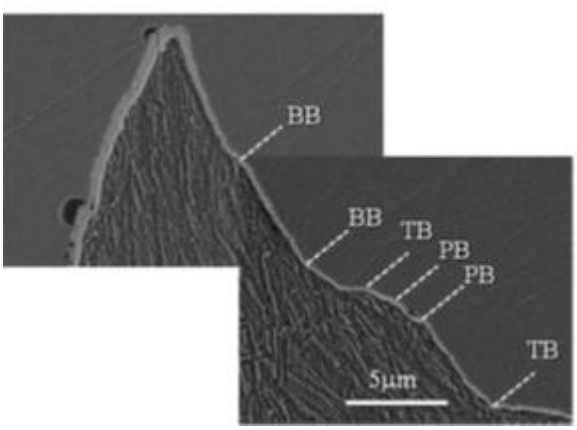

(b) Corresponding FEG–SEM Micrograph

(c) Calculated Slip Traces of the Stage I of Crack Propagation

Figure 2.20. Microstructure of the 0.6CV/270 Sample below the Fracture Surface

The microstructural examination at the Stage I seen in Figure 2.20 has shown that:

• The crack deflects at the interphase boundaries between blocks, packets and twins of the ferritic phase, but not to a significant extent in the interphase boundaries within a single block.

• The bainite block size is the crystallographic parameter controlling the crack propagation at this stage. However, its effect on the fatigue strength remains unclear, partially because it cannot be isolated from other microstructural features that are also likely to be affecting the mechanical behavior.

On another study, Sourmail et al investigated[36] fatigue applications in high Si high C steels nanostructured bainite at the conditions of notched ($K_t = 2$) and tension-tension ($R = 0.1$), and compare them with two high strength steels tested in identical conditions. Results which describe the fatigue strength of the test samples at 10^7 cycles are shown in Table 2.2.

Table 2.2. *Fatigue Strength of Industrially Produced Nanostructured Bainites and Two References*

	06CV-250	*06CV-270*	*1CSi-220*	1CSi-250	*100Cr6* *[Linkewitz, 1998]*	*50CrMo4* *[Schmidt, 2012]*
UTS / MPA	2003	1822	2224	2072	2350	1180
$S_{a,50\%}$ at $N = 10^7$	350	330	205	245	355	305

References were not available in the exact testing conditions used for the rotation bending fatigue, results can only be compared with one another. A comparison of the fatigue strength achieved on 0.6C wt% and higher carbon material suggests a significant difference between these two types of grades. Results do not indicate particular advantages of this microstructure in comparison to conventional lower bainite (bainitized 100Cr6) or quenched and tempered materials. Further work is thus necessary in order to determine whether nanostructured high Si bainitic steels may offer benefits in terms of fatigue performance.

2.5. Objective & Main Contribution

2.5.1. Objective

Steels with high silicon content form carbon-free bainite after isothermal bainitic transformations. The aim of this study is to investigate the fatigue behavior of a lower bainitic structure in 60SiMn5 which is a Si-Fe-C steel. The investigation was done by comparing the fatigue life of a carbide-free lower bainitic structure obtained from 60SiMn5 steel with the fatigue life of a structure which has a tempered martensitic microstructure obtained from the same steel under varying loads. In other words, S-N of a high strength lower bainitic structure in 60SiMn5 steel was examined by comparing it with a high strength tempered martensitic structure in 60SiMn5 steel. In order to make the comparison correct, it was aimed to compare the lower bainitic structure with the tempered martensitic structure which has been austenized at the same temperature and has had similar mechanical properties as lower bainite's. For this reason, mechanical properties of materials such as hardness, yield strength, tensile strength and modulus of elasticity were also discussed in this thesis.

In this study, samples were examined in terms of high cycle fatigue life. High cycle fatigue occurs under dynamic loads below yield strength, and it is considered that steels, which are subjected to dynamic loading at their own yield strength values, have similar life times with each other. Therefore, it is essential in order to compare samples in similar mechanical properties and achieve controlled test conditions that different microstructures have similar yield strength values to each other. In order to determine this, firstly the hardness values of the samples were examined. Hardness measurement is one of the easiest and first ways to determine the mechanical properties of a sample. However, as it is known from the literature, hardness tests give better idea about tensile strength rather than yield strength of a sample. For this reason, it is recommended to perform tensile tests following hardness tests in order to check the affinity of yield strength values.

The steels produced in this study are not highly preferred in industrial use, because in order to obtain 100% bainite or 100% martensite, more austenitizing temperatures are to be preferred in this study than in industrial production. That is, the comparison in this study about fatigue lives was made to contribute to the literature rather than to industrial knowledge. Nevertheless, it is known that silicon-containing spring steels are used in places which need long life usage under repeated high stress values such as leaf springs in the suspension systems of heavy vehicles as seen in Figure 2.21. Considering these service type and service life of leaf springs, it is appropriate to study high cycle fatigue while stress ratio ($\sigma_{min}/\sigma_{max}$) is zero on the fatigue specimens. In the same way, considering the working methods of leaf springs, it was decided to perform fatigue tests on rectangular specimens by repeated bending fatigue method. Since the steels studied in this thesis are relatively hard steels (UTS > 1400 MPa) and high cycle fatigue was to be studied, it was expected that the fatigue specimens break through the fatigue propagation section very quickly after fatigue initiation (See Figure 2.2). Therefore, this study focused on total fatigue duration rather than regarding fatigue propagation duration. In order to minimize fatigue propagation duration which is until the fracture of the fatigue specimen just after the fatigue initiation, it was planned to design the fatigue specimen as thin as possible.

Figure 2.21. Leaf Springs of a Heavy Duty Truck [Shot by J. Gill, 2000]

In summary, before the design of fatigue specimen, a fatigue test machine was designed and manufactured in compliance with the aim of the thesis. Afterward, fatigue specimen was designed, produced according to the criteria coming from the fatigue test machine and the mechanical properties of the specimens, and the fatigue tests were done with these specimens. At the end of the thesis, fatigue lives of the specimens which were in desired microstructures were compared by using S-N curve, and the specimens, which were fractured, were examined by fractographic examinations. The flowchart summarizing the methodology of the thesis is shown in Figure 2.22.

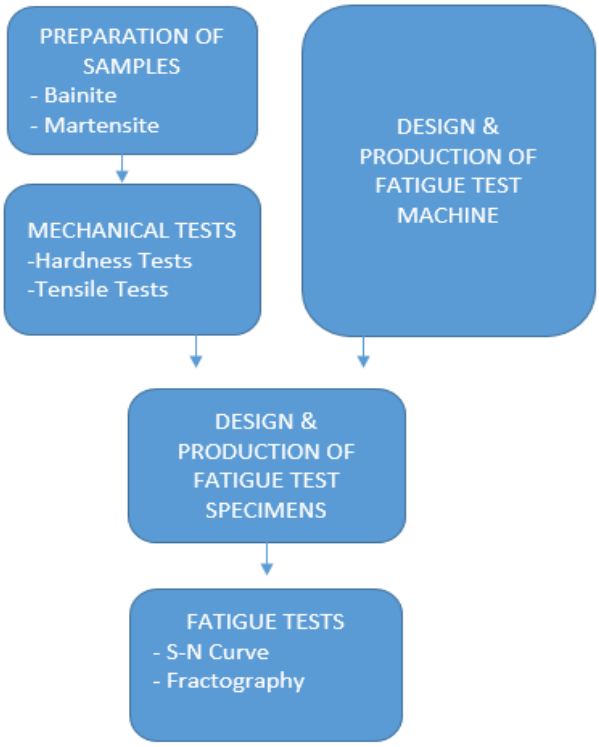

Figure 2.22. Methodology of the Thesis

2.5.2. Main Contribution

The bending fatigue analysis of a carbide-free bainitic structure on rectangular fatigue specimen has been the first in the literature. Krouse-type fatigue specimen was used as rectangular specimen type in this thesis study. Fatigue on Krouse-type specimen was studied with relatively lower strength steels in the literature before. Therefore, the study on high strength steels with this type of fatigue specimen was also be the first in the literature. Therefore, in this study, a new fatigue test machine and modified Krouse-type fatigue specimens were designed and produced for this purpose. The reason why the high strength steels were not tested with this method before this thesis study is probably carbon loss which may be up to a depth of 500 μm that occurs on the surface of fatigue specimens after heat treatment process. When it is considered that the wall thickness of Krouse-type specimen, which is about 1 mm, such a carbon loss from the surface could make the fatigue tests meaningless. Because, as is known from the literature, fatigue is a phenomenon starting from the surface of the sample, and so the microstructure that is desired to be tested on the surface of the specimen ought to be preserved without deterioration. Therefore, the production process of the test specimens was made considering this information.

CHAPTER 3

EXPERIMENTAL PROCEDURE

3.1. Material

60SiMn5 steel which has high silicon content was used in the experiments to obtain carbide-free lower bainitic structure. The material was preferred as a flat bar in order to extract tensile and fatigue specimens in suitable dimensions. Figure 3.1 shows the 60SiMn5 steel flat bar with section dimensions of 14 mm X 90 mm used in the experiments. The material content (spectrometer analysis) of the steel is shown in Table 3.1.

Figure 3.1. 60SiMn5 Steel Flat Bar

Table 3.1. *Ladle Chemical Composition (%) of 60SiMn5*

	C	*Si*	*Mn*	*P*	*S*	*Cr*	*Mo*	*Ni*	*Al*	*Cu*	*Sn*
Min	0,55	1,00	0,90								
Max	0,65	1,30	1,10	0,025	0,025				0,025	0,35	
Sample	0,60	1,20	1,00	0,010	0,003	0,19	0,03	0,07	0,022	0,13	0,012

3.2. Heat Treatment

The materials were splitted up into small pieces of approximately 10 mm X 10 mm X 20 mm for heat treatment processes. Then, these samples were subjected to metallographic process, and got prepared for microstructure and hardness measurements.

In fatigue tests, carbide-free lower bainite and tempered martensite specimens with similar hardnesses were to be compared. Therefore, the lower bainite sample were obtained first. To obtain carbide-free lower bainite, the samples were first austenitized in the muffle furnace, and then kept at a relatively low temperature in the salt bath for bainitization (See Figure 3.2).

Then, tempered martensite tests were carried out at different heat treatment processes until they reached the same hardness value as bainite's. The same muffle furnace was used for the austenization of tempered martensite samples. Following the austenization process, the samples were quenched in a bucket filled with quenching oil. In the quenching process, oil was used instead of water to prevent cracking of the samples. Tempering was then carried out using the same furnace at different temperatures until the same hardness levels were achieved as lower bainite's.

(a) Muffle Furnace *(b)* Salt Bath

Figure 3.2. Heat Treatment Set-up

3.3. Characterization of the Sample

3.3.1. Metallography

After the heat treatment process, it was necessary to cut the samples first, and then bury them into bakelite in order to examine the microstructures of them under the microscope and to perform the hardness tests. The cut surfaces are to be the area where both microstructure examinations and hardness measurements are to be taken. Therefore, the cut surfaces stay on the top while the samples are buried to the bakelite. After embedding the samples in bakelites, the surfaces of the samples were subjected to grinding and polishing. For microstructure examinations and hardness measurements, the surfaces of the samples ought to be smooth and shiny as shown in Figure 3.3.

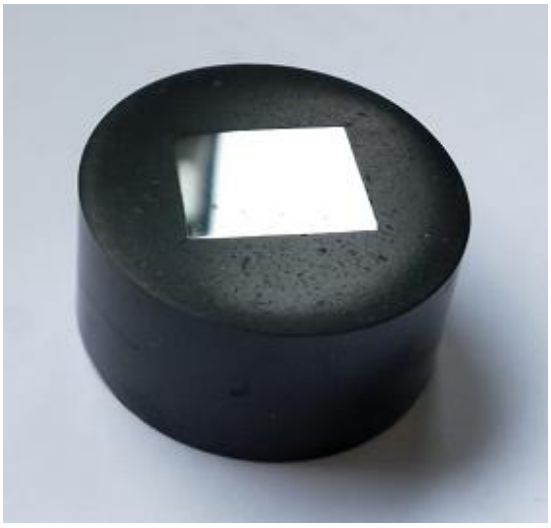

Figure 3.3. A Bakelite Sample

3.3.1. Microstructure

The surfaces of the bakelite samples were etched with solution containing 2% nital after polishing. After this, the surface is ready to be examined under an optical microscope. The samples were examined under Nikon Optihot 100 and Huvitz Digital Microscope HDS-5800 for microstructure examinations.

3.3.2. Hardness Tests

In order to determine the consistency of the mechanical properties in the microstructure, the Vickers hardness values of the prepared samples were examined with a Buehler Microhardness Indenter, first. This hardness measurements were done under the force of 1 kgf. Then the macro hardness values were taken with Emco Universal Digital Macro Hardness Testing Machine in order to determine the mechanical properties of the samples at the macro level. These hardness measurements were done under the force of 30 kgf.

3.3.3. Tensile Tests

Tensile test specimen dimensions were determined according to ASTM E8 / E8M – 13a rectangular tensile testing standard. The dimensions were modified according to the dimensions of jaws of the tensile test device and according to maximum force which tensile test device is able to apply. The dimensions of the tensile test specimen are as indicated in Figure 3.4. Accordingly, gauge-length is determined as 50 mm.

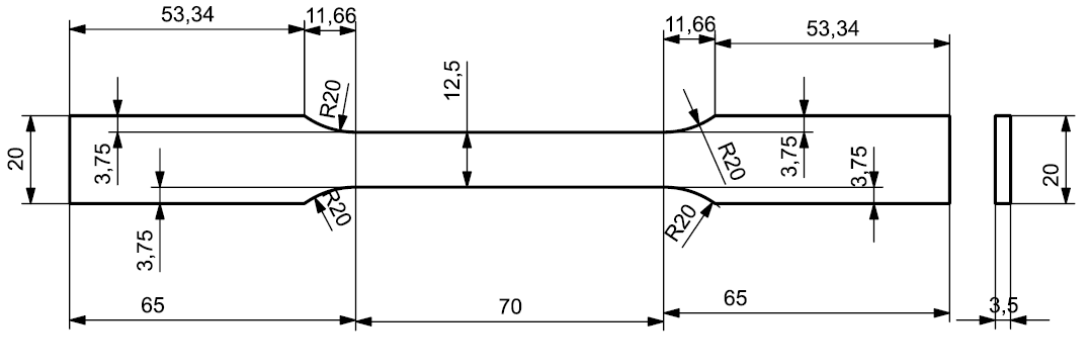

Figure 3.4. Technical Drawing of Tensile Test Specimen[37]

Tensile test specimens were obtained from the determined 60SiMn5 steel flat bar toward its rolling direction. In order to obtain these specimens, the sheet metal was subjected to wire erosion, sawing and grinding operations, respectively. The semi-finished product manufactured by wire erosion process is as shown in Figure 3.15.

These semi-finished tensile test specimens with a thickness of 14 mm were cut longitudinally with a saw and two tensile test specimens of approximately 6.5 mm thickness were produced from each of them. Then, these parts were grinded on both sides by 1.5 mm each and tensile specimens with a final thickness of 3.5 mm were obtained. Final tensile test specimen produced is as shown in Figure 3.6.

Figure 3.5. A Semi-Product Tensile Test Specimen

Figure 3.6. A Tensile Test Specimen

Final tensile test specimens were subjected to heat treatment processes under the specified heat treatment conditions after the hardness measurements. These heat-treated tensile test specimens were then subjected to tensile testing with Instron Tensile Testing Device (See Figure 3.7). Tensile tests were carried out under 10 tonne-force in quasi-static condition at a speed of 1 mm/min. At the end of tensile tests, yield strength, ultimate tensile strength and elongation data were obtained. The appearance of the tensile test specimens before and after the tests are as seen in Figure 3.8 and Figure 3.9, respectively.

Figure 3.7. Instron Tensile Testing Device

Figure 3.8. Tensile Test Specimens before Tensile Tests

Figure 3.9. Tensile Test Specimens after Tensile Tests

3.4. Fatigue Test Machine & Set-up

3.4.1. Design

A fatigue test machine has been designed according to run the revised Krouse-type specimen with a stress ratio which is equal to zero (R = 0). The design of the fatigue test machine is basically based on the fact that a slider-crank mechanism applies dynamic loading to the specimen with single amplitude loading. The load on the specimen is adjusted by the amount of displacement that the mechanism is able to apply to the specimen. This happens through reciprocating motion of the slider-crank mechanism. This mechanism is driven by rotational movement of a BLDC (brushless direct current) inverter motor. This inverter motor is driven by an electronic inverter card which is set at frequency value of 1000 rpm. This set frequency value comes to the inverter card as a signal and it is able to be adjusted in a software on the central processing unit. The CPU is also used to start the test and check the end of the test.

The CPU also receives information from the fatigue specimen via sensors and checks whether the specimen is broken. It calculates the test time as long as the test is in progress and stops the mechanism and test time when the specimen is broken. The test time is displayed on the LED display connected to the CPU. In addition, the CPU sends a text message to the identified phone number via the SMS module to inform the end of the test when the test is finished. All of these actions are managed by the CPU and the software on it. The flowchart describing the operating system of the fatigue test machine is shown in Figure 3.10. Moreover, the electronic circuit diagram describing the system management of the CPU and software codes on Arduino® Uno R3 DIP & Arduino® Leonardo hardwares of the CPU are shown in appendices section of this thesis study.

The fatigue test machine also needs an interior lighting system and a lubrication system. Arduino® Uno R3 SMD is used for its management. Lighting is provided with the voltage from this Arduino® output directly by connecting to the LEDs. The lubrication unit is designed so that oil in the oil tank drops continually onto the

mechanism. Excess oils, which are dropped to and accumulated in the sump, are returned to the oil tank by means of an oil pump which works 30 seconds at each 30 minutes. This ensures lubrication circulation. The oil pump is controlled by the same Arduino® software. The electronic circuit diagram describing the interior lighting system and the lubrication unit and their software codes are as shown in appendices section of this thesis study.

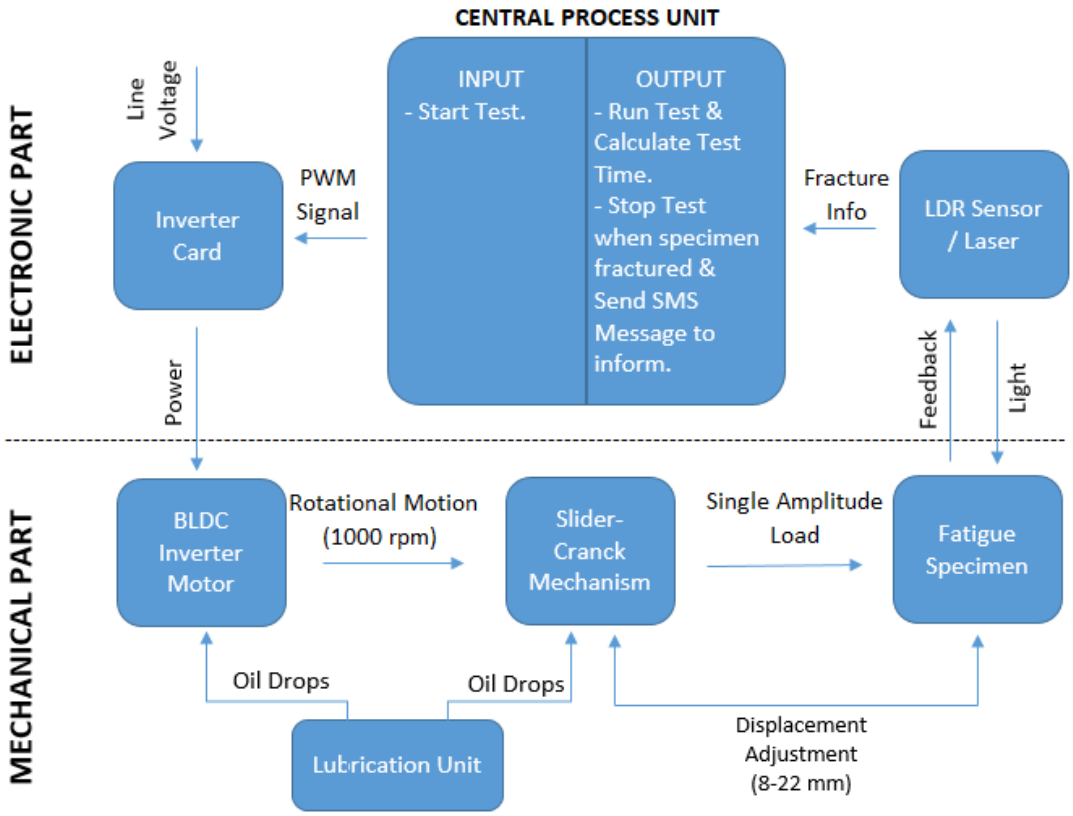

Figure 3.10. Flowchart of Fatigue Test Machine & Set-up

In accordance with this design, the hardware of the fatigue test machine is modeled via Siemens® NX 12.0 CAD program. The 3D modeling of the fatigue test machine and the fatigue test set-up which involves the fatigue test machine are as shown in Figure 3.11 and Figure 3.12, respectively.

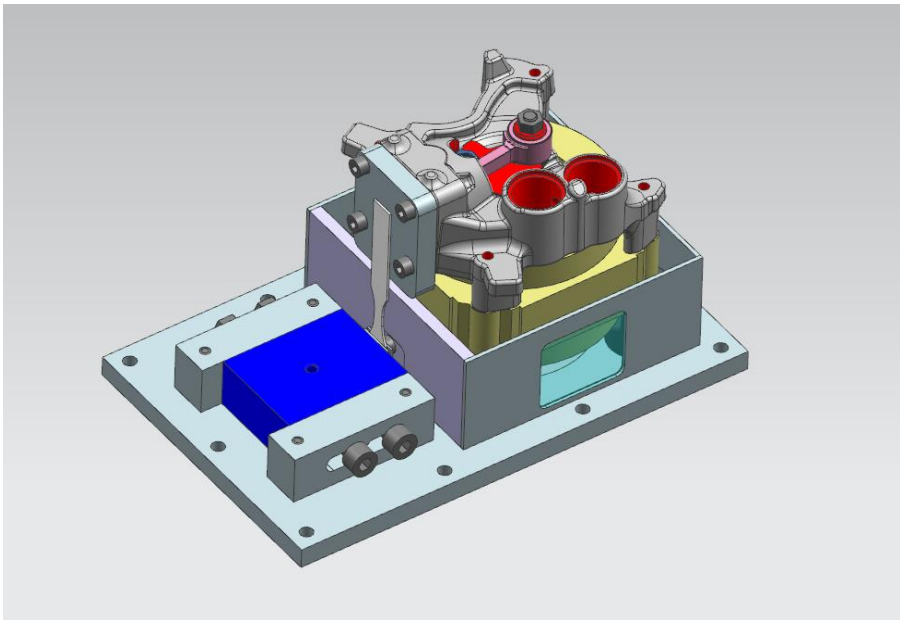

Figure 3.11. Model of Fatigue Test Machine

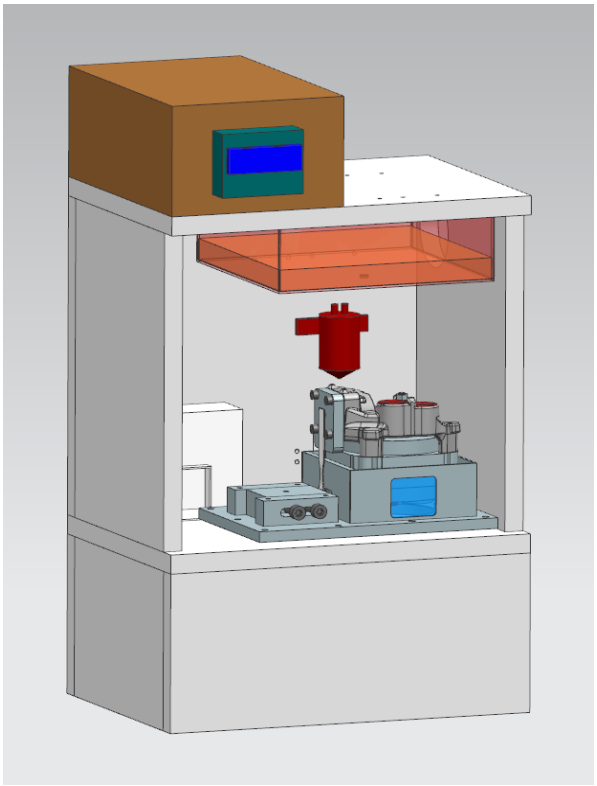

Figure 3.12. Model of Fatigue Test Set-up

3.4.2. Production

After the design of the test system was finished, then it was produced. Arçelik VNTZ 165 domestic hermetic compressor motor group was used as slider-crank mechanism. Other parts were manufactured and assembled according to the design. The prototypes of the fatigue test machine and the fatigue test set-up are as shown in Figure 3.13 and 3.14, respectively.

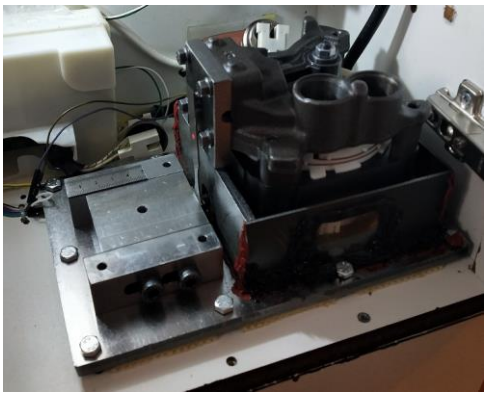

Figure 3.13. Fatigue Test Machine

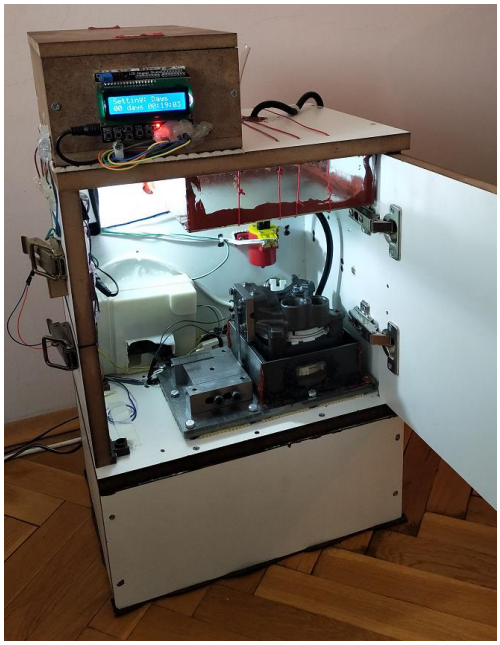

Figure 3.14. Fatigue Test Set-up

The electronic hardware and the lubrication system of the fatigue test machine are also shown in Figure 3.15 and Figure 3.16, respectively.

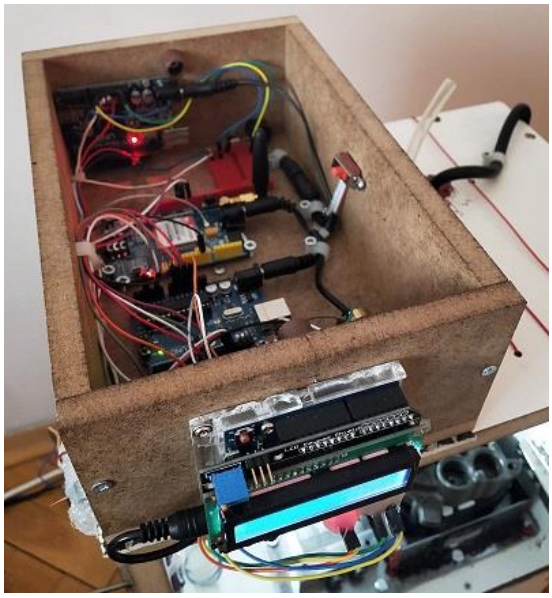

Figure 3.15. Electronic Hardware of Fatigue Test Machine

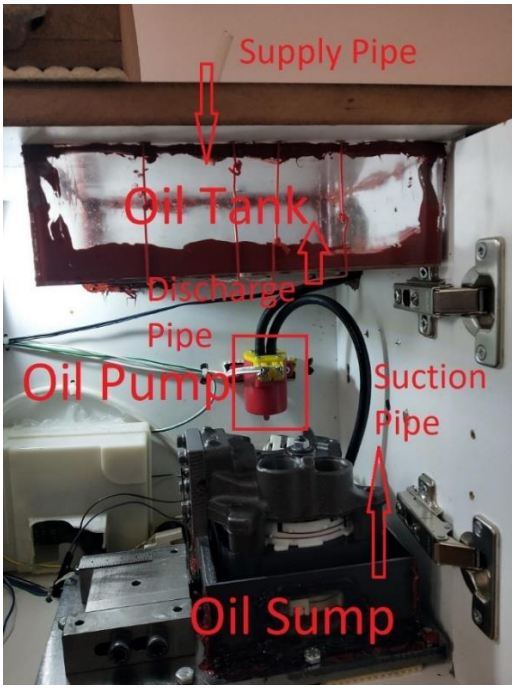

Figure 3.16. Lubrication System of Fatigue Test Machine

3.5. Design & CAD Analyses of Fatigue Specimen

Siemens® NX 12.0 CAD program was used for the design process of the fatigue specimen. The part was first designed so that it could be mounted and tested on the fatigue test machine. It was then optimized to achieve the desired stress values and stress distribution in the bending region. In the optimization process, structural stress and structural modal analyses were applied numerically to the part by using Nastran Solver module of the same CAD program. The part was modeled and analyzed repeatedly until the desired values were obtained in the analyses. After the desired values were obtained as a result of these iterations, the 1st mode shape and value of the part was checked by applying structural modal analysis to the part as the last process. With this method, the desired fatigue specimen design was obtained. Figure 3.17 shows a sample section from the design process of the part.

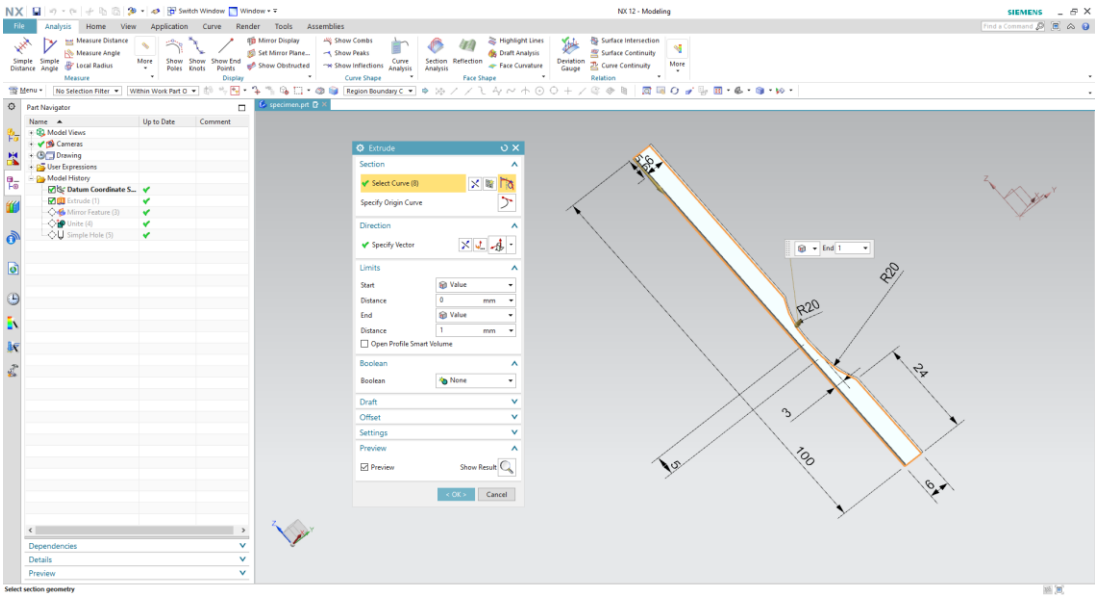

Figure 3.17. Designing Process of Fatigue Specimen

Structural stress analysis was carried out in the “Pre / Post” section of the CAD program. The part was assumed to be isotropic, and the mechanical properties of the material were assigned to the part. The part was meshed with CTETRA (10) type in 3D tetrahedral type. Then, considering the way the part would work, appropriate constraints and force were added to the part, and then solution part was run. Figure 3.18 shows the application of constraints and force to the meshed model.

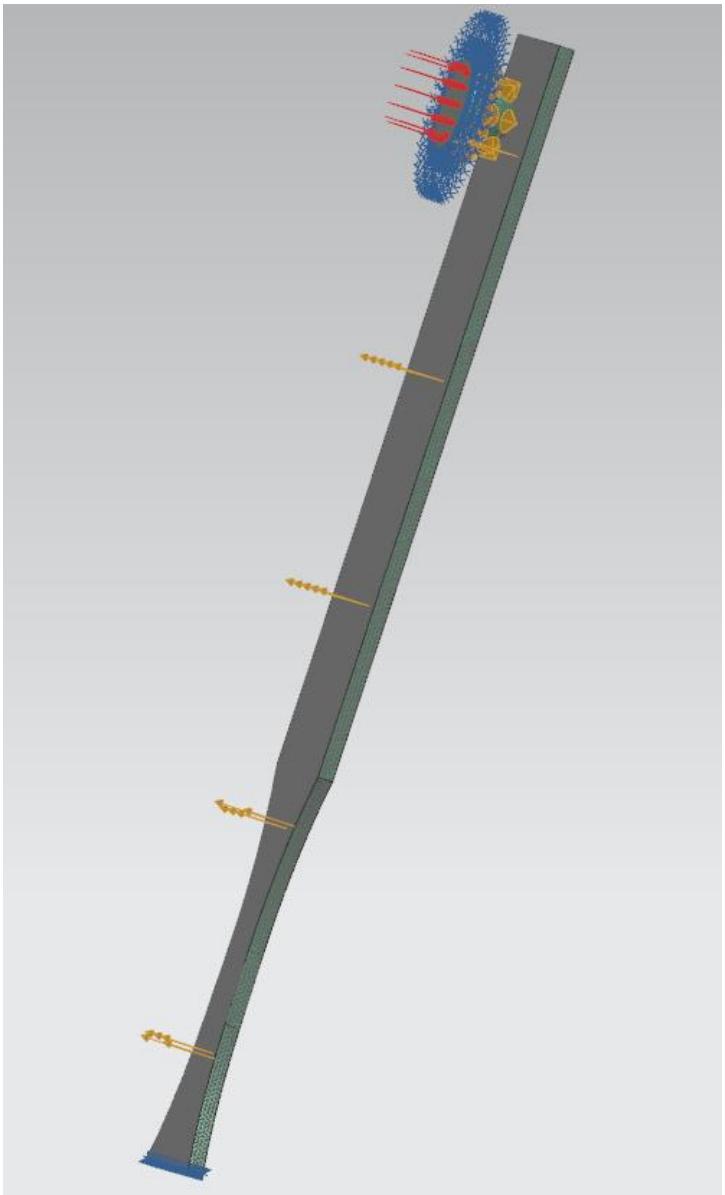

Figure 3.18. Application of Constraints & Exerted Force on Meshed Fatigue Specimen Model for Numerical Stress Analysis

In the solution section, the analysis type is selected as “Structural”, and the solution type is selected as “101 SOL 101 Linear Statistics - Global Constraints”. In this way, displacement, stress distribution and stress values on the sample were solved numerically. Figure 3.19 shows the solution screen of the analysis.

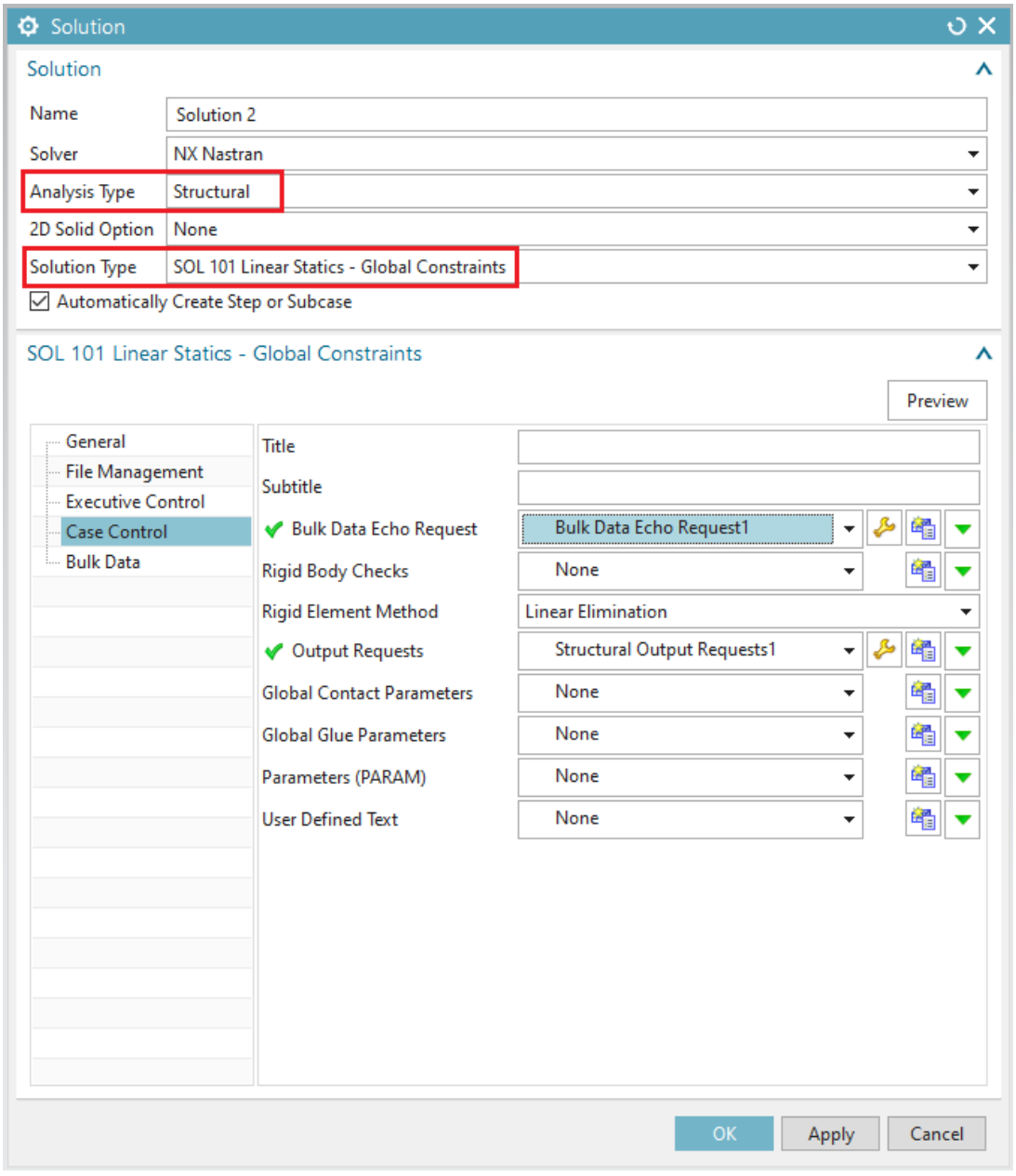

Figure 3.19. Solution Type of Numerical Stress Analysis on Fatigue Specimen Model

Structural modal analysis was also done in the “Pre / Post” section of the CAD program. The part was assumed to be isotropic, and the mechanical properties of the material were assigned to the part. The part was meshed with CTETRA (10) type in 3D tetrahedral type. Then, the constraint was added to the part according to where the part was fixed on the fatigue test machine. Figure 3.20 shows how the constraint is applied to the meshed model. In addition, it is ought to be noted that the smaller the mesh size, the greater the accuracy of the numerical analysis, but the longer the analysis duration. Therefore, the optimal mesh size is needed to find.

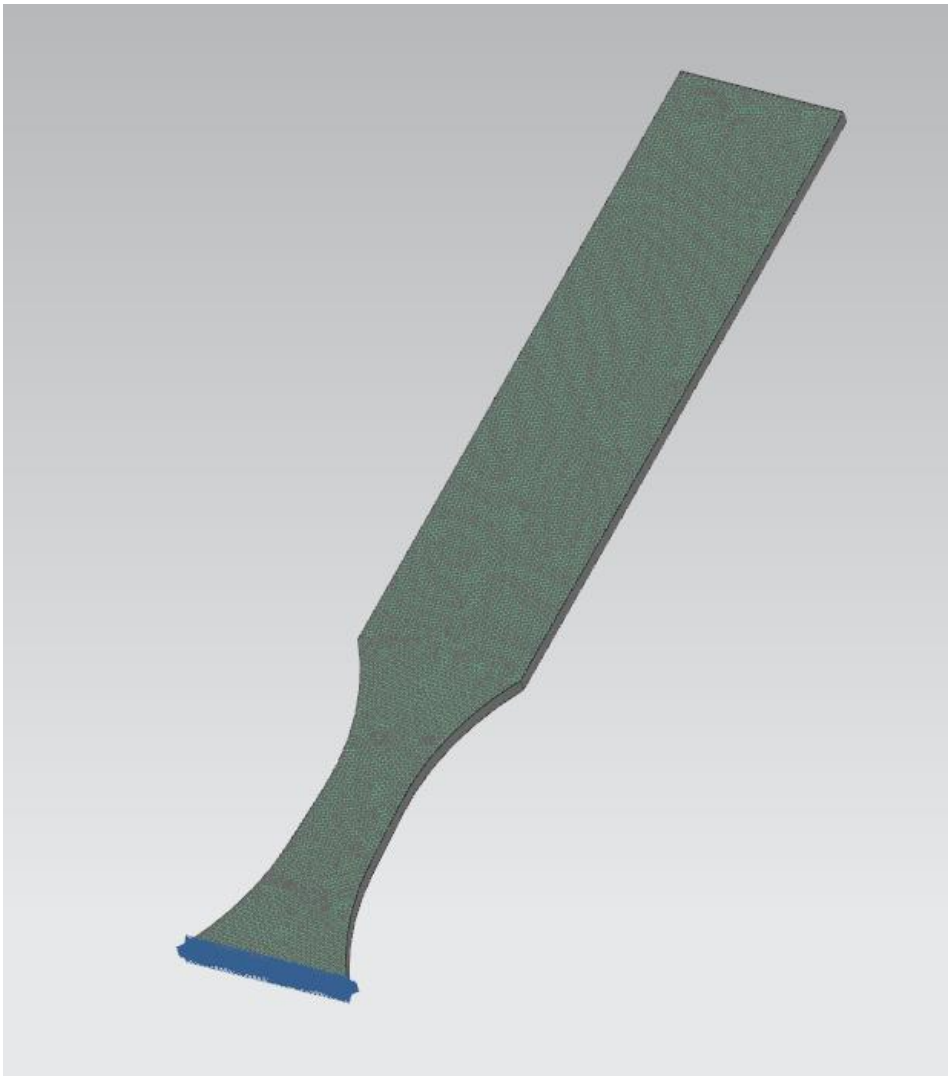

Figure 3.20. Application of Constraint on Meshed Fatigue Specimen Model for Numerical Modal Analysis

In the solution section, the analysis type is selected as “Structural”, and the solution type is selected as “SOL 103 Real Eigenvalues”. In this way, 1st mode value and shape of the fatigue specimen were solved numerically. Figure 3.21 shows the solution screen of the analysis.

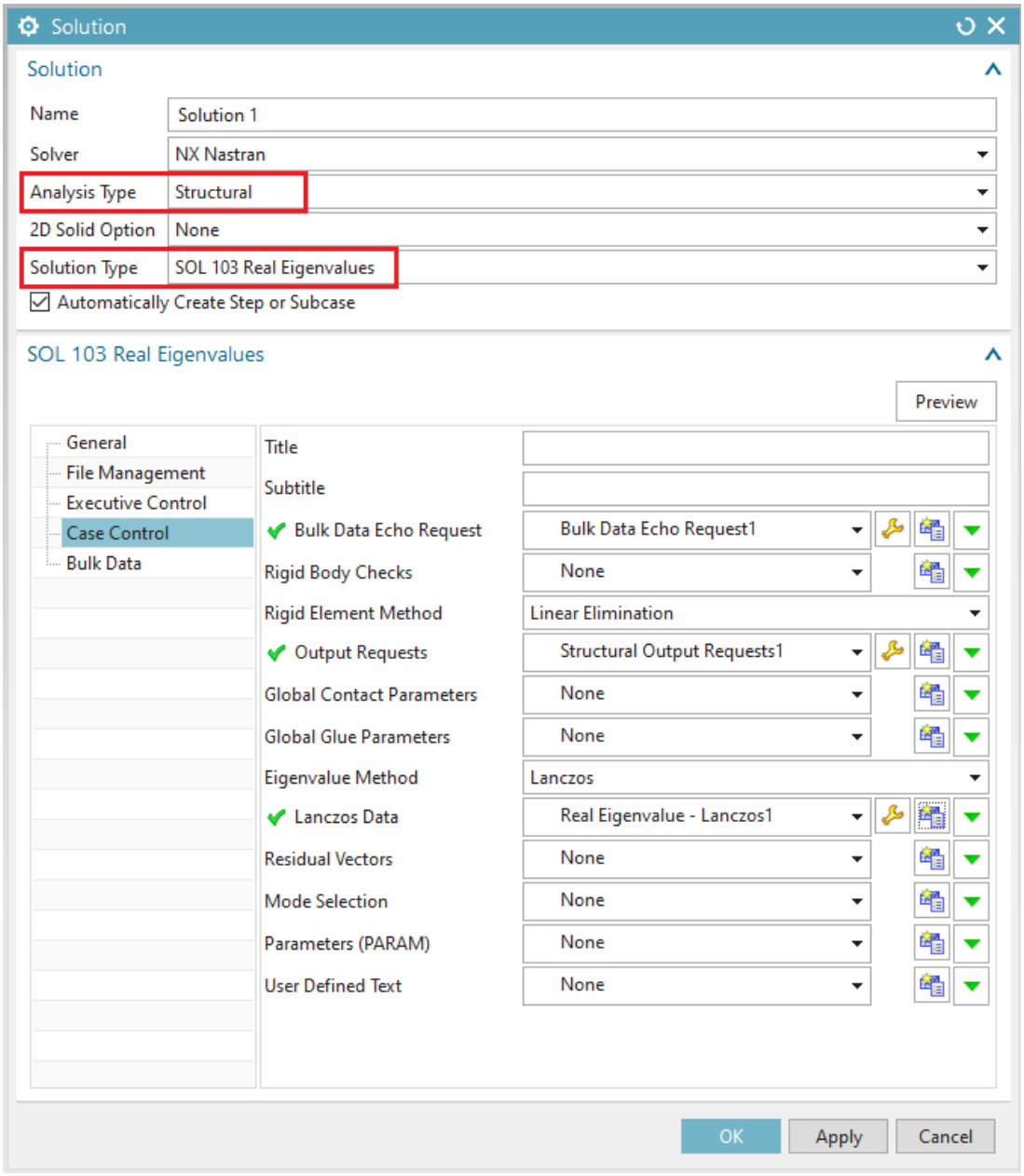

Figure 3.21. Solution Type of Numerical Modal Analysis on Fatigue Specimen Model

3.6. Production of Fatigue Specimen

The production process of the fatigue samples was carried out in 5 stages.

3.6.1. Wire Erosion Process

60SiMn5 steel flat bar was used for fatigue specimens, and it was cut into slices in 2.5 mm thickness each with wire erosion before heat treatment processes. Fatigue specimens were cut in the manner that they would bend in the rolling direction during the fatigue tests. The raw 60SiMn5 steel flat bar undergoing to wire erosion is as shown in Figure 3.22. Moreover, the wire erosion process is illustrated in Figure 3.23.

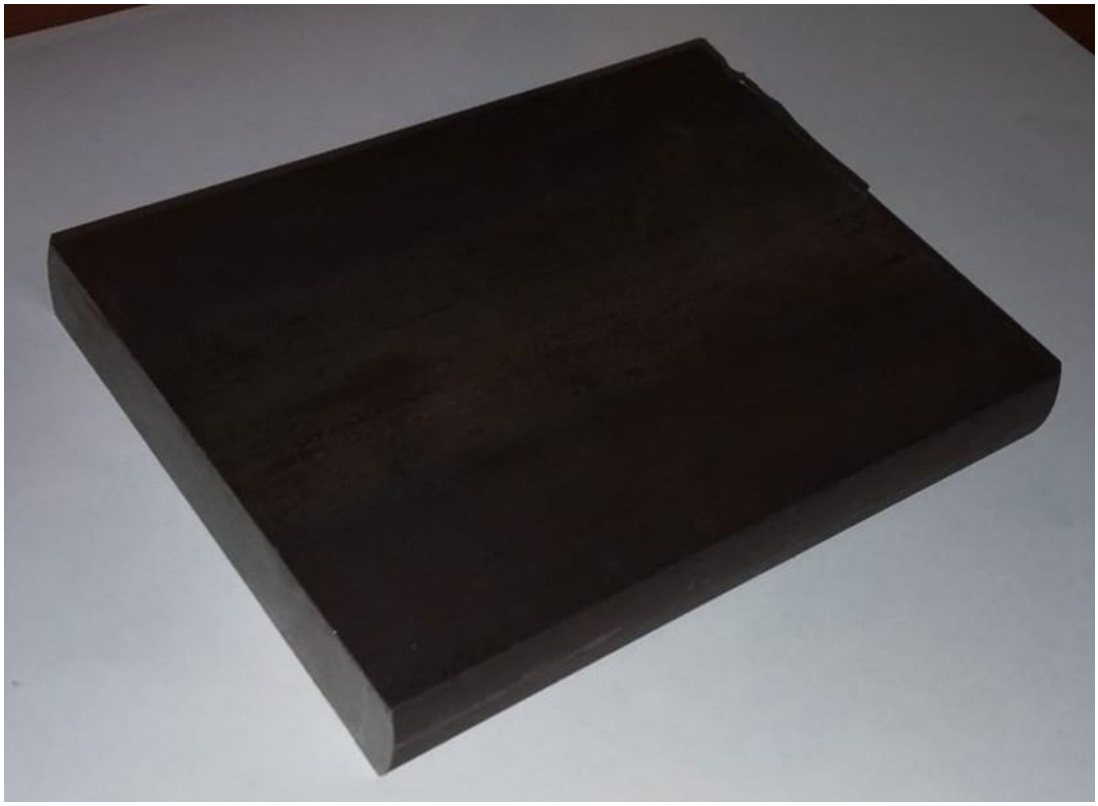

Figure 3.22. 60SiMn5 Steel Flat Bar before Wire Erosion Process

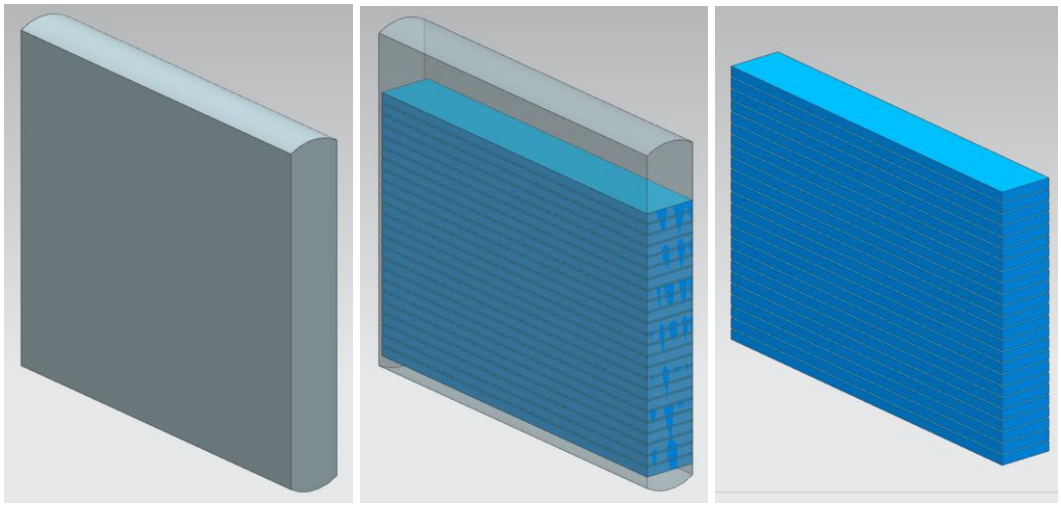

(a) Before Process *(b)* Transition Stage *(c)* After Process

Figure 3.23. Illustration of Wire Erosion Process Stages

In this way, 24 semi-finished fatigue specimens were obtained from a 100 mm long flat bar. The wire erosion machine where the process was performed is as shown in Figure 3.24.

Figure 3.24. Wire Erosion Machine

3.6.2. Heat Treatment Process

The semi-finished parts extracted from the wire erosion process were fastened to each other as shown in Figure 3.25 and underwent to the heat treatment processes which were specified according to the results of hardness and tensile tests. In this way, they were got prepared for machining process. The semi-finished fatigue specimens which were heat-treated are shown in Figure 3.26.

Figure 3.25. Fatigue Specimens before Heat Treatment Process

Figure 3.26. Fatigue Specimens after Heat Treatment Processes

3.6.3. First Grinding Process

The first grinding operation was performed to the heat-treated specimens in order to remove any distortion caused by the heat treatment processes and in order to prepare the specimens for CNC machining. At the end of this operation, the cross-sectional size of the specimens was decreased to 2 mm X 12 mm from 2.5 mm X 14 mm as illustrated in Figure 3.27. Since the microstructure is important on the part surface, the part surface is supposed not to be heated up. For this reason, grinding operations were performed relatively slower than a normal grinding process and using water as coolant. The speed of the grinding wheel in this process is 1850 rpm and its diameter is about 500 mm.

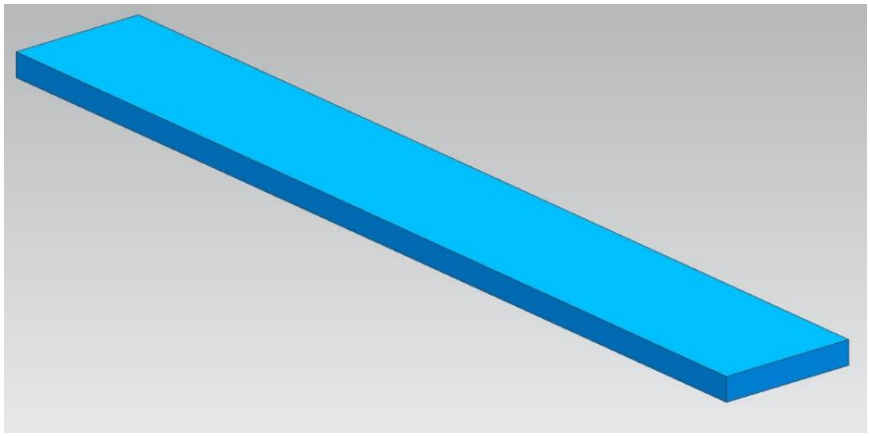

(a) Before Process

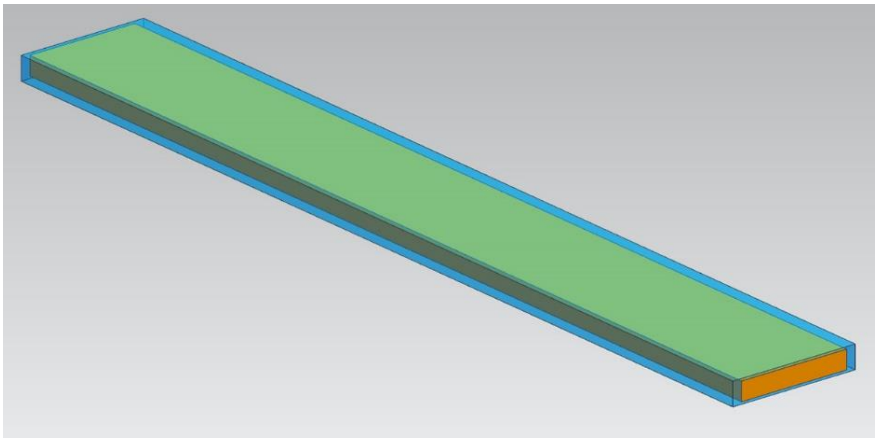

(b) Transition Stage

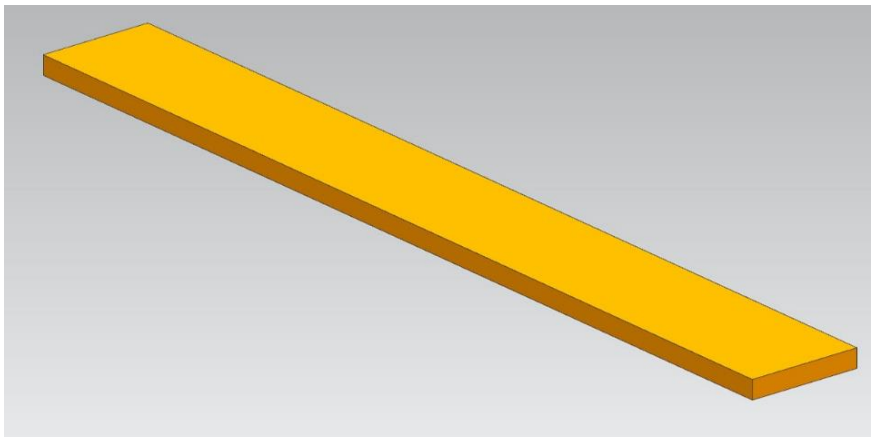

(c) After Process

Figure 3.27. Illustration of First Grinding Process Stages

This grinding process consists of 4 steps. All grinding steps were carried out by grouping the specimens with 6 pieces.

Step 1: The specimens were attached in the rolling direction as shown in Figure 3.28. 0.25 mm of cutting depth was removed from one side of the specimen. The speed of the cutting depth removal is approximately 0.008 mm/min.

Step 2: The other side of the specimens were attached, too, as in step 1, and removed approximately 0.25 mm of cutting depth. This step was completed when the specimen thickness became 2 mm. The speed of the cutting depth removal is approximately 0.008 mm/min.

Step 3: The specimens were linked face to face as oriented in Figure 3.29 and attached to the grinding machine laterally. In this way, 1 mm of cutting depth was removed from the edge of the specimens. The speed of the cutting depth removal is approximately 0.015 mm/min.

Step 4: The other edges of the specimens were grinded, too, as in step 3. 1 mm of cutting depth was removed and this process was continued until the specimen width decreased to 12 mm. The speed of the cutting depth removal is approximately 0.015 mm/min. At the end of this process, the parts became ready for CNC machining as shown in Figure 3.29.

Figure 3.28. Fatigue Specimens during First Grinding Operation

Figure 3.29. Fatigue Specimens after First Grinding Operation

The grinding machine where the process was performed is as shown in Figure 3.30.

Figure 3.30. Grinding Machine

3.6.4. CNC Machining Process

The specimens coming from the first grinding process were placed into the prepared mold as shown in Figure 3.31 and processed on the CNC machine. This CNC machining operation involves drilling the holes on the specimen and milling the profile geometry of the bending region. A tool with a relatively large diameter (Φ 8 mm) was used to make the machining surface in the bending region smoother with relatively small depth of cut per pass (0.05 mm). In addition, a relatively lower tool speed (250 rpm) was applied to ensure that the desired material microstructure on the surface machined would not be disturbed by heating-up. The CNC machining operation process is illustrated as shown in Figure 3.32. The specimens were obtained at the end of the operation as shown in Figure 3.33.

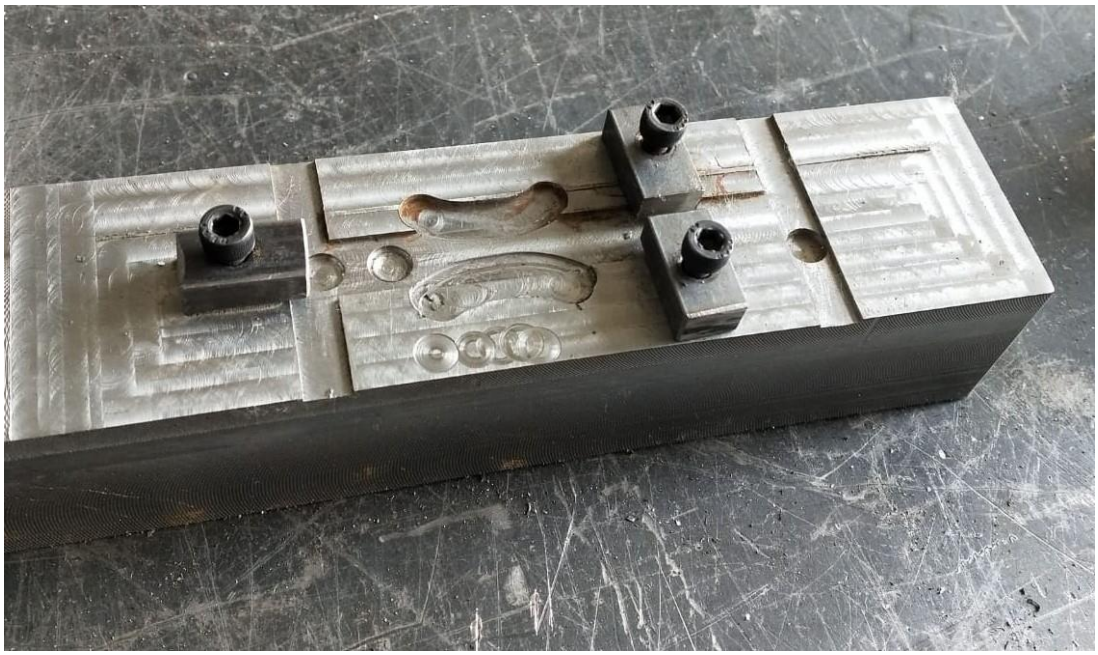

Figure 3.31. The Mold of Fatigue Specimens for CNC Machining Operation

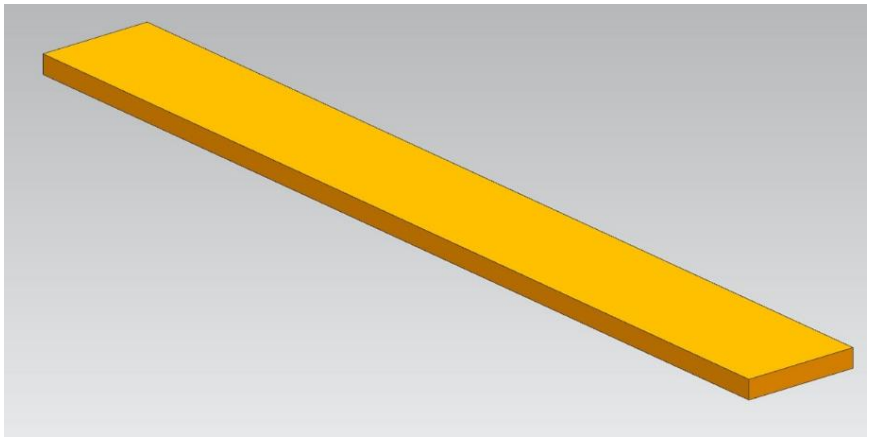

(a) Before Process

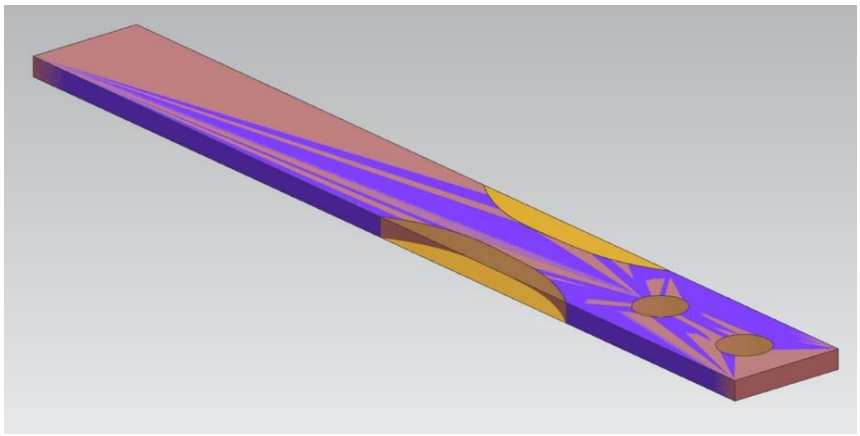

(b) Transition Stage

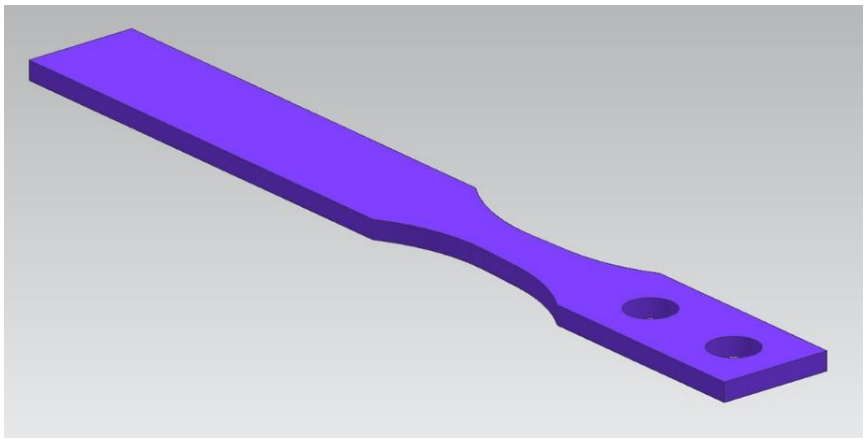

(c) After Process

Figure 3.32. Illustration of CNC Machining Process

Figure 3.33. Fatigue Specimens after CNC Machining Operation

The CNC machine where the process was performed is as shown in Figure 3.34.

Figure 3.34. CNC Machine

3.6.5. Finish Grinding Process

Finish grinding operation was performed to remove burrs remained from CNC machining and bring the parts to their final thickness. As a result, the wall thickness of the parts was reduced from 2 mm to 1 mm as illustrated in Figure 3.35. Since the microstructure is important on the part surface, it is supposed to be that the part surface is not heated up. For this reason, grinding operations were performed relatively slower than a normal grinding process and using water as coolant. The speed of the grinding wheel is 1850 rpm, and its diameter is about 500 mm. This grinding process consists of 4 steps. All grinding steps were carried out by grouping the specimens with 6 pieces.

Step 1: The specimens were attached in the rolling direction as in the first grinding operation. 0.25 mm of cutting depth was removed from one side of the specimen. The speed of the cutting depth removal is approximately 0.005 mm/min.

Step 2: The other side of the specimens were attached as in step 1 and removed approximately 0.25 mm of cutting depth. This step was completed when the specimen thickness became 1.5 mm. The speed of the cutting depth removal is approximately 0.005 mm/min.

Step 3: The specimens were turned onto to other face and attached as in step 1 and the 0.25 mm of cutting depth was removed again. Since the specimens are thoroughly thin, there is a high risk of distortion of the specimens due to surface tensions. For this reason, the parts were attached to the machine in 45^{o} oriented manner as shown in Figure 3.36, and the speed of the cutting depth removal was reduced considerably (0.003 mm/min). Reducing the speed of the cutting depth removal is also important in terms of preserving the desired microstructure to keep the surface cold and smooth during grinding process.

Step 4: The other side of the specimens was turned back, and the same procedure was applied as in step 3. This process was continued until the specimen thickness decreased to 1 mm which is its final thickness. At the end of this process, the specimens came to their final conditions as shown in Figure 3.37.

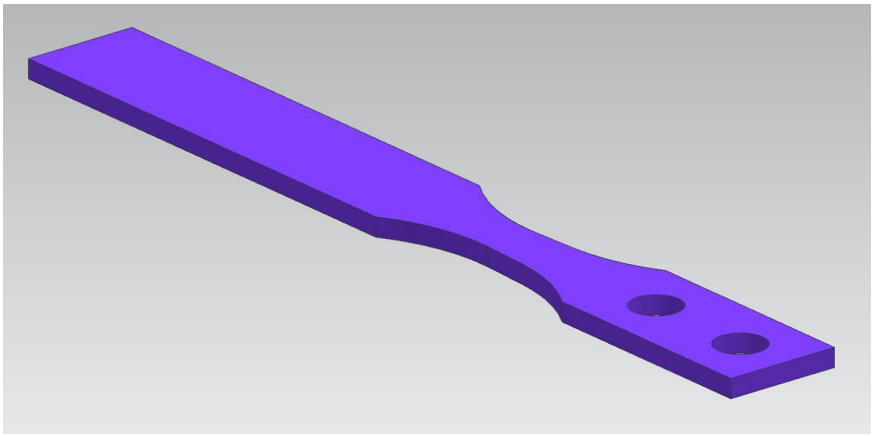

(a) Before Process

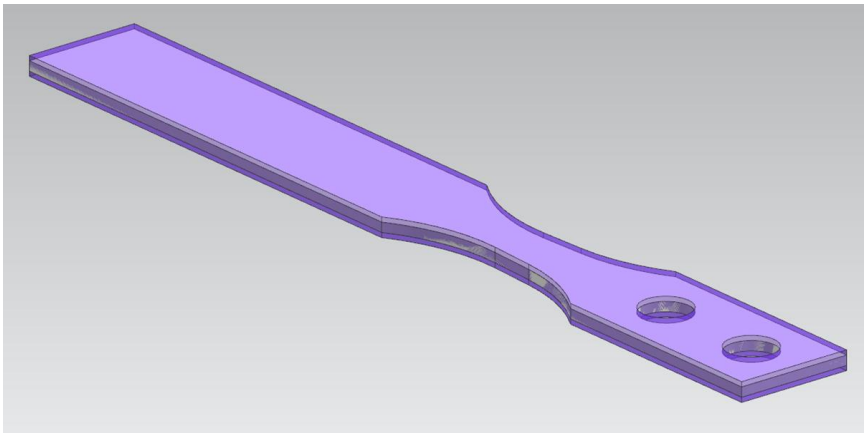

(b) Transition Stage

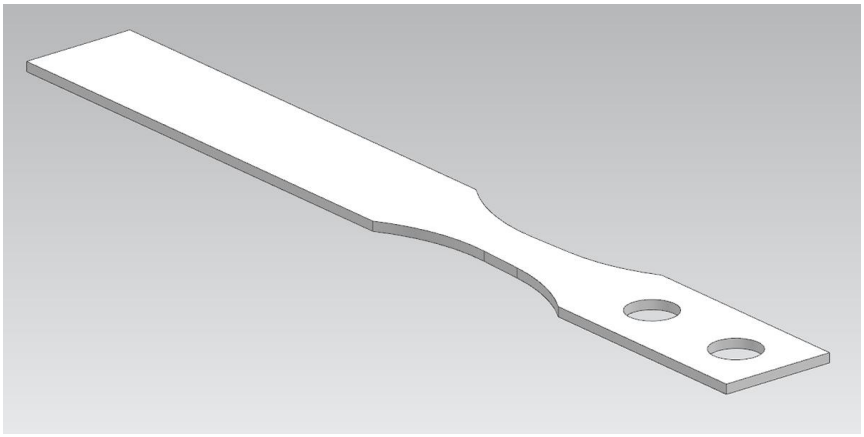

(c) After Process

Figure 3.35. Illustration of Finish Grinding Process

Figure 3.36. Fatigue Specimens during Finish Grinding Operation

Figure 3.37. Finished Fatigue Specimens

The final version of the fatigue specimen which is ready for fatigue testing is as shown in Figure 3.38.

Figure 3.38. Fatigue Specimen

3.7. Dynamometer Tests of Fatigue Specimen

Dynamometer measurement was performed to calculate how much maximum bending stress occurs on the fatigue specimens according to varying displacement. The dynamometer is a test system that measures how much bending force corresponds to how much displacement value at which the specimen is pushed. These displacement and force values are transmitted to the computer via sensors on the pushing pin, and data is generated. The bending force values are substituted into the simple beam equation to calculate how much maximum bending stress value is created at varying displacement values. In this way, the actual force values on the specimen and the maximum bending stress values were calculated analytically. Since the measurements were made as quasi-static (10 mm/min), they could be directly compared with numerical stress analyses. The dynamometer test and the settlement of the dynamometer test system are as shown in Figure 3.39 and Figure 3.40, respectively.

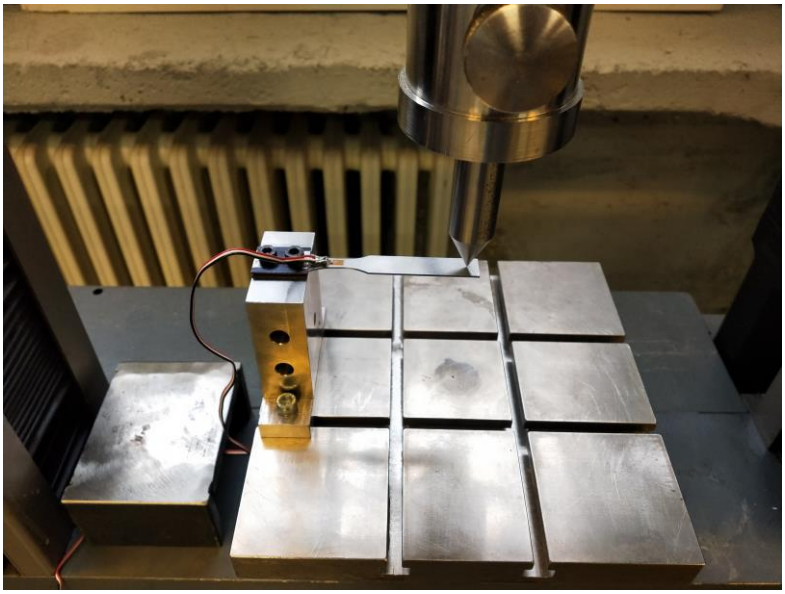

Figure 3.39. Dynamometer Test of Fatigue Specimen

Figure 3.40. Settlement of Dynamometer Test System

3.8. Strain Gauge Tests of Fatigue Specimen

Strain gauge measurements were performed simultaneously with dynamometer measurements. Strain-gauge is a test component that measures how much strain occurs on the bending region of the fatigue specimen according to varying displacement values of which the specimen is pushed. The amount of displacement is read from the dynamometer test system, while strain data coming from the strain gauge are read simultaneously from the strain indicator instrument. Stress data in the bending region are calculated by multiplying the strain data by Young's modulus of the specimen. In this way, it was experimentally calculated how much displacement value created how much maximum bending stress in the bending region of the specimen. Since these measurements were made as quasi-static (10 mm/min), they could be directly compared with numerical and analytical stress analyses. Settlement of strain gauge on the specimen and the device where the strain data were read are as shown in Figure 3.41 and Figure 3.42, respectively.

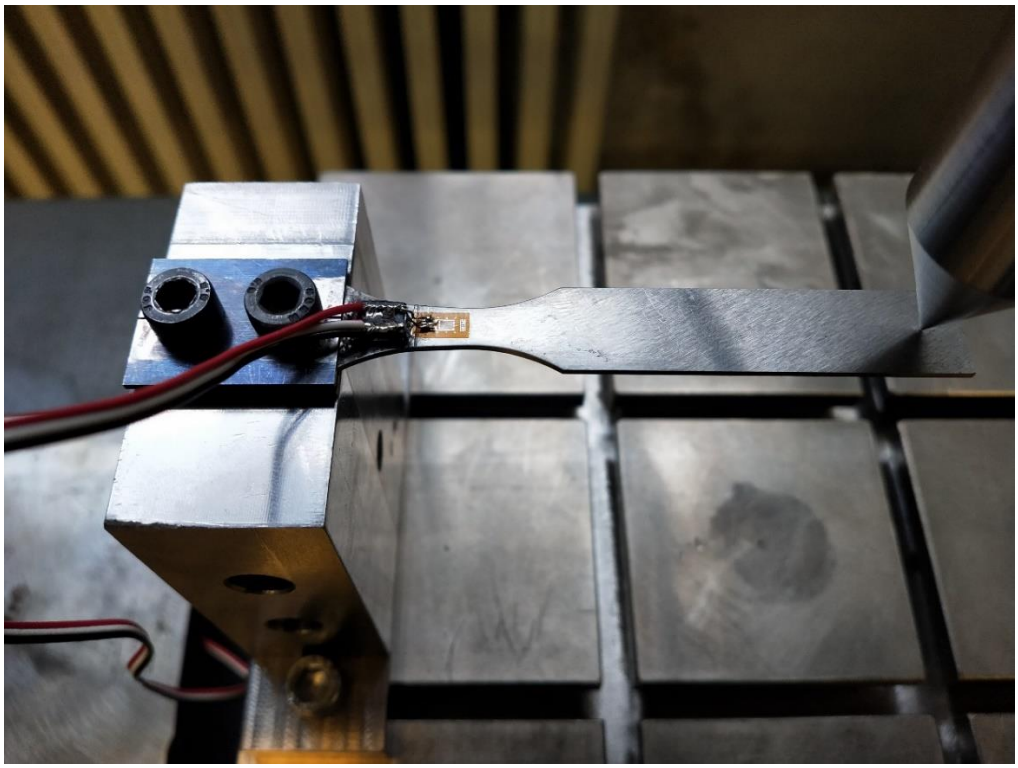

Figure 3.41. Settlement of the Strain Gauge on Fatigue Specimen

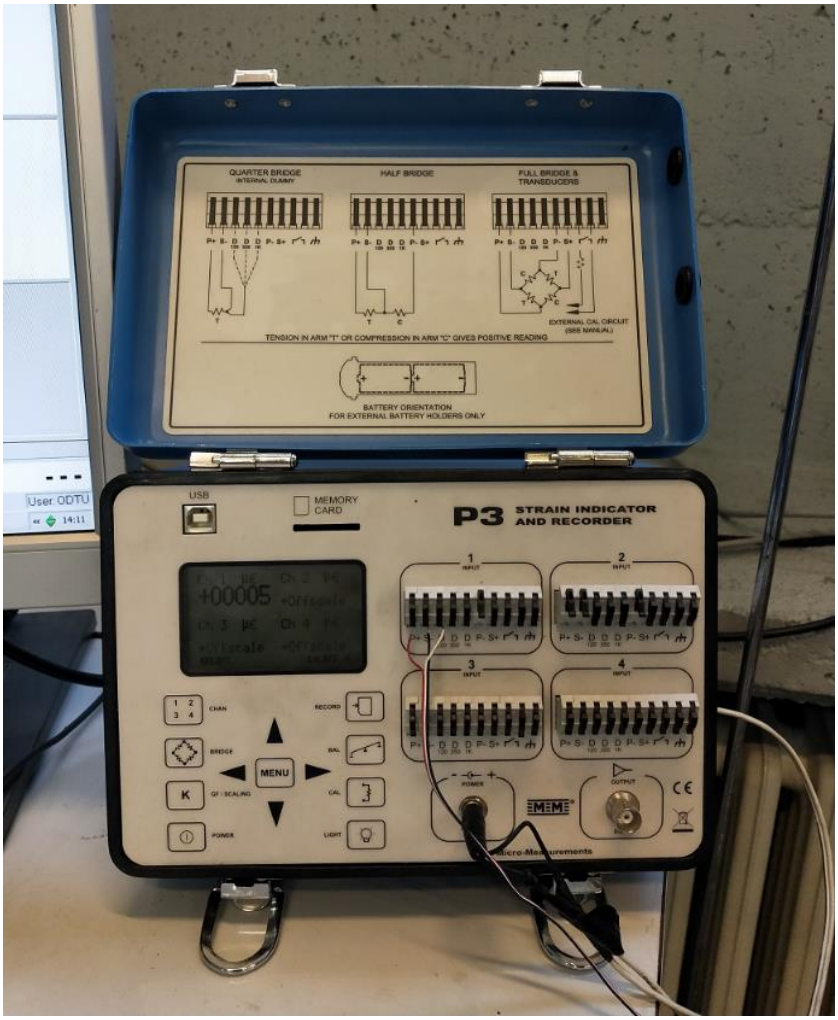

Figure 3.42. Strain Indicator

3.9. Fatigue Tests

Fatigue specimens were tested according to the specified maximum bending stress values. In other words, the fracture times of the specimens were measured at the specified stress values. The fatigue test machine has a displacement range that is able to push the fatigue specimen, and each displacement value corresponds to a stress value desired on the bending region of the fatigue specimen. This displacement value is adjusted before each test in order to reach the desired stress value on the bending region of the fatigue specimen.

To adjust the displacement value, “h distance”, which is the distance between axes of the eccentric shaft and the main shaft of the crank shaft in the mechanism, is adjusted first. “h distance” creates a bending stress, which corresponds to a displacement of 2h, on the fatigue specimen. The fatigue specimen is then fixed to the support as shown in Figure 3.43. This support is attached to the fatigue test machine so that the tip of the pin on the slider touches the fatigue specimen while the slider is at the bottom dead center of cylinder of the mechanism. The orientations, which the fatigue specimen runs on the fatigue test machine with minimum and maximum displacement conditions, are illustrated in Figure 3.44 and Figure 3.45, respectively. In order to eliminate the probability of the pin hitting the fatigue specimen at the bottom dead center, a little initial load was given onto fatigue specimen in each test. The initial load is given by leaning the fatigue specimen to the pin on the slider instead of barely touching to the pin. The initial load corresponds to a displacement of 0.2 mm and is neglected as a stress value.

Figure 3.43. Fixation of Fatigue Specimen to Fatigue Test Machine

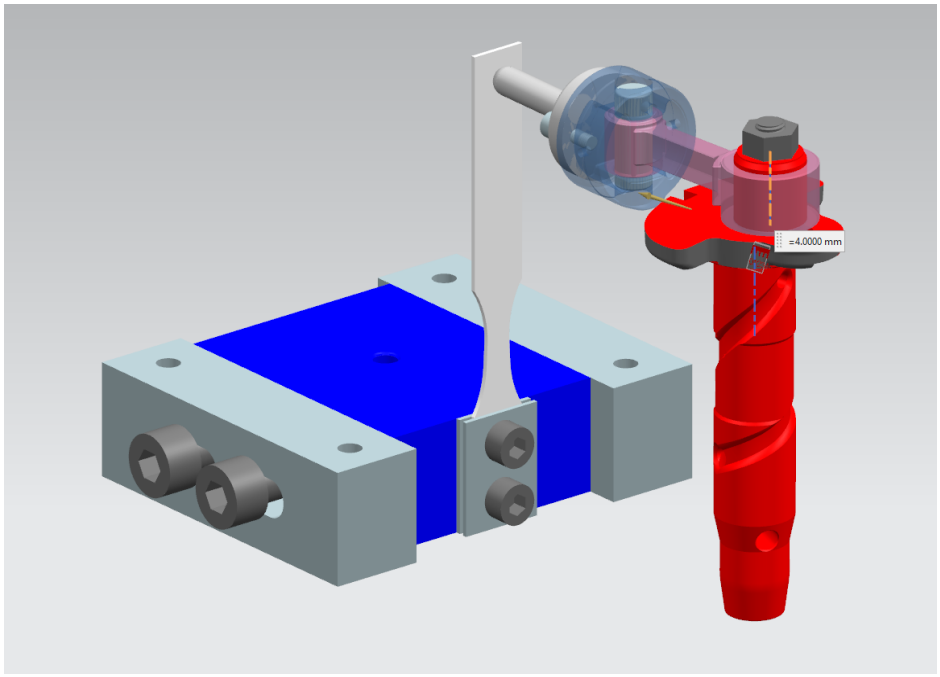

Figure 3.44. Minimum Displacement Orientation of Fatigue Test Machine, which corresponds to h distance of 4 mm on crank shaft & 8 mm Displacement on Fatigue Specimen

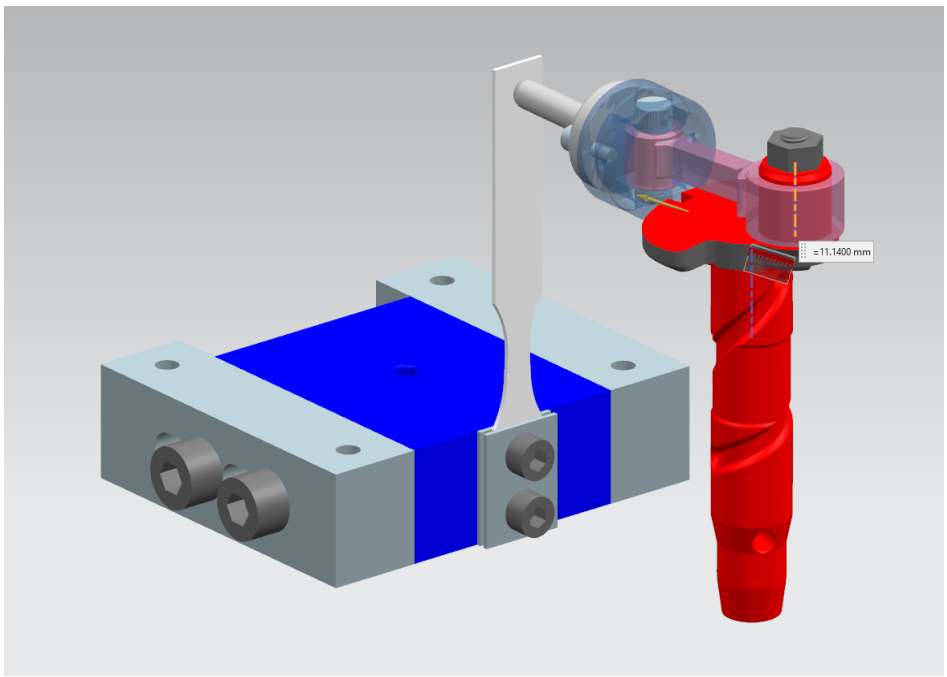

Figure 3.45. Maximum Displacement Orientation of Fatigue Test Machine, which corresponds to h distance of 11 mm on crank shaft & 22 mm Displacement on Fatigue Specimen

The tests were performed at 1000 rpm. The test times according to this operating speed are as indicated in Table 3.2. During the fatigue tests, if the fatigue specimens were not fractured, the tests were ended just after 7 days. When a fracture occured, the fatigue test machine sent a text message to the defined phone number to inform the test ended. Figure 3.46 shows an example text message, which fatigue test machine sent, about the fatigue test has ended.

Table 3.2. *Test Durations with respect to Number of Cycles applied to Fatigue Specimen*

# of Cycle	*Duration of Test*
10^3	1 min
10^4	10 min
10^5	1h 40 min
10^6	16 h 40 min
10^7	7 days

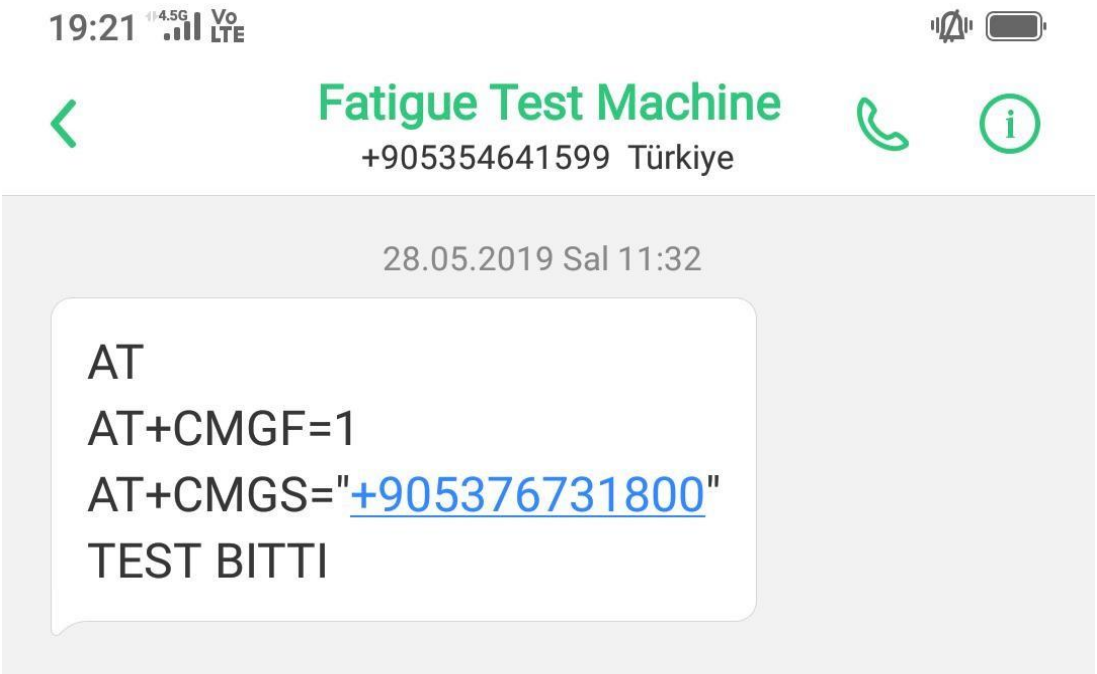

Figure 3.46. An SMS Message Sample which was sent by Fatigue Test Machine to inform the test ended

3.10. Fractography

After the specimens were fractured, the fracture zones were first examined visually, and macro observations were photographed. Then the presence of structures such as striation, tear ridge, cleavage, dimple was examined using Jeol JSM-6400 Scanning Electron Microscope.

CHAPTER 4

EXPERIMENTAL RESULTS

4.1. Heat Treatment and Microstructure

Austenization was carried out in all 60SiMn5 samples at 900 ºC for half an hour. First, lower bainitic structure trial, which was expected to have higher hardness level than tempered martensitic trials, was performed. The sample was kept in salt bath for bainitization process at 250 ºC for 6 hours just after the austenization process. 6 hours bainitation process was preferred, although duration of 3 – 4 hours was expected to be enough, in order to ensure uniform microstructure in whole structure with 100% lower bainite. Thereafter, tempered martensite trials were performed. The samples were quenched in oil just after the austenization process then subjected to tempering at different temperatures for 1.5 hours for each sample until the similar hardness level was obtained with lower bainite sample's. Tempered martensite hardness decreases as the tempering temperature increases. Therefore, the tempering temperature is kept at 550 °C or below. In this study, tempering below 400 ºC has been also tried to obtain equivalent hardness value of tempered martensitic sample to hardness of lower bainitic sample. However, it was nothing short of detecting equivalent hardness value of tempered martensitic samples and lower bainitic sample. Because tempering temperature below 400 ºC is not preferred in tensile and fatigue tests due to that the temper embrittlement problem is expected. All heat treatment parameters which yield one type of carbide-free lower bainitic structure and five types of tempered martensitic structure are shown in Table 4.1.

Table 4.1. *Heat Treatment Parameters of the Samples*

	LB-250	*TM-550*	*TM-500*	*TM-450*	*TM-400*	*TM-375*
Austenization	30 mins @ 900 ºC	30 mins @ 900 ºC	30 mins @ 900 ºC	30 mins @ 900 ºC	30 mins @ 900 ºC	30 mins @ 900 ºC
Quenching	-	Oil	Oil	Oil	Oil	Oil
Heat Treatment	6 hours Salt Bath @ 250 ºC	1,5 hours Tempered @ 550 ºC	1,5 hours Tempered @ 500 ºC	1,5 hours Tempered @ 450 ºC	1,5 hours Tempered @ 400 ºC	1,5 hours Tempered @ 375 ºC

As seen in Figure 4.1, the microstructure of LB-250 consists of almost 100% lower bainitic structure with uniform microstructure as expected. LB-250 is expected to become carbide-free lower bainitic structure due to its silicon content and heat treatment parameters applied. That is, it is expected that retained austenite films with silicon content, which provide strength to the structure, yielded between bainite shaves of LB-250. Furthermore, as seen in Figure 4.2, Figure 4.3, Figure 4.4, Figure 4.5 and Figure 4.6, the microstructures of tempered martensitic trials consist of almost 100% tempered martensitic structures with uniform microstructure as expected. Those tempered martensitic trials are expected not to contain any ferrite phase between needle-shaped structures due to heat treatment parameters applied.

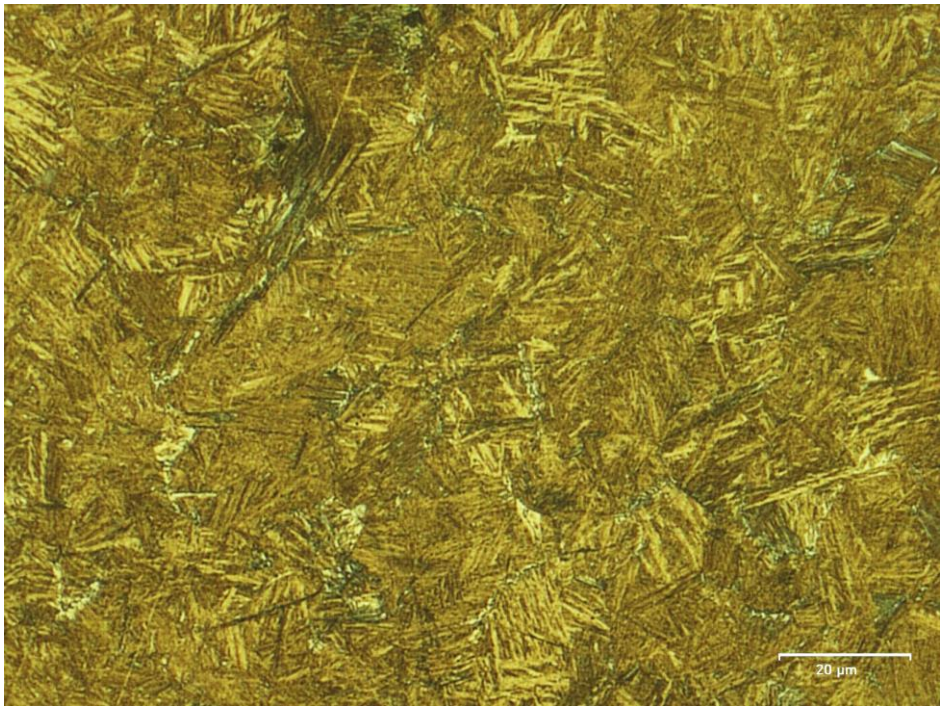

Figure 4.1. Optical Micrograph of LB-250

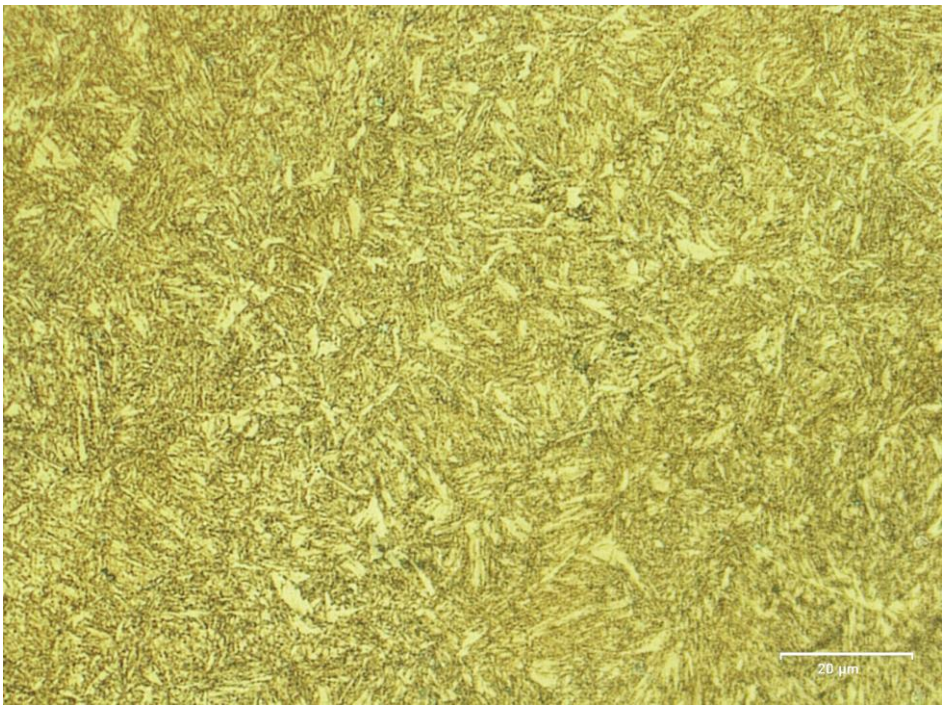

Figure 4.2. Optical Micrograph of TM-550

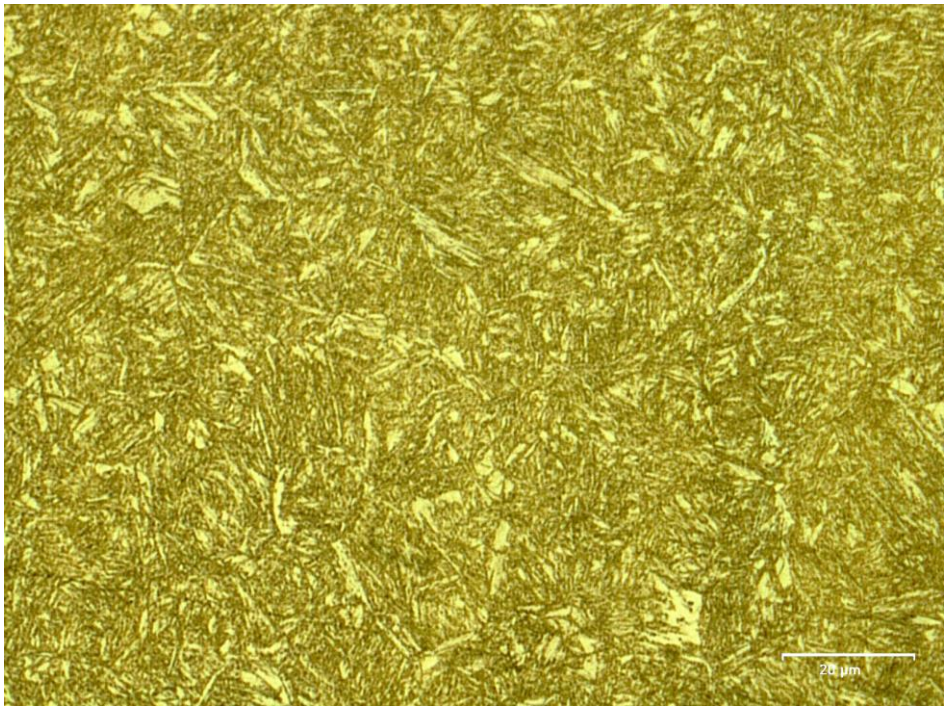

Figure 4.3. Optical Micrograph of TM-500

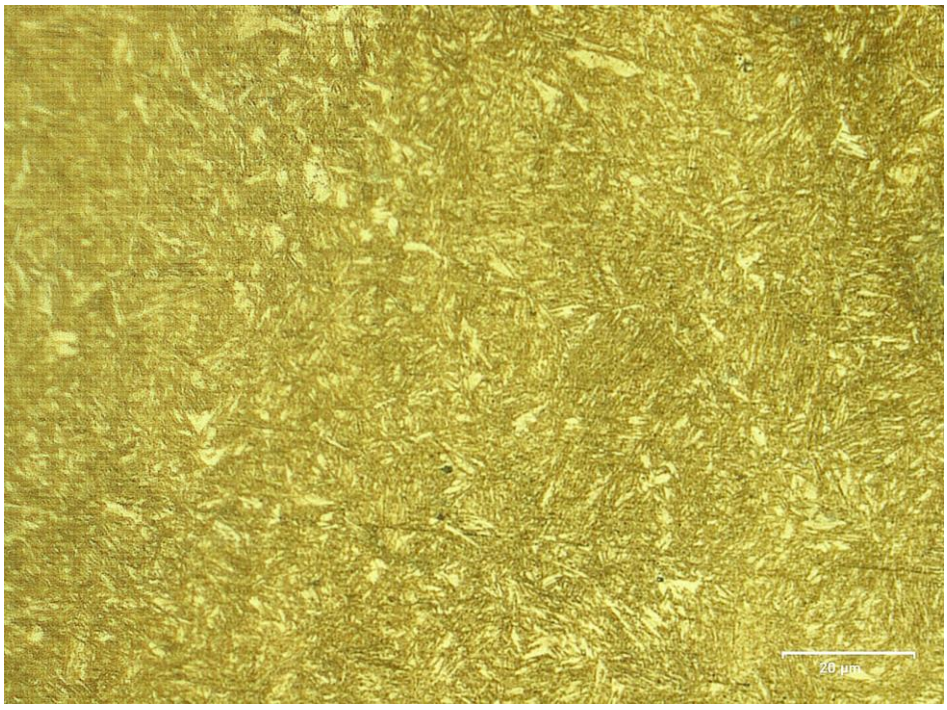

Figure 4.4. Optical Micrograph of TM-450

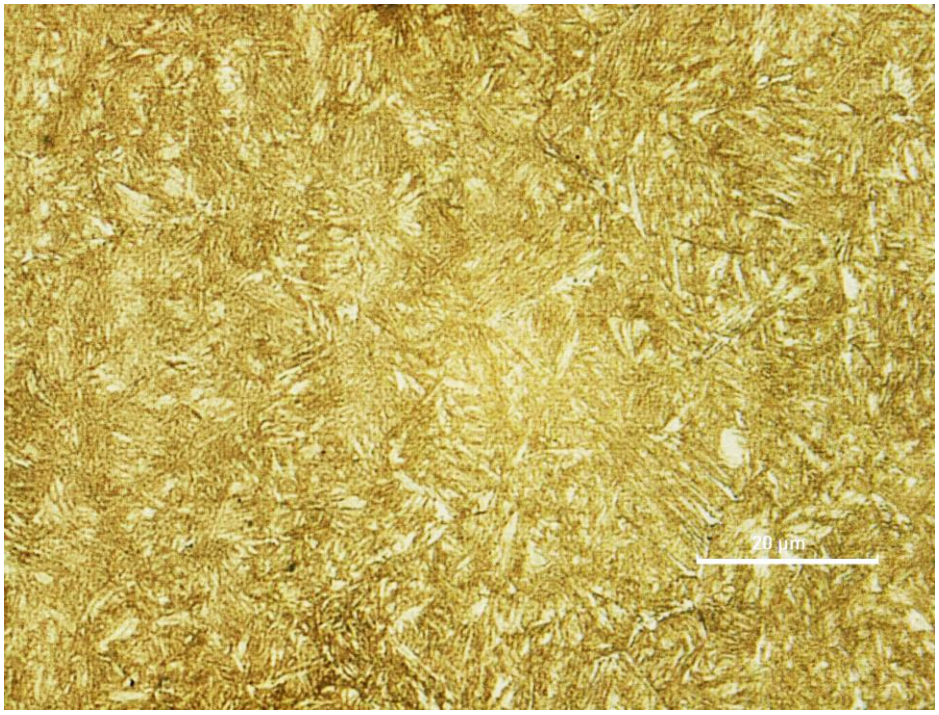

Figure 4.5. Optical Micrograph of TM-400

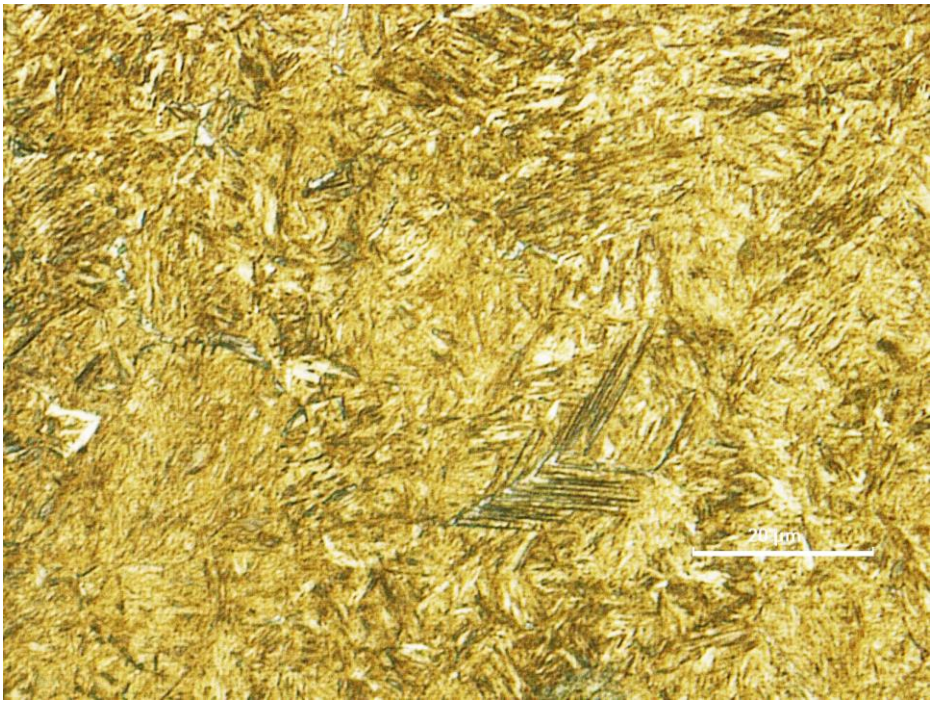

Figure 4.6. Optical Micrograph of TM-375

4.2. Mechanical Tests

4.2.1. Hardness Tests

The hardness measurements have been taken from heat-treated samples. Micro hardness measurements were also performed to see the consistency in the microstructures, but macro hardness measurements were taken into consideration to show the mechanical properties of the samples. Table 4.2 and Table 4.3 show the micro and macro hardness measurement results of heat-treated samples, respectively. In addition, the distribution of the data of all micro and macro hardness measurements according to their heat treatment parameters is as shown in Figure 4.7 and Figure 4.8, respectively.

According to the hardness measurements, the hardnesses of LB-250 sample and the tempered martensitic steel tempered at 375 ºC (TM-375) are very similar. However, it was considered that the comparison of LB-250 and TM-400 has been more reasonable in tensile and fatigue tests since temper embrittlement problem could have been faced if TM-375 was used.

Table 4.2. *Micro Hardnesses of the Samples in 1 kgf Vickers Scale*

	LB-250	TM-550	*TM-500*	*TM-450*	*TM-400*	*TM-375*
Min	570	343	364	427	512	573
Max	609	370	390	460	544	597
AVERAGE	584	357	378	445	528	582

Table 4.3. *Macro Hardnesses of the Samples in 30 kgf Vickers Scale*

	LB-250	TM-550	*TM-500*	*TM-450*	*TM-400*	*TM-375*
Min	586	373	400	467	541	607
Max	611	393	429	486	555	616
AVERAGE	600	382	417	478	549	614

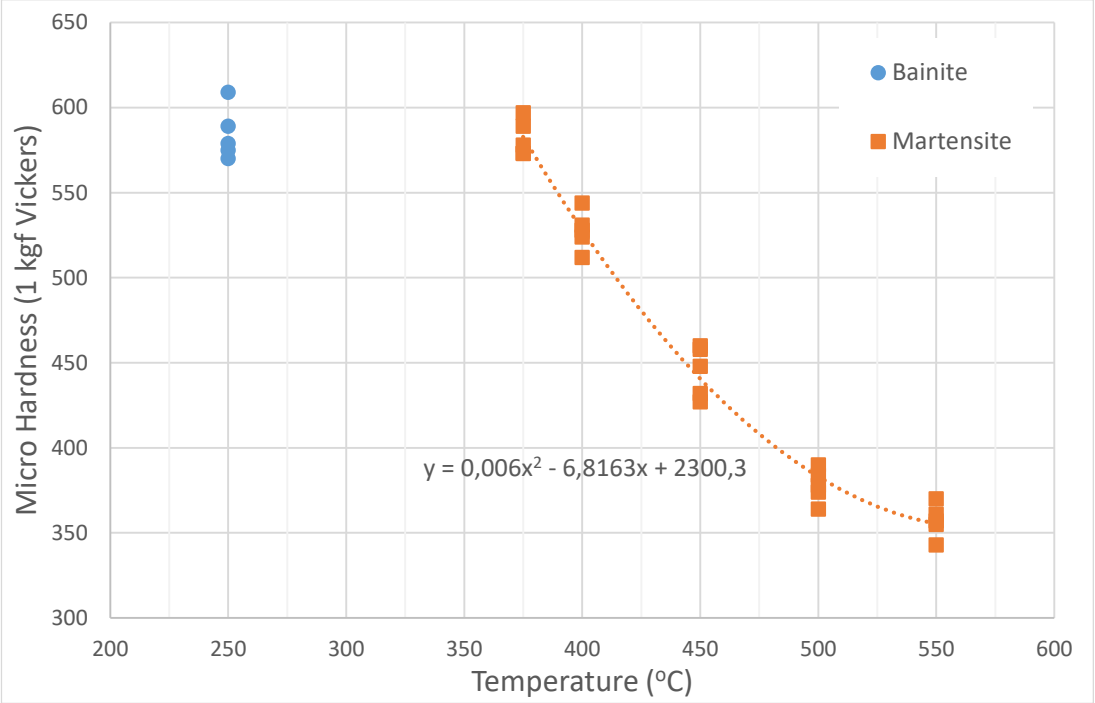

Figure 4.7. Micro Hardnesses of the Samples with respect to Heat Treatment Parameters

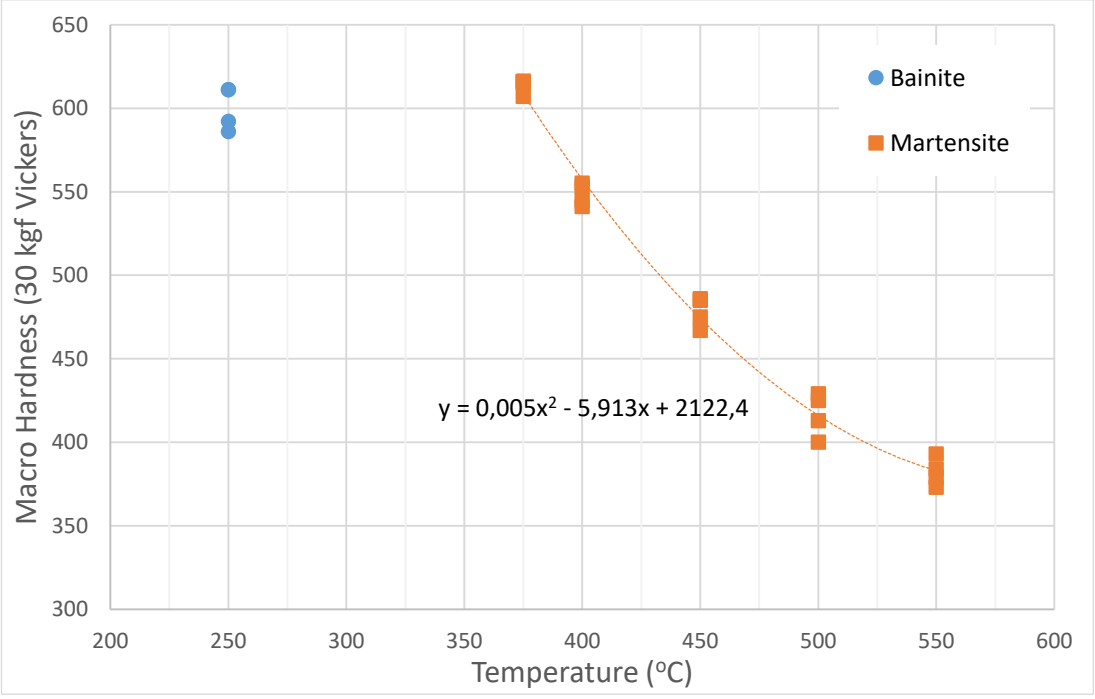

Figure 4.8. Macro Hardnesses of the Samples with respect to Heat Treatment Parameters

4.2.2. Tensile Tests

Two tensile test specimens were used for each of LB-250 and TM-400 samples. The stress-strain curves are shown in Figure 4.9. As expected, modulus of elasticity is the same for each sample; yield strength and ultimate tensile strength values of LB-250 samples were slightly higher than TM-400 samples'. The transition of the curve to the plastic region from elastic region has been sharper in TM-400 samples and smoother in LB-250 samples. While the elongation amounts of TM-400 tensile specimens have been high (4,5% and 4,6%) and more consistent in itself, the elongation amounts of LB-250 tensile specimens have been both high (4,6%) and low (2,8%).

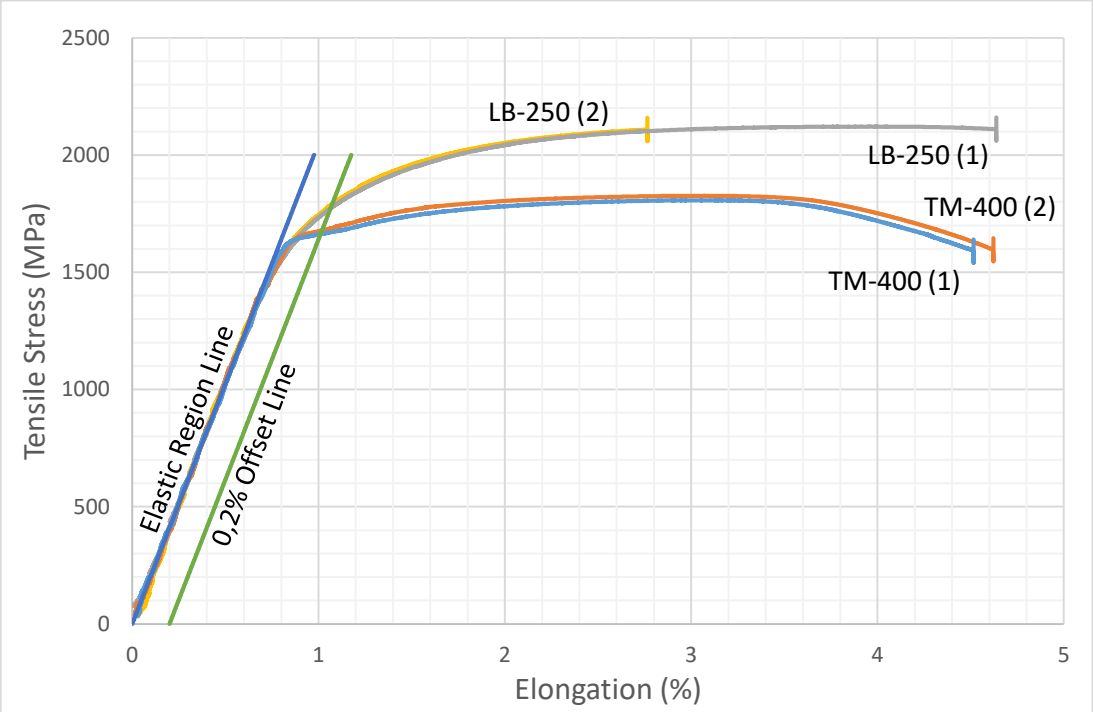

Figure 4.9. Strain versus Stress Curves of LB-250 & TM-400

The results obtained from tensile tests together with the density and poisson's ratio values of the samples have been summarized in Table 4.4. These mechanical properties are essential values for numerical analyses for fatigue specimen design.

Table 4.4. *Mechanical Properties of LB-250 & TM-400*

	σ_y *(MPA)*	*UTS (MPa)*	*E (GPa)*	ε_1 *(%)*	ε_2 *(%)*	$\rho(kg/m^3)^{[38]}$	$v^{[assumed]}$
LB-250	1750	2100	205	4,6	2,8	7850	0,3
TM-400	1650	1800	205	4,5	4,6	7850	0,3

The specimens, which completed the tensile tests are as shown in Figure 4.10 and Figure 4.11. From these inspections, it is seen that TM-400 specimens show more ductile appearance than LB-250 has. TM-400 specimens were broken by necking while LB-250 specimens were broken more abrupt with brittle characteristic.

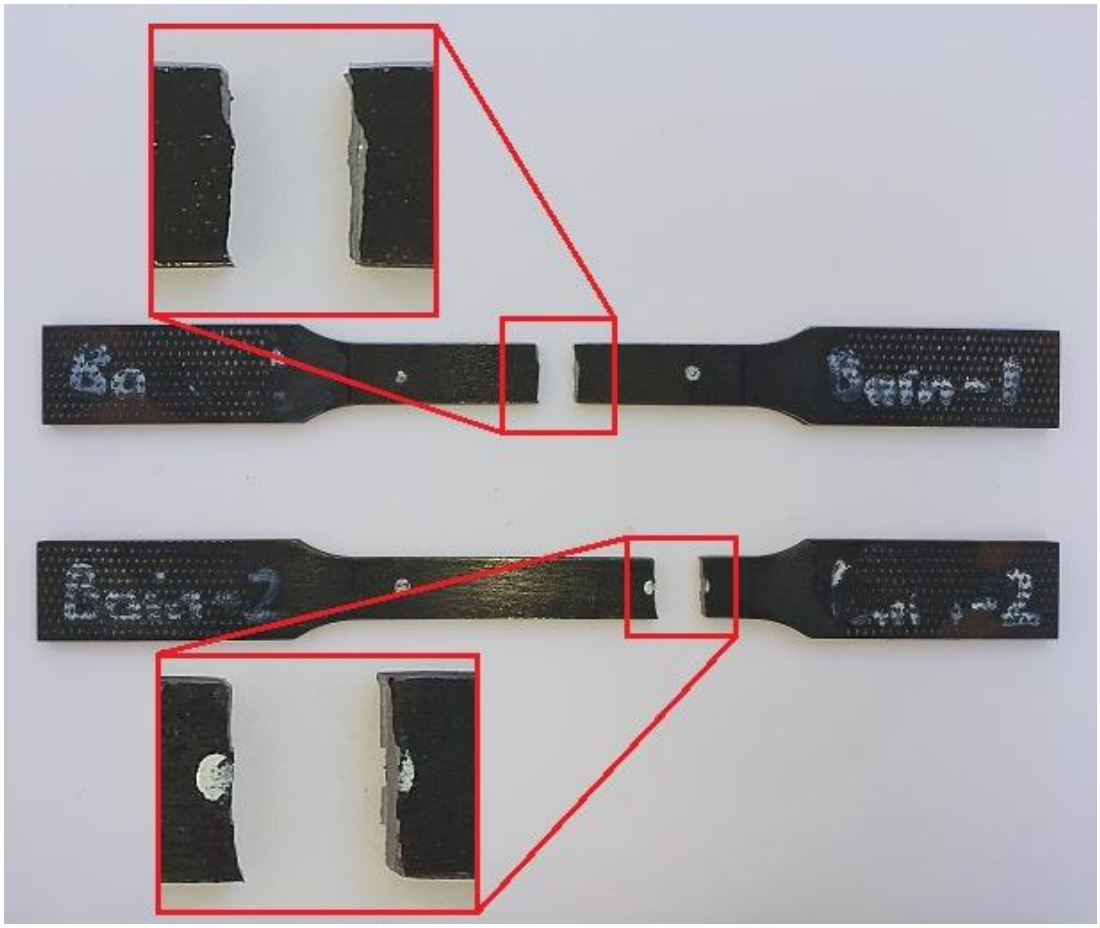

Figure 4.10. Side View of Fractured LB-250 Tensile Test Specimens

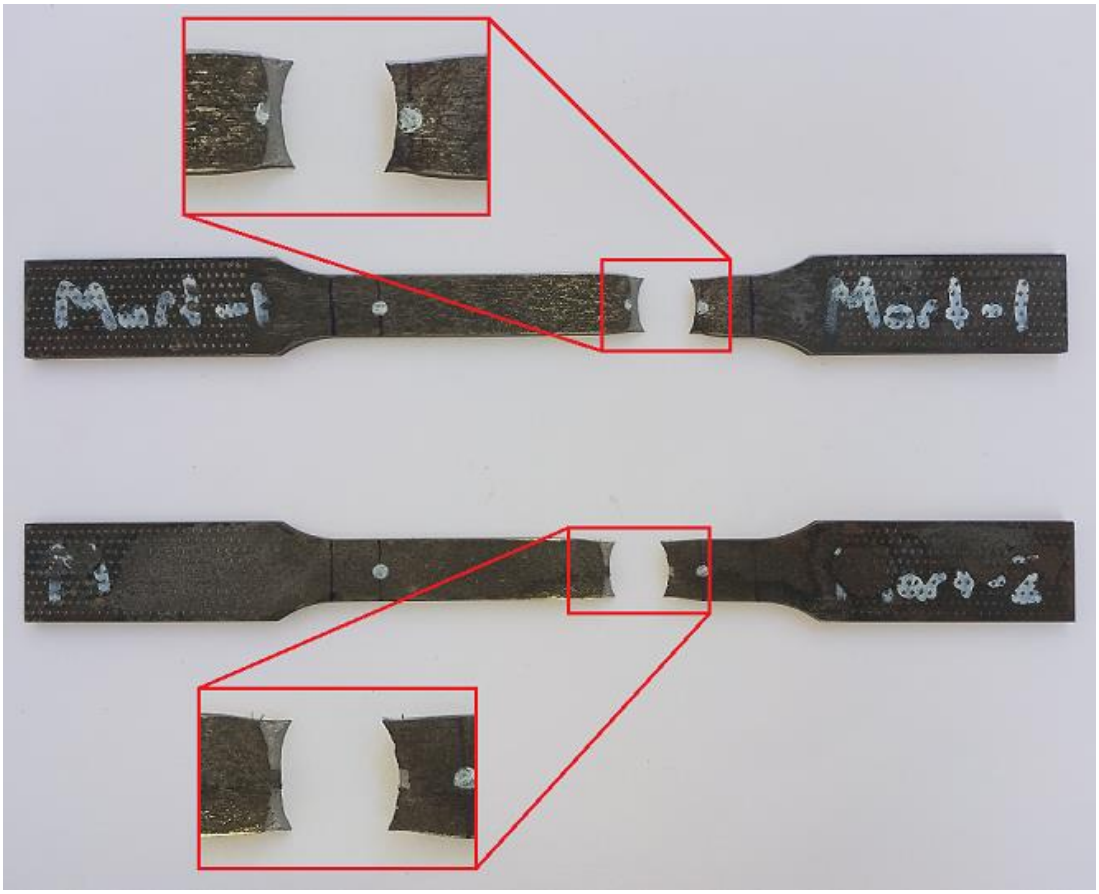

Figure 4.11. Side View of Fractured TM-400 Tensile Test Specimens

The fractured area of LB-400 is smoother and brighter when viewed through the section. From the initiation point of the failure, the tear ridges which spread over the whole cross section are observed. This structure characterizes brittle rupture. When the fractured zone of TM-400 is examined, shear lips are seen at the outer zones and ductile morphology are observed at the centers. These structures characterize ductile rupture. The cross-sectional images of the LB-250 and TM-400 rupture zones are as shown in Figure 4.12 and Figure 4.13, respectively.

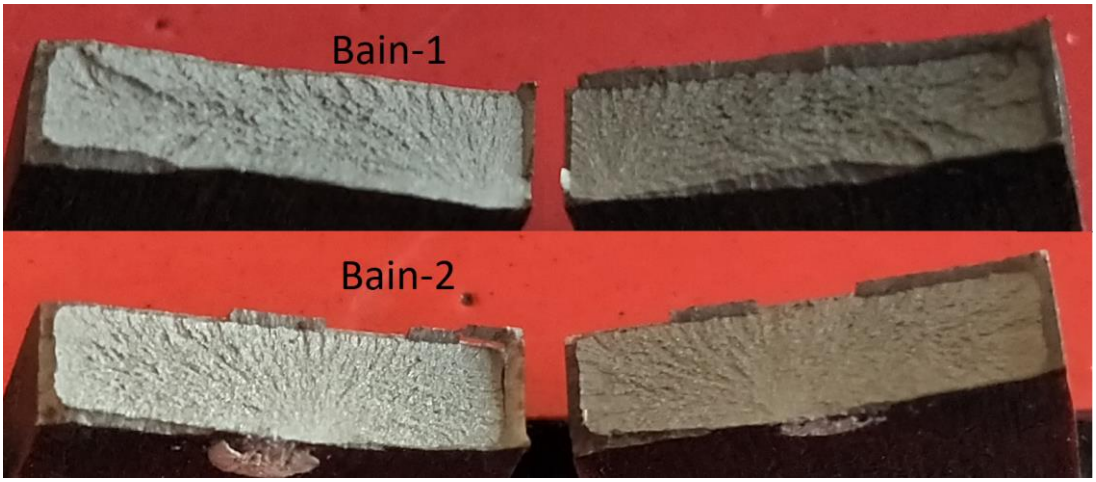

Figure 4.12. Fracture Surfaces of LB-250 Tensile Test Specimens

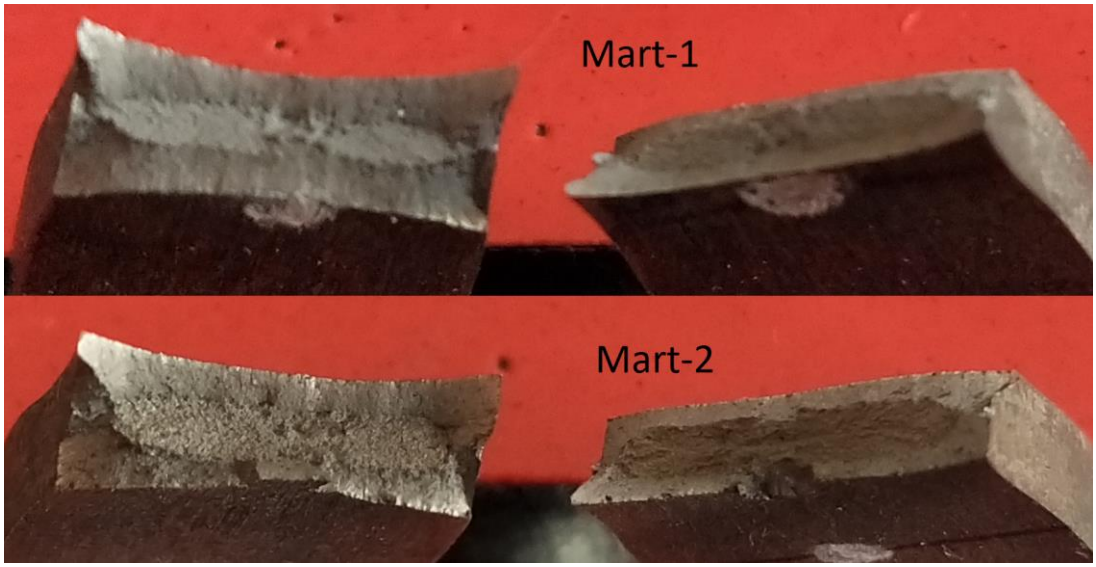

Figure 4.13. Fracture Surfaces of TM-400 Tensile Test Specimens

4.3. Design & CAD Analysis of Fatigue Specimen

4.3.1. Stress Analysis

Using the data in Table 4.4, the fatigue specimen was numerically optimized via structural stress analyses. As a result of the optimization, the stress values expected to

be reached in the bending region of the specimen are as shown in Table 4.5. That is, the maximum displacement (22 mm) of the fatigue test machine is supposed to create a maximum bending stress on the fracture zone of the fatigue specimen about 1500-1600 MPa, and so does the minimum displacement (8 mm) about 500-600 MPa.

The specimen was optimized to allow the specimen to operate within the desired displacement and stress range. The nominal stress value was assumed as the average of elemental stress and nodal stress values obtained from the analyses. Bending forces and maximum bending stresses obtained with respect to the applied displacement range (8 – 22 mm) are shown on the graphs in Figure 4.14 and Figure 4.15, respectively. In addition, the graph values are summarized in Table 4.6 according to maximum and minimum displacement values. According to the values in Table 4.6, it is seen that the criteria specified in Table 4.5 are satisfied at the end of optimization.

Table 4.5. *Optimization Criteria for Numerical Stress Analysis*

Displacement (mm)	*Maximum Bending Stress Range(MPA)*
22	1500-1600
8	500-600

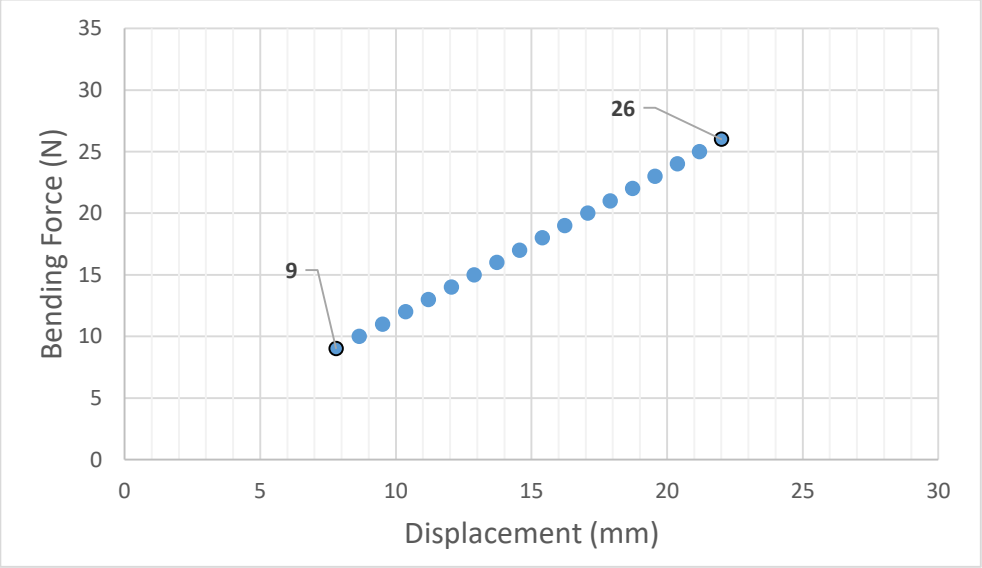

Figure 4.14. Numerical Bending Forces

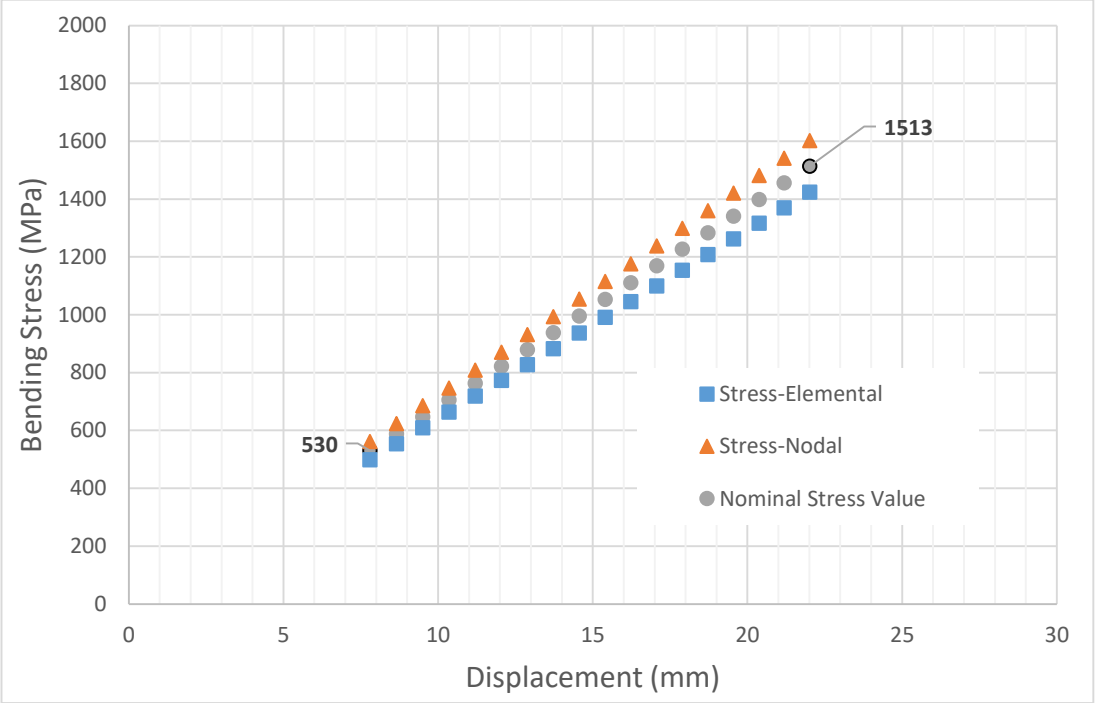

Figure 4.15. Numerical Maximum Bending Stresses

Table 4.6. *Numerical Bending Forces and Maximum Bending Stresses according to Maximum & Minimum Displacements*

Displacement (mm)	*Force (N)*	*Elemental Stress (MPa)*	*Nodal Stress (MPa)*	*Nominal Stress (MPa)*
22	26	1424	1602	1513
8	9	499	561	530

To confirm the assumption that the nominal stress is calculated by averaging elemental stress and nodal stress, the numerical stress analysis (for the maximum displacement of 22 mm) is repeated for the specimen model which is meshed with lower size. As seen in Figure 4.16, the elemental stress value of the specimen meshed with lower size approaches the assumed nominal stress value (1513 MPa).

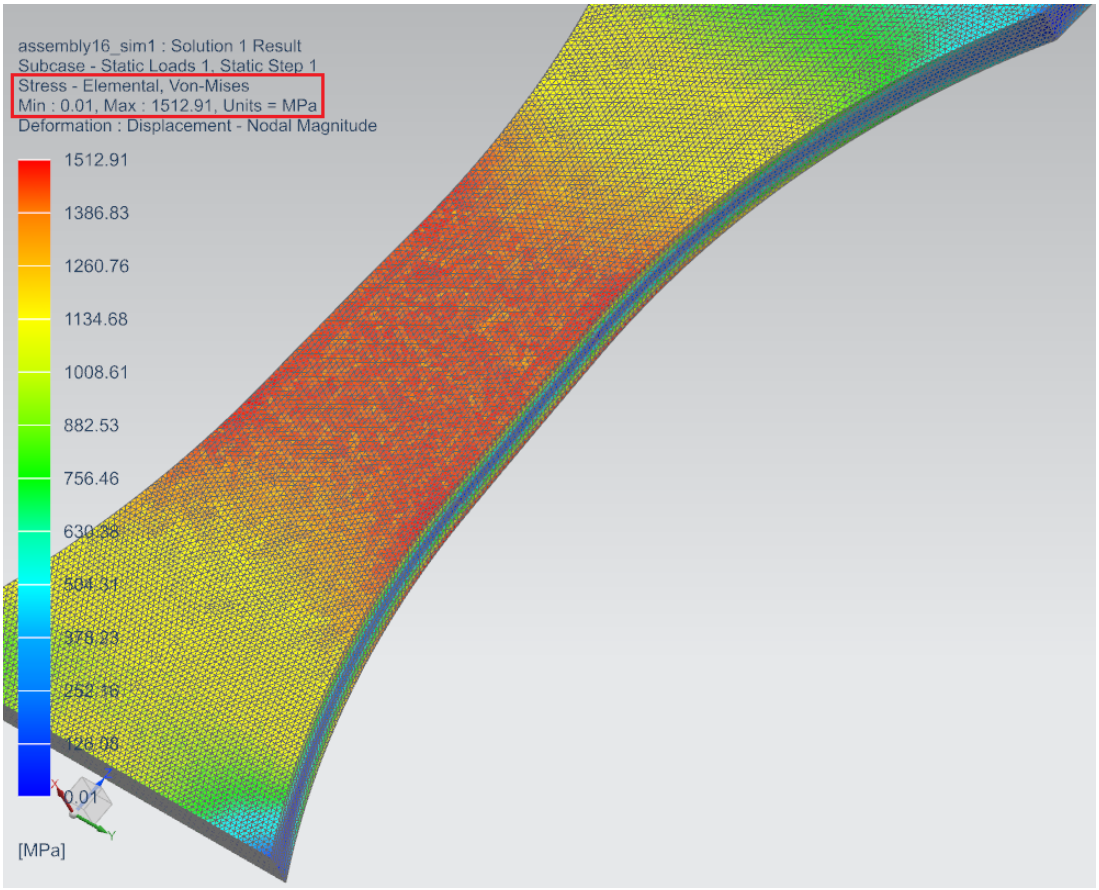

Figure 4.16. Stress Magnitude & Distribution on Bending Region of Fatigue Specimen at Displacement of 22 mm via Elemental Stress Analysis with 0.15 mm Mesh Size

Moreover, the stress distribution on the specimen model at the maximum displacement value (22 mm) is also shown in Figure 4.16. It is seen that the maximum bending stress has been distributed homogenously throughout the bending region of the specimen. This bending region has approximately 30 mm^2 area and connected to the wider regions of the specimen with radii of 20 mm to achieve the desired stress distribution.

In addition, displacement, elemental stress and nodal stress simulation images of the numerical stress analyses of the specimen at the maximum displacement are as shown in Figure 4.17, Figure 4.18 and Figure 4.19, respectively, as examples of stress analyses.

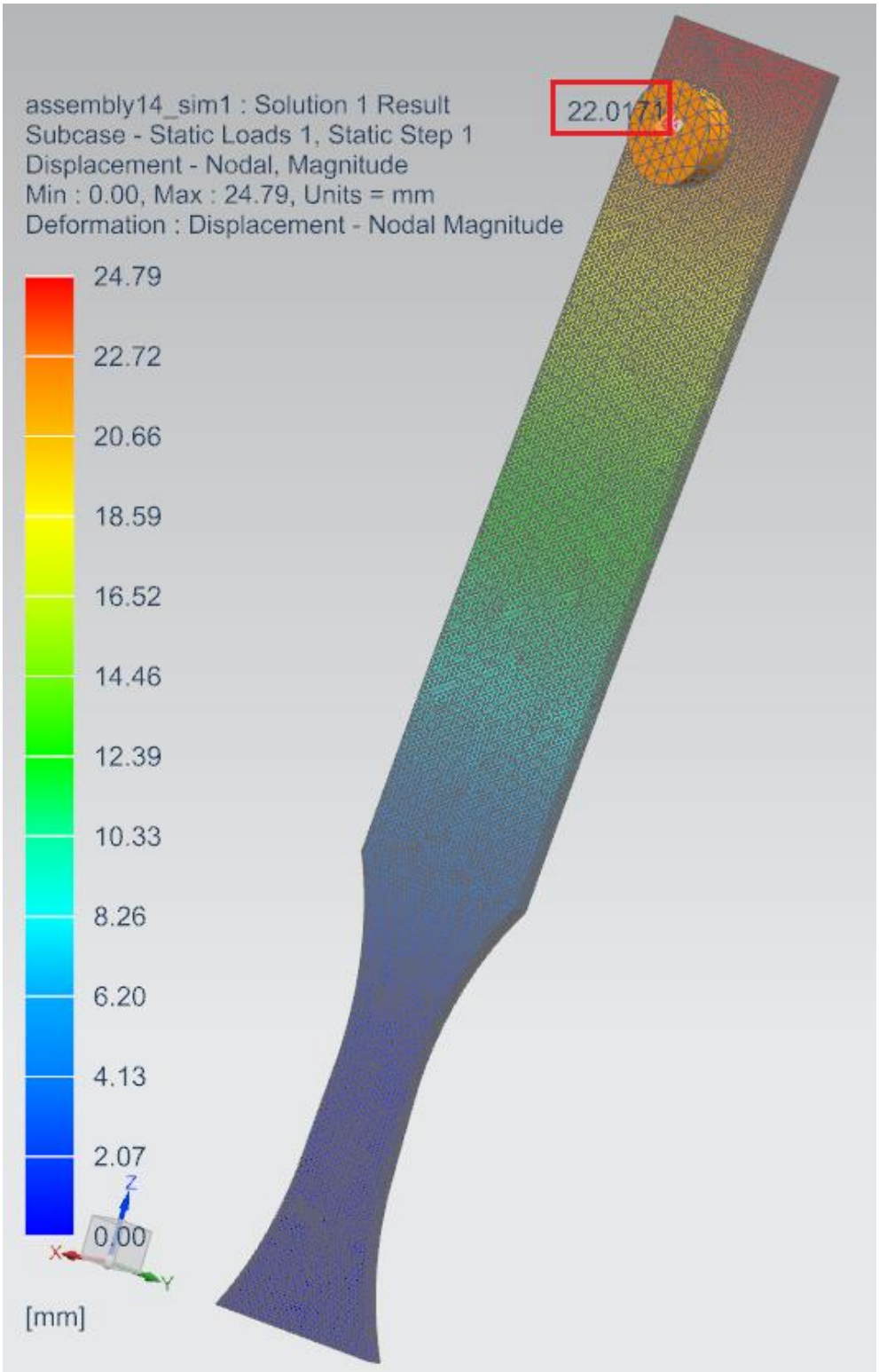

Figure 4.17. Nodal Displacement Analysis of Fatigue Specimen Model with 0.33 mm Mesh Size at Displacement of 22 mm

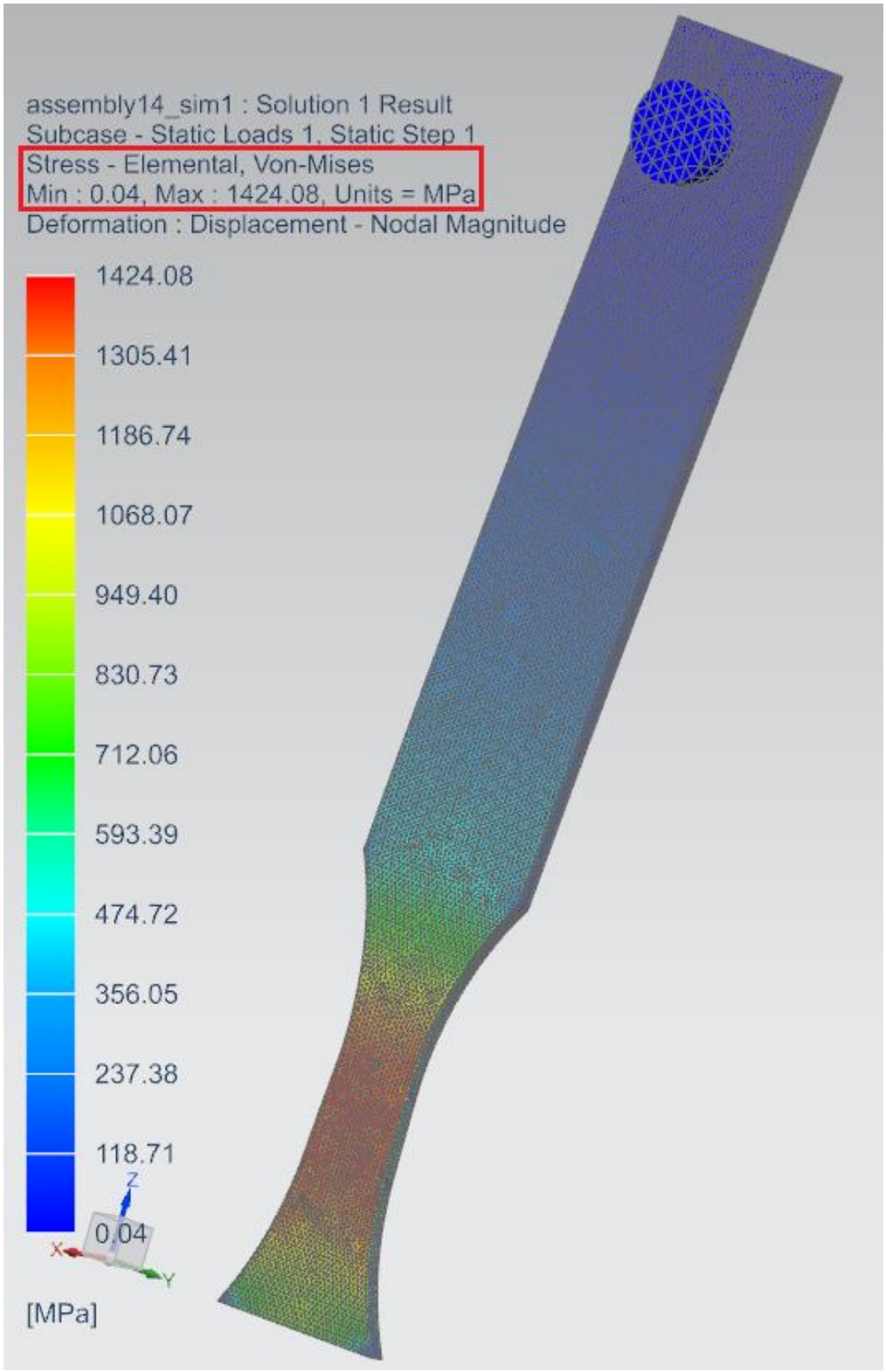

Figure 4.18. Elemental Stress Analysis of Fatigue Specimen Model with 0.33 mm Mesh Size at Displacement of 22 mm

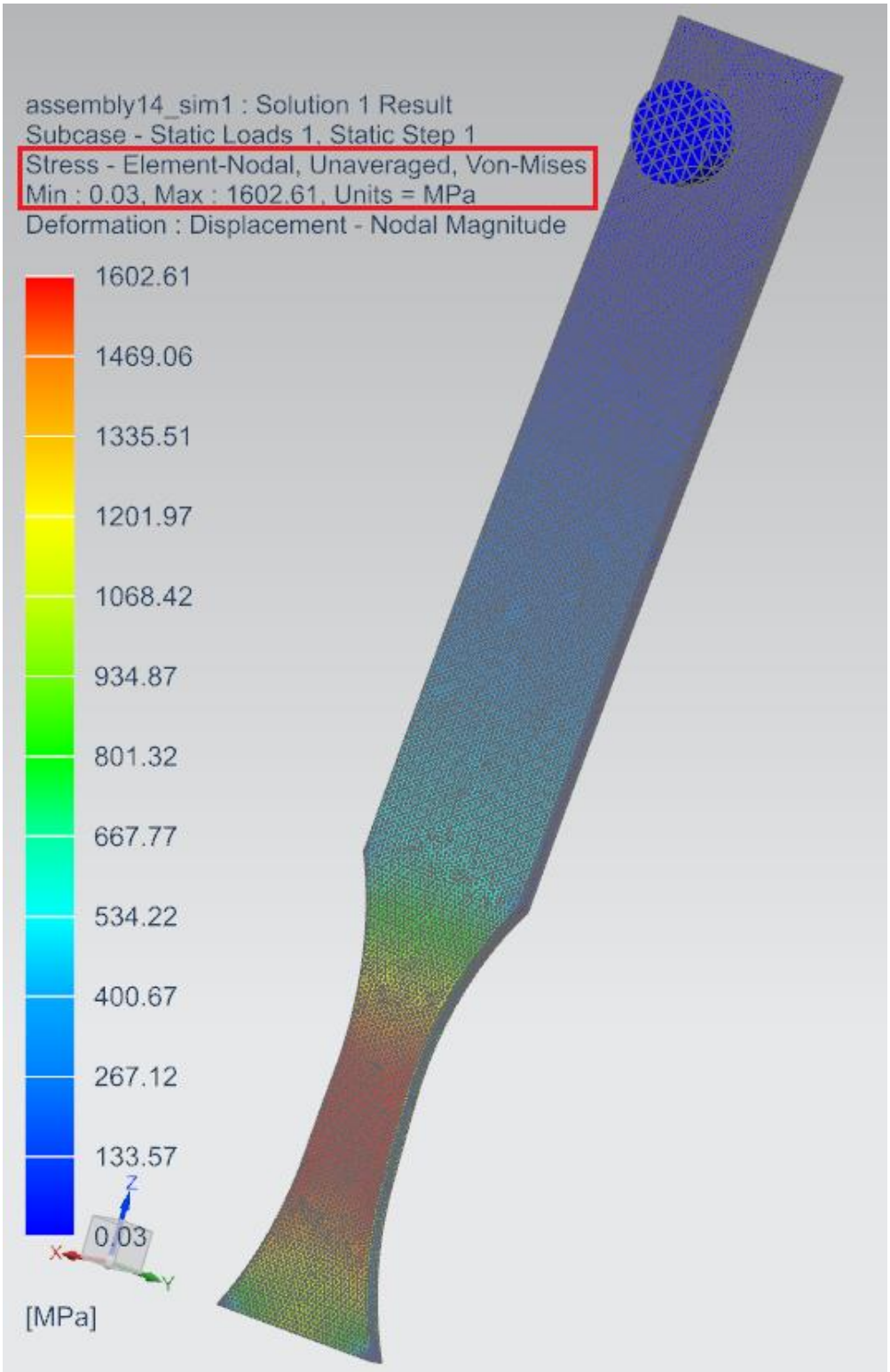

Figure 4.19. Nodal Stress Analysis of Fatigue Specimen Model with 0.33 mm Mesh Size at Displacement of 22 mm

4.3.2. Modal Analysis

As seen from the analysis in Figure 4.20, the 1st mode value, which is compatible with the motion of the fatigue test machine, of the optimized specimen model is 113 Hz. This value is very safe compared to the operating speed of the instrument, 16.7 Hz (1000 rpm), and it has been concluded that the specimen is able to work properly on the fatigue test machine.

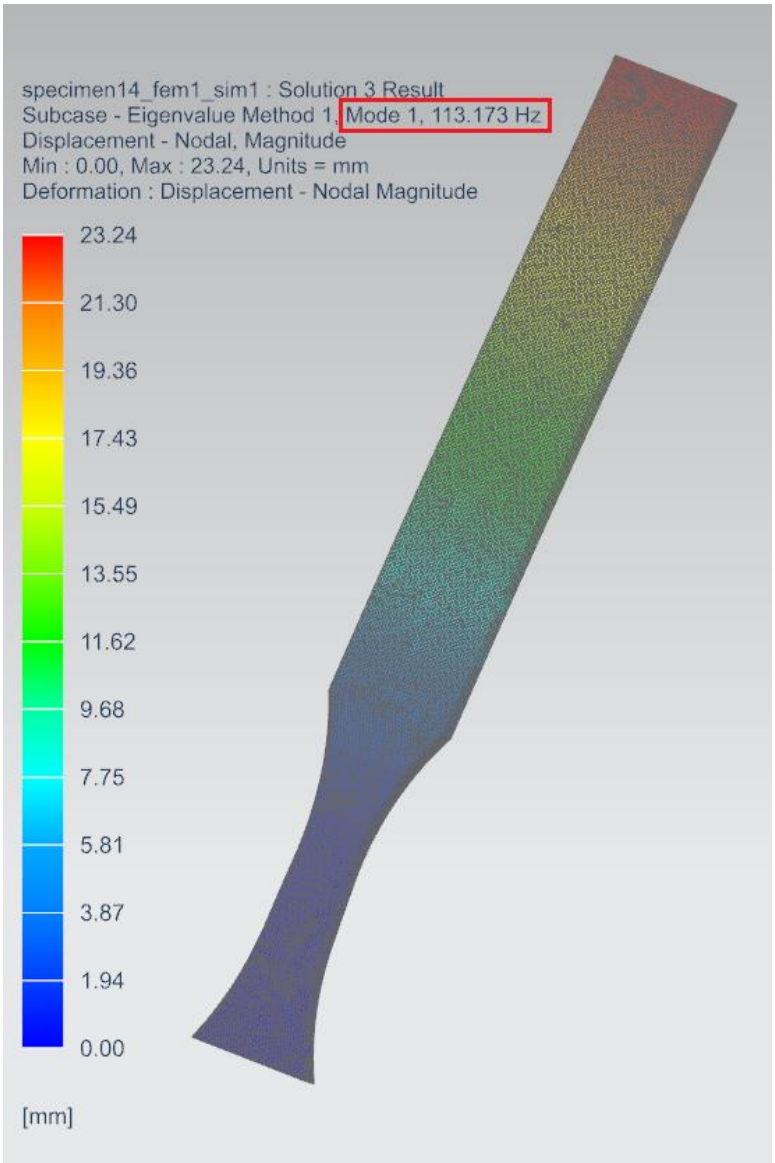

Figure 4.20. Structural Modal Analysis of Fatigue Specimen Model with 0.33 mm Mesh Size at its 1st Mode

4.3.3. Final Dimensions of Fatigue Specimen

As a result of the analyses, the isometric view of the optimized specimen model and technical drawing which shows its dimensions are as shown in Figure 4.21 and Figure 4.22, respectively.

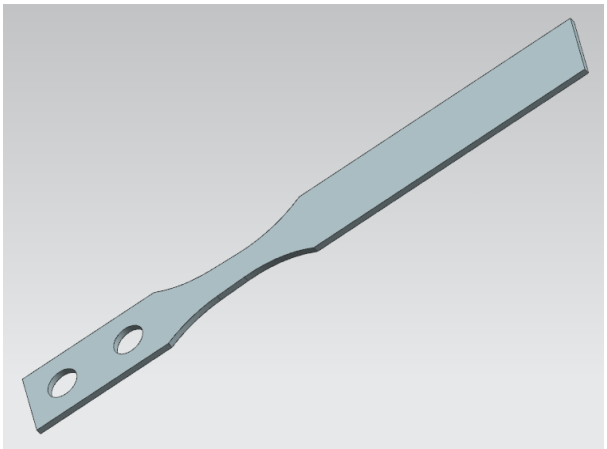

Figure 4.21. Isometric View of Fatigue Specimen Model

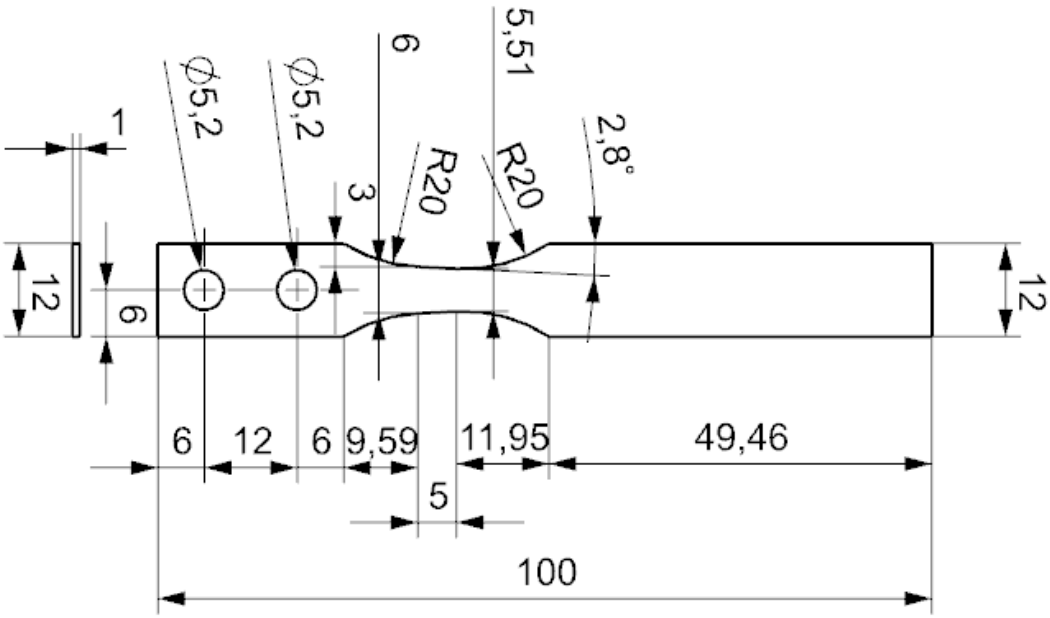

Figure 4.22. Technical Drawing of Fatigue Specimen

4.4. Dynamometer Test Results

Although the force measurement in the displacement range of 8 – 22 mm was sufficient on the fatigue specimen, the force measurement in the displacement range of 0 - 25 mm was taken from the dynamometer. The measurement results are as shown in Figure 4.23. It is seen that the actual measurement data turns into a decreasingly growing trend from linear trend. This is considered as due to the fact that the device pin cannot push on the specimen at exactly 90° as the specimen goes on bending. In order for the simple beam equation to work correctly to calculate the maximum bending stress value, it is assumed that the bending force is applied perpendicular to the specimen as long as the test goes on. Therefore, the force data from the dynamometer has been corrected as if it was always pushing on the sample at an angle of 90°. The corrected force data is also shown in Figure 4.23.

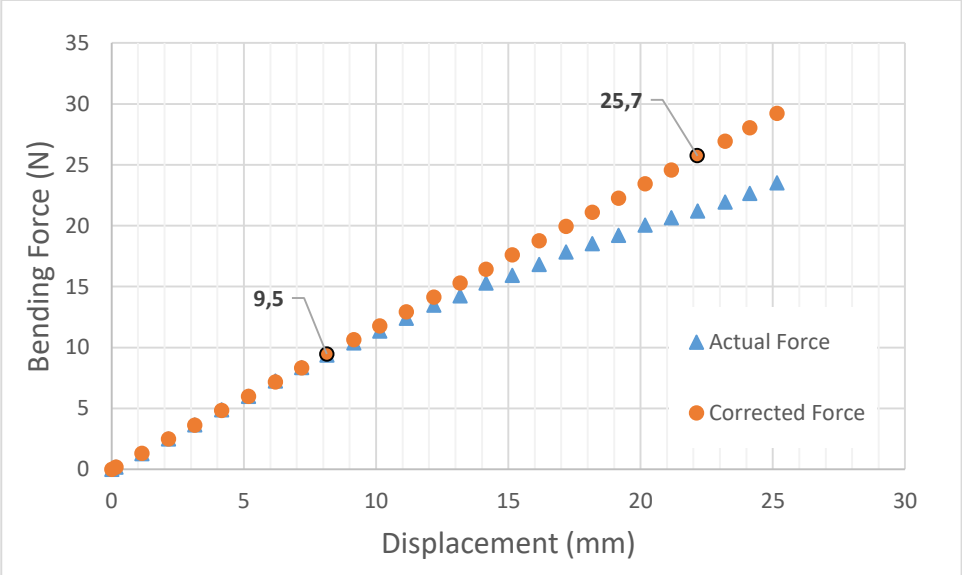

Figure 4.23. Actual and Corrected Bending Forces applied by the Dynamometer

When the corrected force values are substituted into the simple beam equation with the values shown in Figure 4.24, the maximum stress values in the bending region are obtained. Simple beam equation to remind is:

$$\sigma_{max} = \frac{6 \cdot F.L}{w.t^2}$$

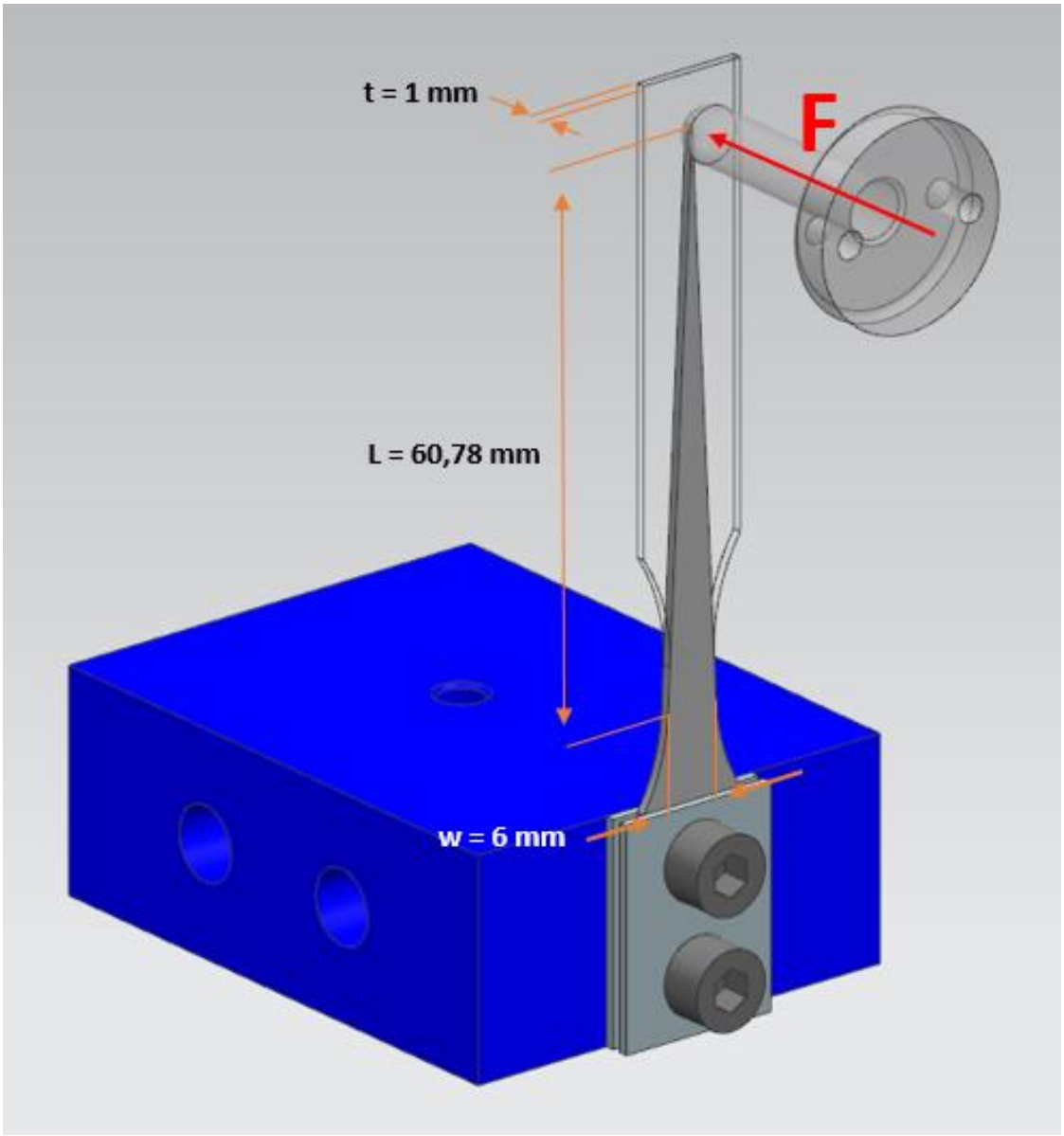

Figure 4.24. Dimensions needed for Simple Beam Equation

The analytical maximum stress values in the bending region according to the varying displacement values are as shown in Figure 4.25.

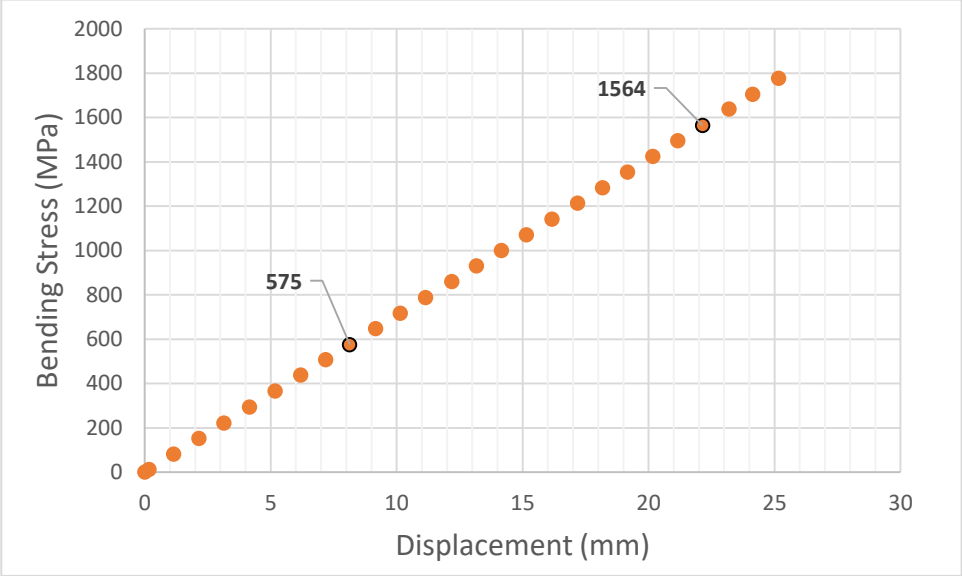

Figure 4.25. Analytical Maximum Bending Stresses

The summary of the results obtained from the dynamometer tests according to the minimum (8 mm) and maximum (22 mm) displacement values of the fatigue test machine is shown in Table 4.7. According to the data in Table 4.7, the criteria specified in Table 4.5 is also satisfied by this analytical approach.

Table 4.7. *Corrected Bending Forces and Analytical Maximum Bending Stresses according to Displacements of 22 & 8 mm*

Displacement (mm)	*Force (N)*	*Maximum Bending Stress (MPa)*
22	25,7	1564
8	9,5	575

4.5. Strain Gauge Test Results

Although strain measurement in the displacement range of 8 – 22 mm was sufficient on the fatigue sample, strain measurements on the displacement range of 0 – 25 mm were taken via the strain gauge. Strain values which were taken from the middle of the bending region according to the displacement values are as shown in Figure 4.26. As expected, strain values are almost aligned linearly on the graph.

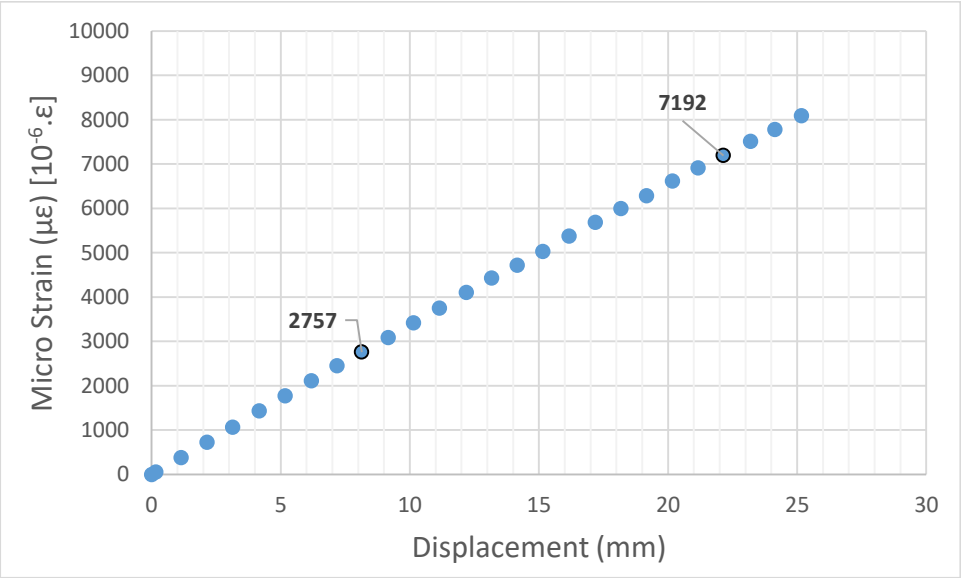

Figure 4.26. Strain Values measured by Strain Gauge

When the strain values are multiplied by 205 GPA Young's Modulus (E) obtained from tensile tests, the stress values in the bending region are able to be obtained experimentally. Stress-strain equation to remind is:

$$\sigma_{max} = \mathrm{E} \cdot \varepsilon$$

By means of the stress-strain equation, the stress values in the bending region according to the varying displacement values are as shown in Figure 4.27.

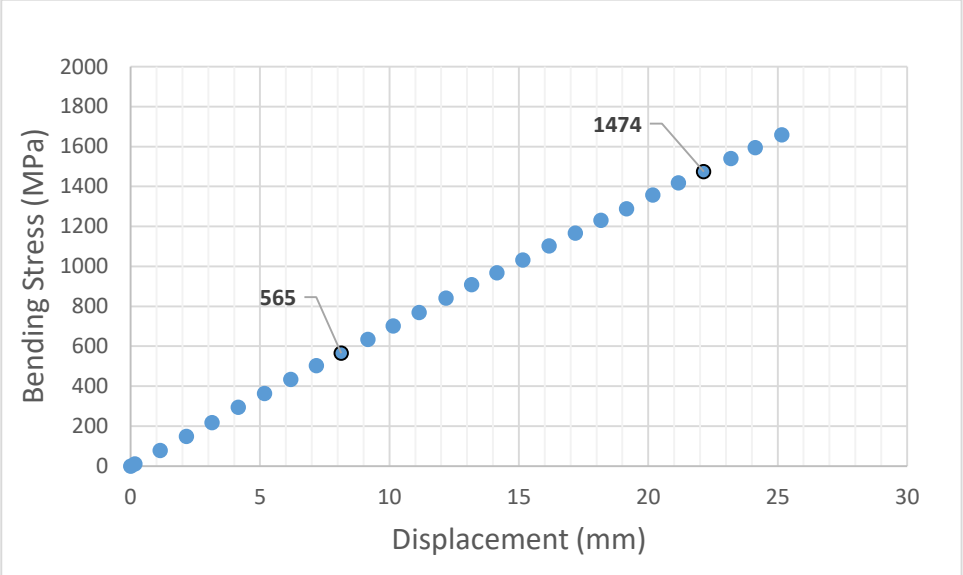

Figure 4.27. Experimental Maximum Bending Stresses

A summary of the results obtained from the strain gauge measurements according to the minimum (8 mm) and maximum (22 mm) displacement values of the fatigue test machine is shown in Table 4.8. According to the data in Table 4.8, the criteria specified in Table 4.5 are almost satisfied by the experimental approach. The experimentally obtained stress data are expected to reflect the stress values on the fatigue specimen in more realistic way. When this experimental stress values obtained are examined in this respect, it is concluded that the fatigue specimen design can work on the fatigue test machine in accordance with the required criteria.

Table 4.8. *Micro Strain Values and Experimental Maximum Bending Stresses according to Displacements of 22 & 8 mm*

Displacement (mm)	*Strain (με)*	*Maximum Bending Stress (MPa)*
22	7192	1474
8	2757	565

4.6. Fatigue Test Results

The samples were subjected to bending fatigue (R = 0) tests at 1000 rpm according to stress amplitude values. The stress amplitude values are half values of maximum bending stress values which are experimentally calculated from strain gauge measurements. In the region where the endurance limit was expected, staircase method was applied to determine the endurance limit exactly. According to the test results, no clear difference was observed between the fatigue life of LB-250 and TM-400 fatigue specimens. The endurance limit value can be assumed as 575 MPa for both fatigue specimen types. In Figure 4.28, fatigue life data of the specimens obtained from the fatigue tests are shown as comparative. Since the S-N curve was located in a higher stress region (550 – 750 MPa) than that the fatigue test machine is able to provide (275 – 775 MPa), the fatigue test machine was just operated in the displacement range of 16.2 – 22.2 mm during the tests unlike the planned (8 – 22 mm) displacement range.

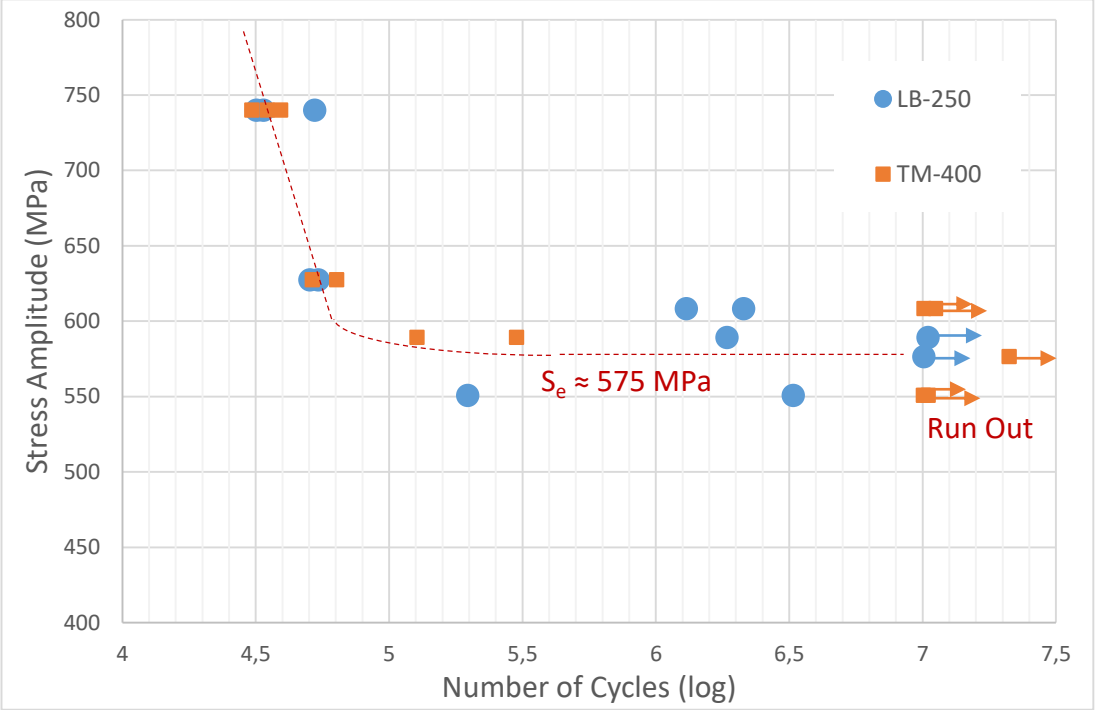

Figure 4.28. S-N Curves of LB-250 & TM-400 Fatigue Specimens

Minitab® 18 program was used to prove that there has been no clear difference between fatigue lives of LB-250 and TM-400 fatigue specimens. According to the variant stress values, fatigue life data of LB-250 and TM-400 fatigue specimens are compared in the analysis of variance table (See Table 4.9) obtained by multiple linear regression method. In the statistical approach, if P-values of fatigue life data of the specimens are greater than 0.05 while the P-value of regression is less than 0.05, this means that there is no clear difference between the fatigue life data. These P-values mentioned are as shown in Table 4.9.

Table 4.9. *Analysis of Variance for Comparison of LB-250 & TM-400 Fatigue Specimens*

Source	*DF*	*Adj SS*	*Adj MS*	*F-Value*	*P-Value*
Regression	2	35820	17910	8,02	0,010
LB-250	1	5170	5170	2,32	0,162
TM-400	1	6290	6290	2,82	0,128
Error	9	20091	2232		
Total	11	55910			

4.7. Fractography

4.7.1. Visual Inspection

During fatigue tests, it was observed that LB-250 specimens have been broken suddenly, and TM-400 specimens have been broken by starting hitting to the pin of the fatigue test machine just a few seconds before breaking. This can be an evidence that the fracture characteristic is brittle in LB-250 specimens and ductile in TM-400 specimens after the fatigue crack has been propagated. These were found to be related to fact that, when the fracture geometries in Figure 4.29 and Figure 4.30 are examined, it is seen that the fracture surface is flat in a LB-250 specimen in accordance with the brittle character, and the fracture surface is serrated after a certain flatness in a TM-400 specimen in accordance with the ductile character. The same can also be seen from the examination of the cross-sectional area of the fractured specimens in Figure 4.31 and Figure 4.32.

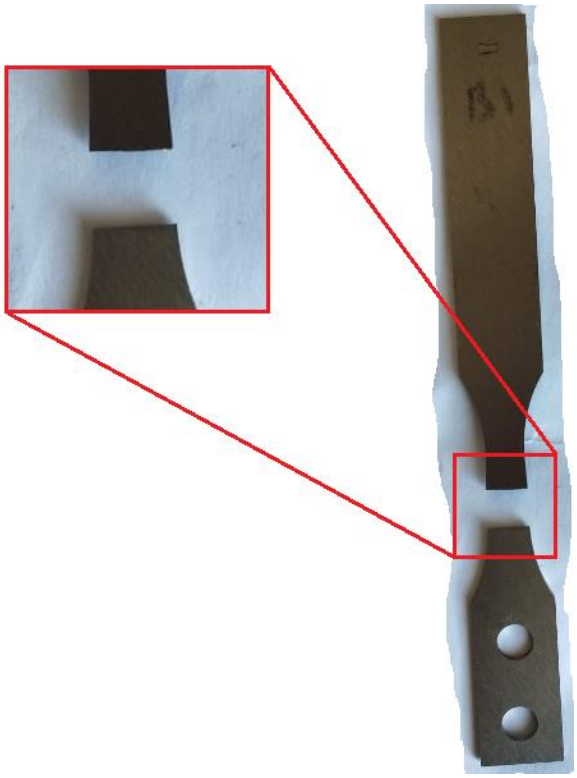

Figure 4.29. Front View of Fracture Geometry of a LB-250 Fatigue Specimen

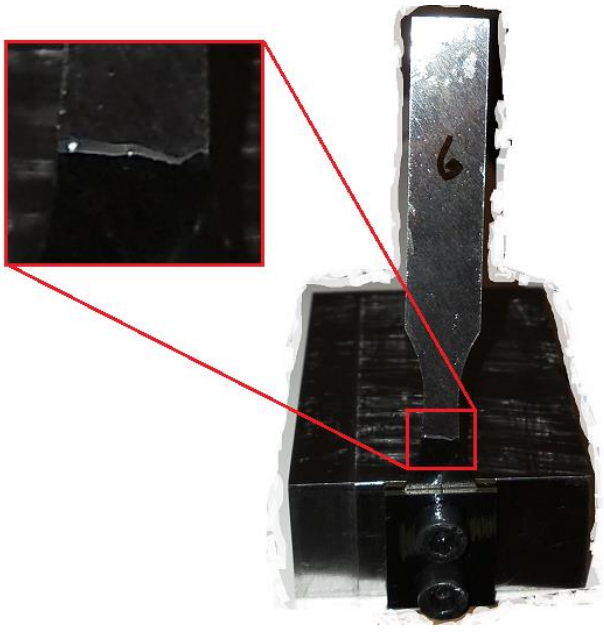

Figure 4.30. Front View of Fracture Geometry of a TM-400 Fatigue Specimen

Figure 4.31. Fracture Surfaces of a LB-250 Fatigue Specimen

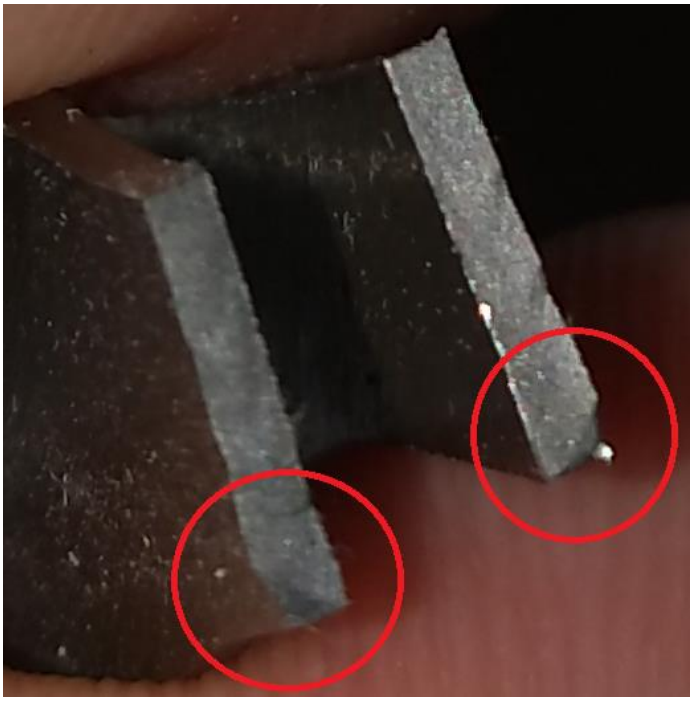

Figure 4.32. Fracture Surfaces of a TM-400 Fatigue Specimen

In addition to the fracture geometry of the specimens, the rupture locations on the fracture zones of LB-250 and TM-400 fatigue specimens are as shown in Figure 4.33 and Figure 4.34, respectively. As seen from these figures, fatigue samples might be broken from anywhere in the bending region. This is an expected feature of the Krouse-type specimen and confirms that stress is distributed homogeneously across the bending region as it is expected from the numerical stress analyses.

Figure 4.33. Fracture Zones of LB-250 Fatigue Specimens

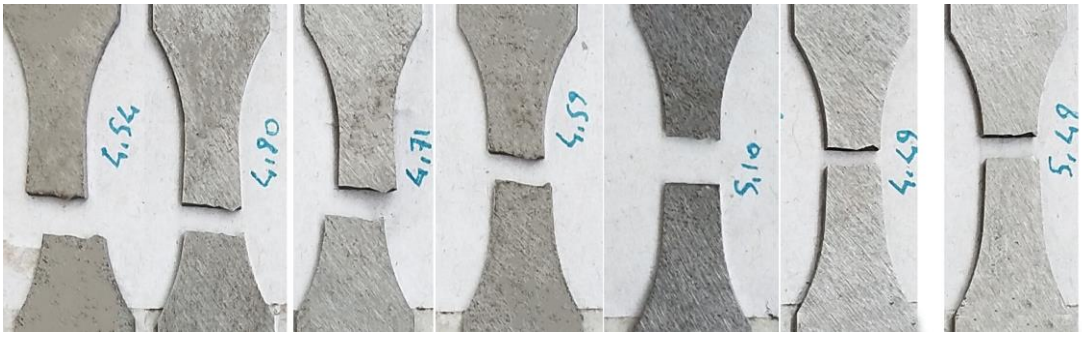

Figure 4.34. Fracture Zones of TM-400 Fatigue Specimens

4.7.2. SEM Inspection

When the samples were examined in SEM, it is seen that fatigue usually started from the corner zones of the tension side of the specimens. Figure 4.35 shows the whole fatigue zone of a LB-250 fatigue specimen, where the fatigue was initiated and propagated.

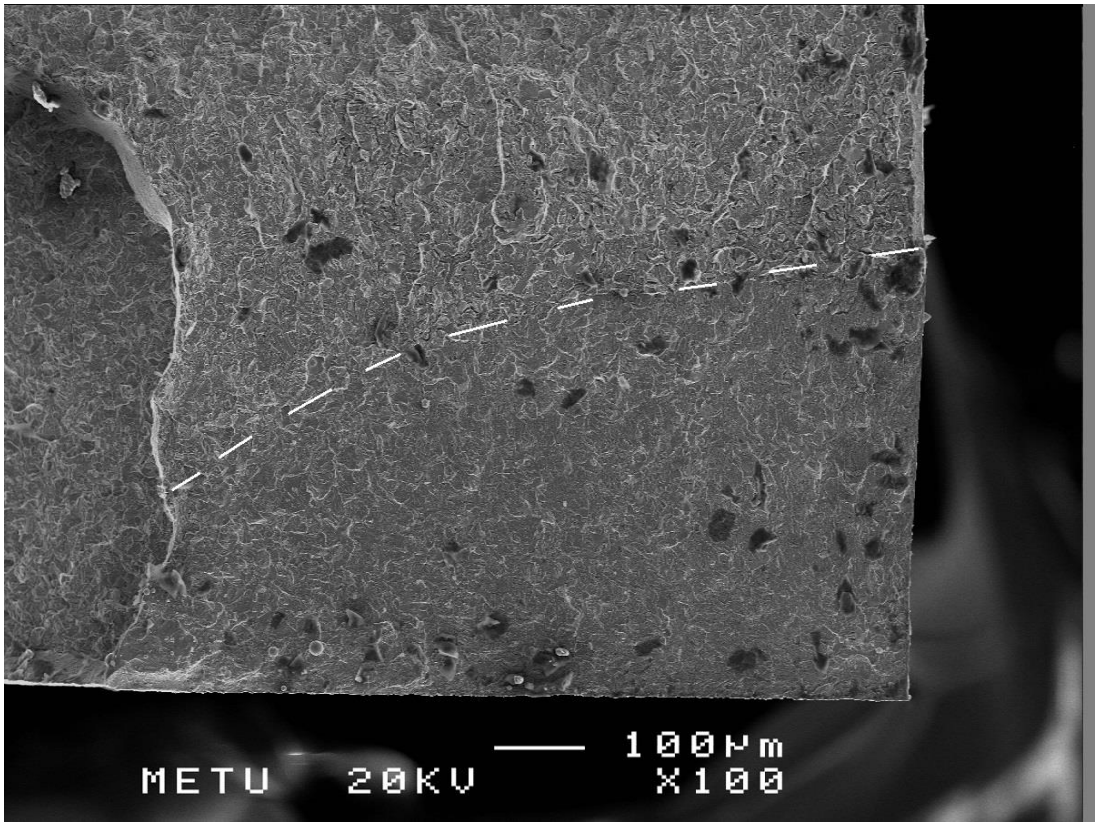

Figure 4.35. Whole Fatigue Zone of a LB-250 Specimen

When fatigue zones are examined, fatigue striations, which are perpendicular to the direction of crack growth, and tear ridges, which are in the direction of crack growh, are easily distinguished. Figure 4.36 and Figure 4.37 show the fatigue zones of a LB-250 fatigue specimen and TM-400 fatigue specimen, respectively.

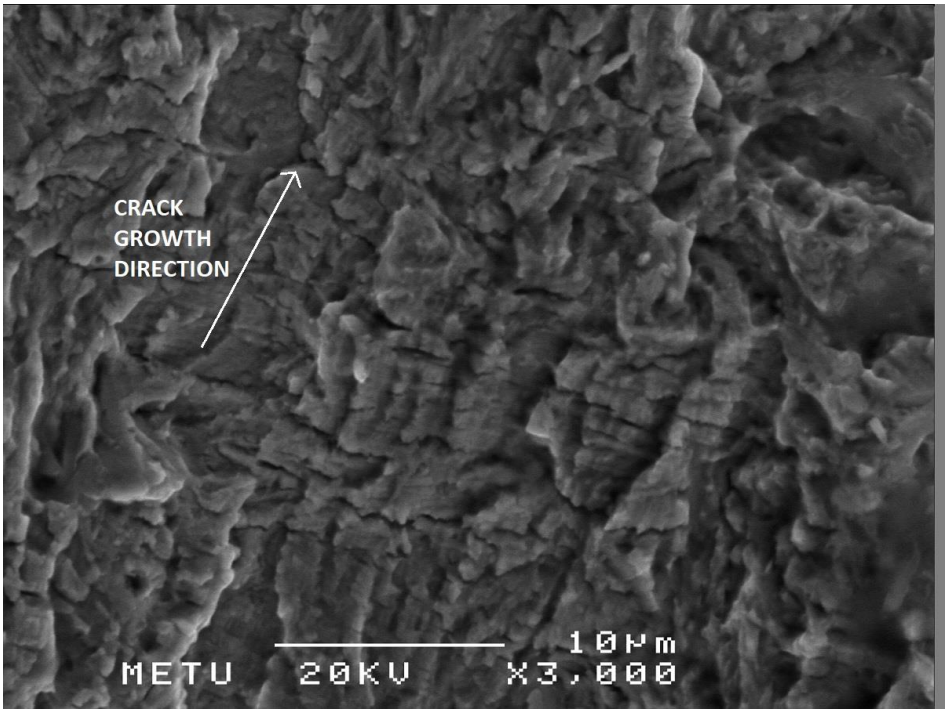

Figure 4.36. Fatigue Zone of a LB-250 Fatigue Specimen

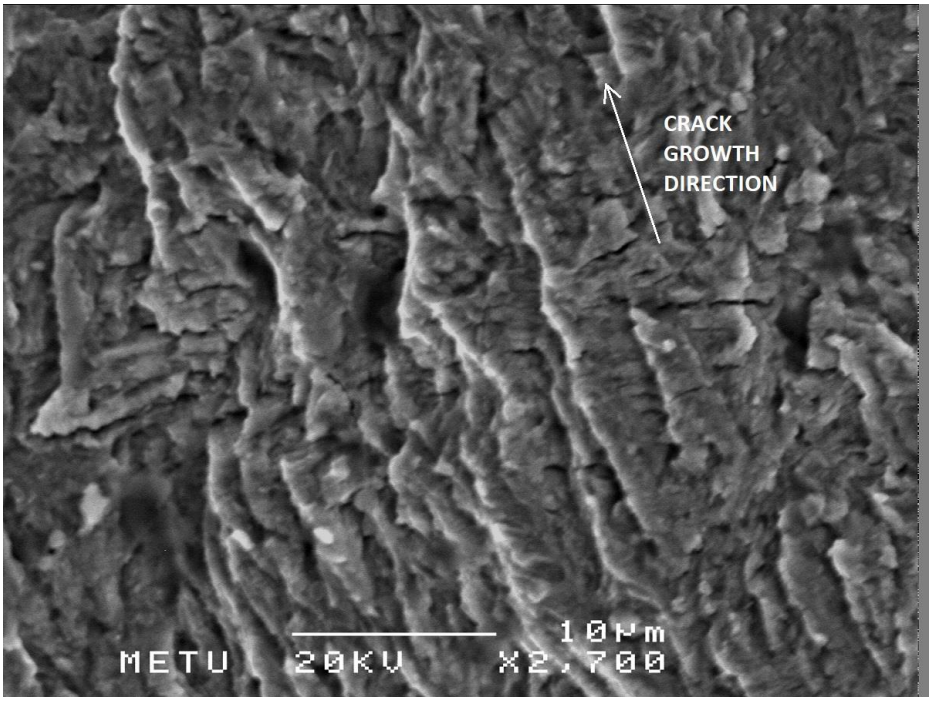

Figure 4.37. Fatigue Zone of a TM-400 Specimen

When the fast fracture zones of the samples are examined, LB-250 specimens generally show cleavages (transgranular cracks) which are observed in brittle fracture behavior (See Figure 4.38 and Figure 4.39). However, intergranular cracks and dimple structures reflecting the ductile fracture behavior are also noteworthy (See Figure 4.40). In the TM-400 specimens, intergranular cracks and dimple structures are observed (See Figure 4.41 and Figure 4.42). In this respect, it can be interpreted that the fast fracture zones examined in SEM coincide with the information obtained from tensile test examinations. In other words, LB-250 specimens are broken in brittle manner while TM-400 specimens are broken in ductile manner at their fast fracture zones.

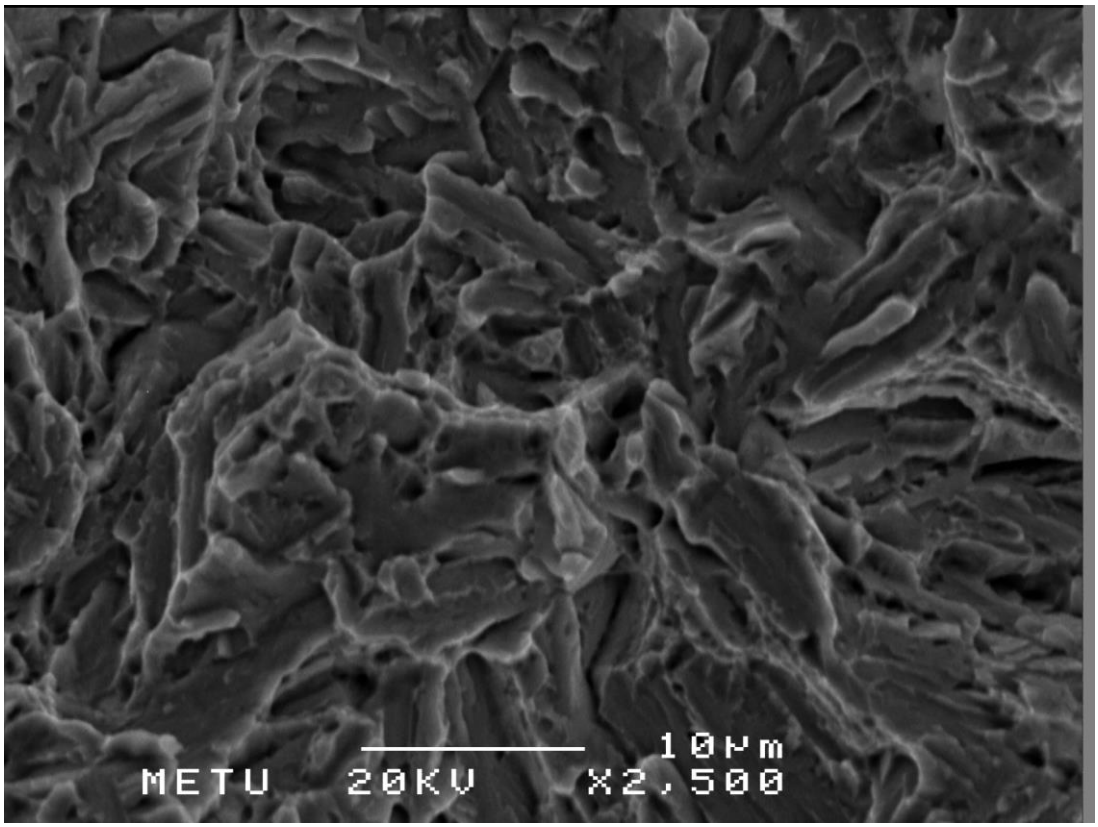

Figure 4.38. Fast Fracture Zone of a LB-250 Fatigue Specimen, which shows cleavages

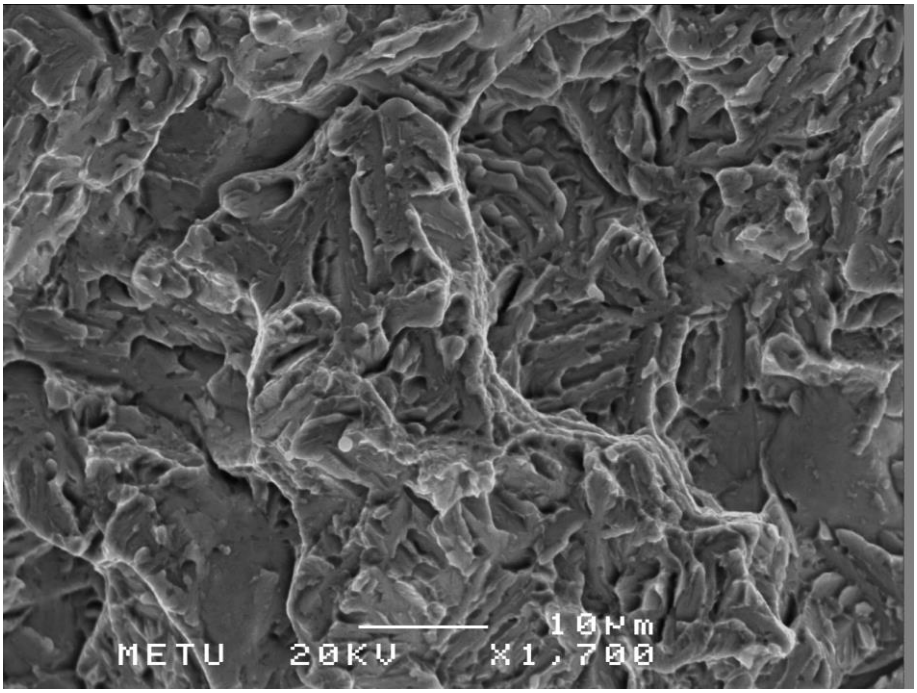

Figure 4.39. Fast Fracture Zone of a LB-250 Fatigue Specimen, which shows cleavages

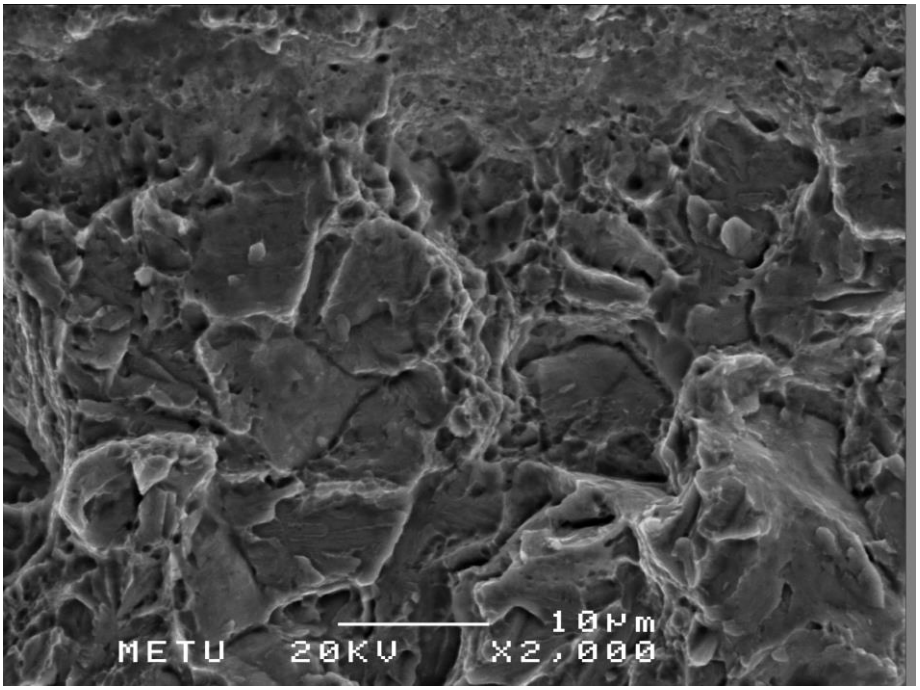

Figure 4.40. Fast Fracture Zone of a LB-250 Fatigue Specimen, which partly shows intergranular cracks and dimples

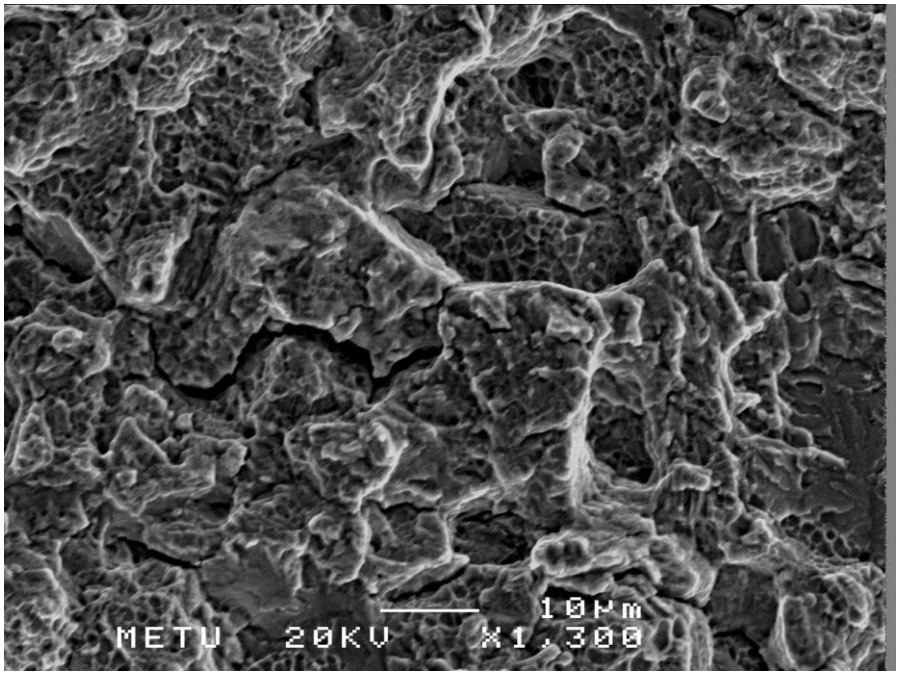

Figure 4.41. Fast Fracture Zone of a TM-400 Fatigue Specimen, which shows intergranular cracks and dimples

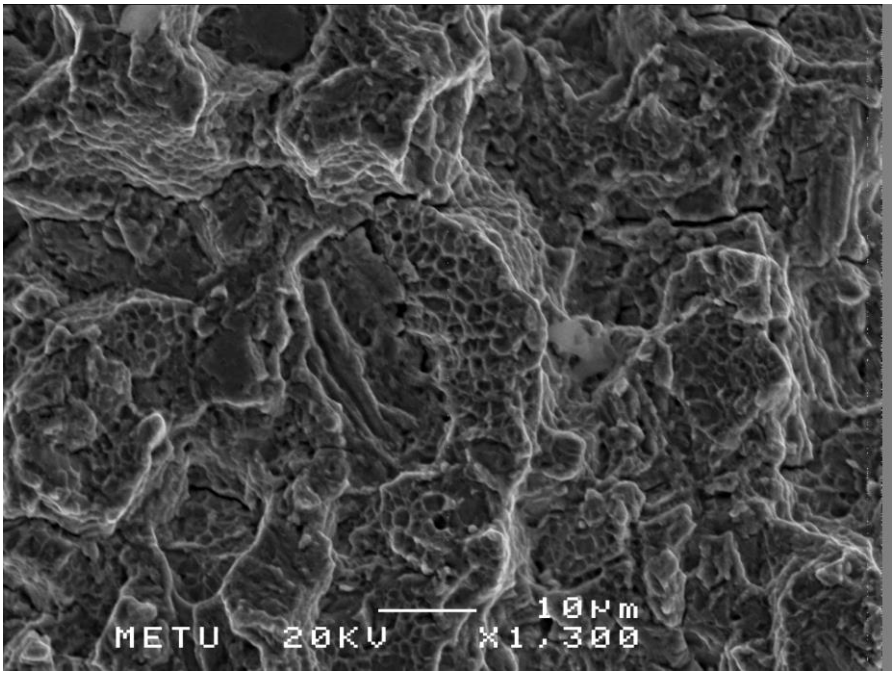

Figure 4.42. Fast Fracture Zone of a TM-400 Fatigue Specimen, which shows intergranular cracks and dimples

CHAPTER 5

DISCUSSION

In this thesis, mechanical properties of two different structures produced from 60SiMn5 steel were examined and their bending fatigue lives were compared. One of these structures is a carbide-free lower bainite which has been bainitized at 250 ºC, while the other is tempered martensite which has been tempered at 400 ºC. According to the studies in the literature, there is no clear difference between fatigue lives of high strength bainitic and high strength martensitic structures. The aim of this thesis is to compare the fatigue lives of high strength lower bainitic and high strength tempered martensitic structures in 60SiMn5 steel, which are in different microstructure but with similar mechanical properties and to see whether using carbide-free lower bainite offers an advantage in terms of fatigue life. In this section, the results presented in the experimental results chapter about this context were evaluated and commented about.

5.1. Material

According to the tensile test results, it is seen that yield and tensile strength values are consistent with hardness test results. That is, LB-250 samples have higher tensile strength value (2100 MPa) than TM-400 samples' (1800 MPa); but when evaluated in terms yield strength values (1750 & 1650 MPa), it can be assumed that the samples show similar mechanical properties. The most important feature in this study in terms of similar mechanical properties is accepted as yield strength value. The reason is because the fatigue lives of high strength (UTS > 1400 MPa) steels with similar yield strengths are considered to be close to each other under the same dynamic loads. When two different groups of samples obtained in this thesis study are evaluated with these mechanical properties, it can be concluded that the comparison of these two samples is correct in terms of fatigue life.

The fracture surfaces of the ruptured tensile specimens and the fast fracture zones of the fractured fatigue specimens were evaluated in terms of surface morphology. Accordingly, it is seen that LB-250 specimens break in brittle manner while TM-400 specimens break with ductile behavior. It can be interpreted for two reasons why the lower bainites in this thesis are broken in brittle character. The first is that LB-250 specimens are carbide-free; that is, there are no structure such as cementite, which can provide toughness, in the ferrite phase of the bainitic structure in steels which are with high silicon content. The second is the accumulation of carbide in retained austenite between bainite shaves in carbide-free bainite, instead of carbide deposition into the ferrite phase unlike in conventional lower bainite. This retained austenite can provide high strength to the structure while increasing its brittleness at the same time. If the steel used (60SiMn5) was preferred as a steel with higher carbon content (> 1%), although carbide-free bainite is formed, it is expected that a more ductile carbide-free bainitic structure could be obtained because bainites would be more small-sized. Therefore, ductile fracture behavior could not be achieved in these samples, probably due to the relatively low carbon content (0.6%).

On the other hand, it is considered that why tempered martensites in the thesis break in ductile manner is because of tempering process. It is known in the literature that untempered martensite samples are relatively hard materials and expected to break in accordance with brittle behavior. Tempering is a process utilized to reduce the hardness of martensitic structures by reducing the internal stresses and thus to restore ductility. It is usually considered that the ductility of the martensitic structures increases more as the tempering temperature increases (for conditions where the tempering time is kept constant). It can be interpreted that why TM-400 specimens break in ductile manner is because of relatively higher tempering temperature. The "relatively higher tempering temperature" term mentioned here is not according to the TM-550 samples, but according to the tempering temperatures above the temper embrittlement zone (250 – 400 ^{o}C). It is also considered that the tempering applications penetrate into whole microstructure of the TM-400 samples when taking

into account that samples are quite thin and their tempering durations are reasonably long (1.5 hours). These are the most probably reasons why TM-400 samples break in accordance with ductile behavior.

5.2. Stress Analyses

In the displacement range (8 – 22 mm) where the fatigue test machine operates, the fatigue specimens have been optimized so that the desired maximum bending stress values be formed in the bending regions of the fatigue specimens. This optimization was performed by numerical stress analyses. Then, samples were produced according to optimized fatigue specimens. In order to confirm that numerical analyses were correct, dynamometer and strain gauge measurements were performed on the fatigue specimens produced. Maximum bending stress was calculated analytically using the simple beam equation by substituting the force values measured from the dynamometer to the equation. The comparison of the force values obtained from the dynamometer with the force values obtained from numerical analyses is as shown in Figure 5.1. As a result, the trend of these forces data which are very close to each other confirms the numerical analyses. However, strain gauge measurements are required for further verification. In strain gauge measurements, strain values are obtained from the strain gauge on the bending region, and thus stress values in the bending region are able to be calculated experimentally. The comparison of numerical, analytical and experimental stress values is shown in Figure 5.2. Accordingly, it can be concluded that all stress analyses are accurate. However, it is recommended that experimentally obtained stress values are used when subtracting the S-N curve because they are expected to reflect the test set-up better.

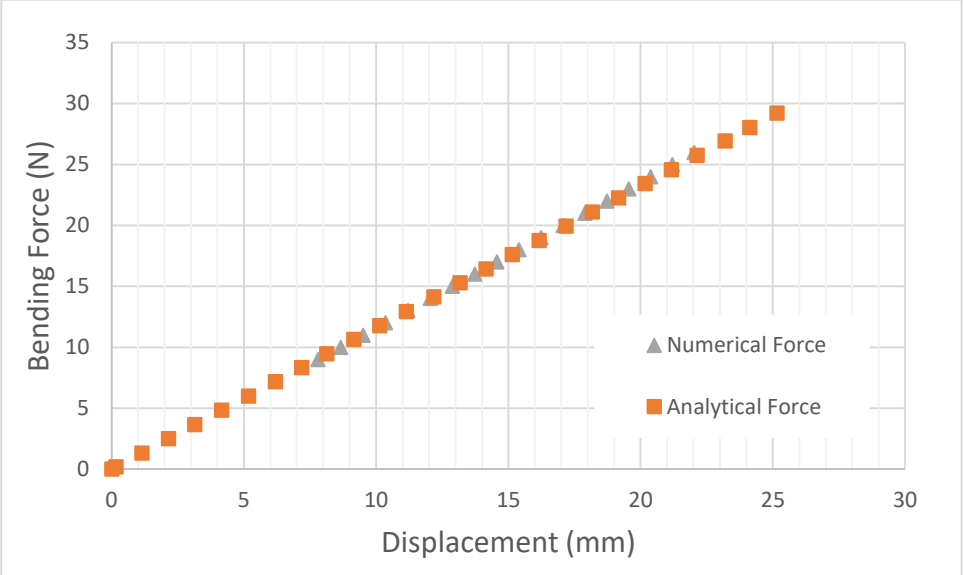

Figure 5.1. Numerical and Analytical (Corrected) Bending Forces

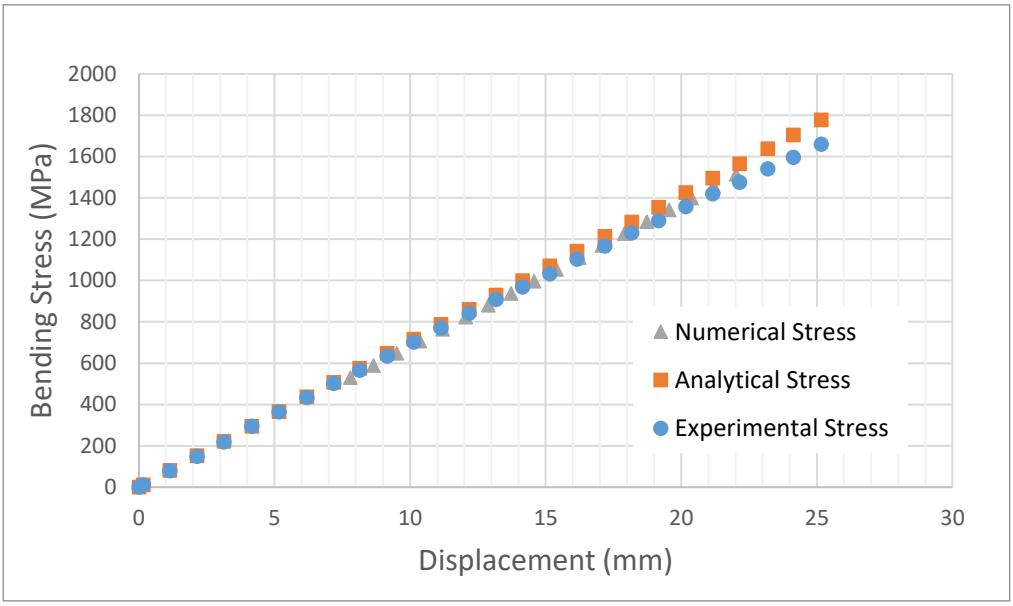

Figure 5.2. Numerical, Analytical and Experimental Maximum Bending Stresses

5.3. Fatigue Life & Endurance Limit

According to the statistical evaluations, LB-250 specimens have been no advantage in terms of fatigue life compared to TM-400 specimens. Fatigue lives of LB-250 and TM-400 specimens are obtained similar to each other as in the literature which compares bainitic and martensitic structures according to their fatigue lives. The lives of the fatigue specimens operated in the range of 625 – 750 MPa (stress amplitude) are very close to each other, regular and in the range of $10^{4.5}$ – 10^{5} cycles as shown in Figure 4.28. From just below 625 MPa (550 – 610 MPa), the lives of the fatigue specimens ranges from 10^{5} to infinite. However, in this stress range, the correlation between stress values applied to the specimens and fatigue lives are impaired. This zone can be defined as the endurance limit because 6 pieces of the 7 pieces of LB-250 specimens and 5 pieces of the 7 pieces of TM-400 specimens exceeded 10^{6} cycles, which is defined as infinite life limit. Broken one piece of LB-250 and two pieces of TM-400 specimens could not exceed $10^{5.5}$ cycles. Therefore, the gap between $10^{5.5}$ and 10^{6} cycles at the endurance limit region can be an evidence that there may be notch, inclusion, metal impurity or sensitivity due to metalworking on fatigue specimens which were broken before $10^{5.5}$ cycles. It is as shown in Table 5.1 that which fatigue specimen type completed the fatigue tests at which fatigue life region. In Table 5.1, red color describes the fracture of the fatigue specimens, while green color describe that fatigue specimens completed the tests without fracture.

Table 5.1. *Fatigue Life and Stress Regions where the Fatigue Specimens completed the Fatigue Tests*

Fatigue Life Region	*High Cycle Fatigue*			*Infinite Life*		
Stress Region (MPa)	*625 - 750*	*550 - 610 (Endurance Limit Region)*				
# of Cycles	$10^{4,5}$-10^{5}	10^{5}-$10^{5,5}$	$10^{5,5}$-10^{6}	10^{6}-$10^{6,5}$	$10^{6,5}$-10^{7}	*Run Out (>10^{7})*
# of LB-250	5	1	0	4	0	2
# of TM-400	5	2	0	0	0	5

In addition, it should be noted as an interesting point that 4 pieces of 6 pieces of LB-250 specimens exceeding 10^6 cycles were fractured until $10^{6.5}$ cycles and the other 2 specimens continued to run without any fracture even after 10^7 cycles. All 5 pieces of TM-400 specimens exceeding 10^6 cycles continued to run without any fracture after 10^7 cycles. This may be an evidence for that fatigue propagation can continue very slowly in LB-400 specimens even if they have passed the infinite life (> 10^6 cycles) threshold while fatigue propagation at TM-400 specimens has stopped completely. The fact that the fatigue lives of LB-250 specimens are so inconsistent in itself can be related to inconsistency in the elongation values obtained from the tensile tests. Likewise, the consistency of fatigue lives of TM-400 specimens in itself can be attributed to the high and consistent elongation values obtained from the tensile tests. Therefore, it can be interpreted that ductility is one of the factors affecting fracture tougness and it may be effective on fatigue crack initiation and propagation. The observations from Figure 4.9, Figure 4.12 and Figure 4.13, which can be an evidence for this phenomenon, are summarized in Table 5.2.

Table 5.2. *Rupture Properties of LB-250 & TM-400 Tensile Test Specimens*

	Elongation	*Crack Initiation Side*
LB-250 (1)	4,6%	from the the corner as one point
LB-250 (2)	2,8%	from the middle of long edge as one point
TM-400 (1)	4,5%	from long edges as shear lips
TM-400 (2)	4,6%	from long edges as shear lips

If the endurance limit value is considered as run-out of the specimens without fracture after 10^7 cycles, it can be considered as 575 MPa, which is the average value of endurance limit region, for TM-400 specimens. Fatigue fracture is still observed at lower boundary of endurance limit region for LB-250 specimens. Even when the 10^7 cycle limit is considered as $10^{5.5}$, the same case happens. However, considering the clutter of fatigue life data in the range of 550 - 610 MPa, it is not possible to distinguish the endurance limit of LB-250 and TM-400 specimens because there is no guarantee that the TM-400 samples will not break below 550 MPa which is the lower boundary of endurance limit region. In order to determine the endurance limit exactly according to the run-out of the specimens without fracture after 10^7 cycles, it is recommended to perform tests below 550 MPa, but the number of the specimens in this study was insufficient. However, in this thesis study, the endurance limit value is expected among endurance limit region where fatigue tests were done, and it can be assumed as 575 MPa for both types of fatigue specimens.

It was mentioned in the literature review section that there is no clear difference between endurance limits of high strength bainitic and martensitic structures in the literature. Likewise, in this thesis, there was no significant difference between the fatigue life and endurance limits of LB-250 samples, a high strength carbide-free lower bainitic structure and TM-400 samples, a high strength tempered martensitic structure; and their endurance limit values were obtanined as approximately 575 MPa. This endurance limit value is consistent with the endurance limit value of approximately 700 MPa determined in the literature for high strength (UTS > 1400 MPa) steels, because the stress ratio (R = 0) used in this study is greater than the stress ratio (R = -1) that gives the endurance limit value of 700 MPa in the literature. So the endurance limit in this study is expected slightly lower than the endurance limit in the literature. Because the bigger the stress ratio, the greater the mean tension stress in the bending region, thus it is expected that fatigue initiation and propagation to be faster. Therefore, the increase of the stress ratio is expected to be a factor that decreases the endurance limit value. With these results, it has been also shown that bending fatigue

application in ASTM B 593 – 96 Standard can be applied to high strength steels by revising Krouse-type specimen specified in the standard.

CHAPTER 6

CONCLUSION

In this thesis, LB-250 samples, which are high strength carbide-free lower bainitic structure, and TM-400 samples, which are high strength tempered martensitic structure, were heat-treated to obtain similar mechanical properties and investigated in terms of fatigue behaviors. A new type of fatigue test machine was designed for the fatigue tests; and Krouse-type fatigue specimen, specified in B 593 – 96 Standard, was revised according to this fatigue test machine and high strength (UTS > 1400 MPa) steel application. The following conclusions have been drawn from the fatigue testing of martensitic and bainitic samples:

- A bainitic structure, which has an UTS of 2100 MPa and a yield strength of 1750 MPa, has been obtained by transforming the 60SiMn5 steel to bainite at 250 ^{o}C which is just above M_s. On the other hand, oil quenching of the same steel and tempering at 400 ^{o}C have yielded a UTS of 1800 MPa and a yield strength of 1650 MPa.
- The bainitic specimen showed brittle behavior both in tensile tests and at fast fracture zones of fatigue specimens. On the other hand, the martensitic specimen showed ductile behavior both in tensile tests and at fast fracture zones of fatigue specimens.
- It is observed that there is no clear difference between the fatigue life and endurance limit of both bainitic and martensitic specimens, which is in agreement with the studies in literature.
- The endurance limits of both bainitic and martensitic specimens, defined according to 10^6 cycles at R = 0 condition, was found to be approximately 575 MPa. This result is also close to that of high strength (UTS > 1400 MPa) steels which were tested at R = -1 condition in the literature.

- The bainitic specimens, that did not fracture until $10^{6,5}$ cycles, and the martensitic specimens, that did not fracture until $10^{5,5}$ cycles, have shown infinite life behavior by running without any failure even after 10^{7} cycles.
- It has been demonstrated that the bending fatigue application, in ASTM B 593 – 96 Standard, is applicable to high strength steels by revising Krouse-type specimen specified in the standard.

REFERENCES

[1] Lynch, *Some Fractographic Contributions to Understanding Fatigue Crack Growth*, 2017.

[2] *Crash Plane Broke up in Mid-Air*, The Guardian, 27th May 2002.

[3] Jeníček, *Effect of Silicon on Stability of Austenite during Isothermal Annealing of Low-alloy Steel with Medium Carbon Content in the Transition Region between Pearlitic and Bainitic Transformation*, 2017.

[4] Bhadeshia, *Bainite in Steels*, Theory and Practice, 3rd Edition, p.339, 2015.

[5] Bhadeshia, *Bainite in Steels*, Theory and Practice, 3rd Edition, p.339-340, 2015.

[6] Rementeria, *On the Role of Microstructure in Governing the Fatigue Behaviour of Nanostructured Bainitic Steels*, 2015.

[7] Sourmail, *Evaluation of the Potential of High Si High C Steels Nanostructured Bainite for Wear and Fatigue Applications*, 2012.

[8] Zhang, *Low-cycle Fatigue-cracking Mechanisms in FCC Crystalline Materials*, 2014.

[9] Mughrabi, *Microstructural Mechanisms of Cyclic Deformation, Fatigue Crack Initiation and Early Crack Growth*, 2015.

[10] Budynas, Nisbett, *Shigley's Mechanical Engineering Design*, 8th Edition in SI Units, p. 275, 2008.

[11] Budynas, Nisbett, *Shigley's Mechanical Engineering Design*, 8th Edition in SI Units, p. 274, 2008.

[12] Siemens PLM Community, *What is a SN-Curve?*, 29 August 2019.

[13] Xue, *Fatigue Life Assessment of a High Strength Steel 300 M in the Gigacycle Regime*, 2012.

[14] Siemens PLM Community, *What is a SN-Curve?*, 29 August 2019.

[15] Müller, *Accuracy of Fatigue Limits Estimated by the Staircase Method using Different Evaluation Techniques*, International Journal of Fatigue, 2017.

[16] ASTM B 593 – 96, *Standard Test Method for Bending Fatigue Testing for Copper-Alloy Spring Materials*, 2003.

[17] Cyders, *Modeling and Experimental Comparison of Effects of a Forging Post Process on Additive Manufactured Metallurgy*, 2017.

[18] ASTM B 593 – 96, *Standard Test Method for Bending Fatigue Testing for Copper-Alloy Spring Materials*, 2003.

[19] ASTM B 593 – 96, *Standard Test Method for Bending Fatigue Testing for Copper-Alloy Spring Materials*, 2003.

[20] Haidyrah, *An Experimental Study on Bending Fatigue Test with a Krouse-Type Fatigue Specimen*, November 2014.

[21] Haidyrah, *Characterization of bending Fatigue Mini-specimens for Nuclear Materials*, 2015.

[22] Sun, *Effects of Stress Ratio on Crack Growth Rate and Fatigue Strength for High Cycle and Very-high-cycle Fatigue of Metallic Materials*, Mechanics of Materials, Volume 69, Issue 1, Pages 227-236, February 2014.

[23] Sourmail, *Evaluation of the Potential of High Si High C Steels Nanostructured Bainite for Wear and Fatigue Applications*, 2012.

[24] Bakır, *The Comparison of Bainitic Transformations and Mechanical Properties of 60SiMn5 and 55Cr3 Steels*, September 2019.

[25] Sij Group, *Siqual 5142 Steel*, Designation by Standards, 2016.

[26] Bhadeshia, *Nanostructured Bainite*, 2009.

[27] Caballero, *Design of Novel Bainitic Steels: Moving from Ultra Fine to Nanoscale Structures*, 2013.

[28] Caballero, *Atomic Scale Observations of Bainite Transformation in a High Carbon High Silicon Steel*, 2006.

[29] Beladi, *Characterization of Nano-structured Bainitic Steel*, 2012.

[30] Kundrák, *X-ray Diffraction Investigation of White Layer Development in Hard-turned Surfaces*, 2011.

[31] Sij Group, *Siqual 5142 Steel*, Designation by Standards, 2016.

[32] Yoshino, *The Cooperative Relation between Temper Embrittlement and Hydrogen Embrittlement in a High Strength Steel*, Metallurgical Transactions, Volume 5, p.363-370, February 1974.

[33] Bhadeshia, *Bainite in Steels*, Theory and Practice, 3rd Edition, p.339-340, 2015.

[34] Bhadeshia, *Bainite in Steels*, Theory and Practice, 3rd Edition, p.339, 2015.

[35] Rementeria, *On the Role of Microstructure in Governing the Fatigue Behaviour of Nanostructured Bainitic Steels*, 2015.

[36] Sourmail, *Evaluation of the Potential of High Si High C Steels Nanostructured Bainite for Wear and Fatigue Applications*, 2012.

[37] ASTM E8 / E8M - 13a, *Standard Test Methods for Tension Testing of Metallic Materials*, 2013.

[38] Sij Group, *Siqual 5142 Steel*, Designation by Standards, 2016.

APPENDICES

A. CENTRAL PROCESS UNIT

The circuit diagram of CPU, which describes the management of the fatigue test machine, is shown in Figure A.1.

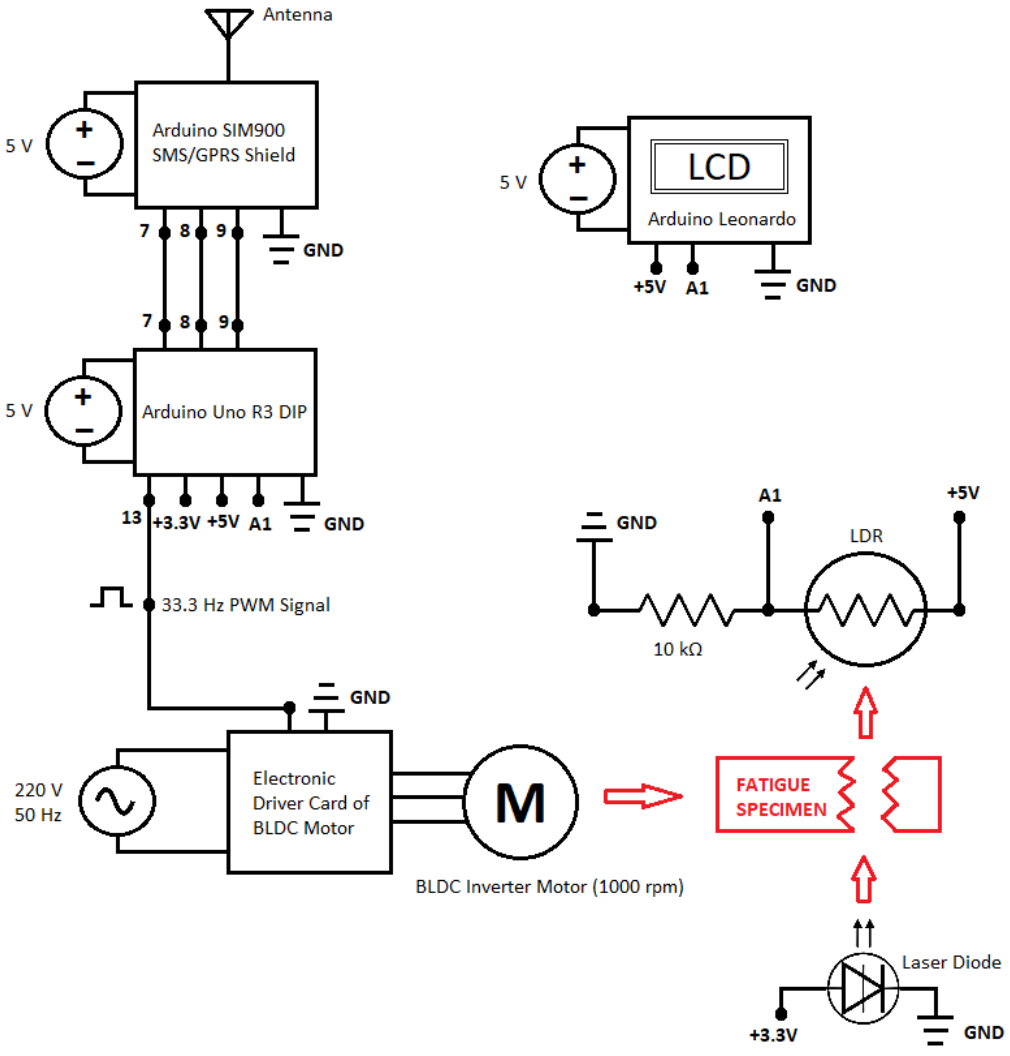

Figure A.1. Circuit Diagram of Central Process Unit

The software codes in Arduino® Uno R3 DIP of CPU are stated below:

```
int motor=13;
unsigned int time;
#include<SoftwareSerial.h>
SoftwareSerial mySerial(7, 8);
void setup() {
pinMode (13,OUTPUT);
Serial.begin(9600);
mySerial.begin(9600);
updateSerial();
}
void loop() {
MOTOR();
ANALOG();
TIME();
updateSerial();
}
void MOTOR(){
  //digitalWrite(13, HIGH);
  //delay(14);
  //digitalWrite(13,LOW);
  //delay(14);
```

```
}
void ANALOG()
{
int sensorValue = analogRead(A1);
Serial.println(sensorValue);
if(sensorValue<800)
{digitalWrite(13, HIGH);
 delay(14);
digitalWrite(13,LOW);
delay(14);}
else
{digitalWrite(13,LOW);
mySerial.begin(9600);
 mySerial.println("AT");
 updateSerial();
 mySerial.println("AT+CMGF=1");
 updateSerial();
  mySerial.println("AT+CMGS=\"+905376731800\"");
 updateSerial();
  mySerial.print("TEST BITTI"); //text content
  updateSerial();
  mySerial.write(26);
}
```

```
}
void updateSerial()
{
  while (Serial.available())
  {
    mySerial.write(Serial.read());
  }
  while(mySerial.available())
  {
    Serial.write(mySerial.read());
  }
}
  void TIME()
{
  Serial.print("Time: ");
  time = millis()/1000;
  Serial.println(time);
  }
```

The software codes in Arduino® Leonardo of CPU are stated below:

```
#include <LiquidCrystal.h>
#include <LCDKeypad.h>
#include <LcdKeypad.h>
#include <LiquidCrystal.h>
#include <LCDKeypad.h>
#define DAYS 0
#define HOURS 1
#define MINUTES 2
#define SECONDS 3
// The LCD screen
LCDKeypad lcd;
// The time model
unsigned int days = 0;
unsigned int hours = 0;
unsigned int minutes = 0;
unsigned int seconds = 0;
unsigned int setting = 0;
void setup() {
  lcd.begin(16,2);
  lcd.setCursor(0,0);
  lcd.print("Setting: Days   ");
```

```
}
void loop() {
  incTime();
  printTime();
  buttonListen();
}
void buttonListen() {
  // Read the buttons five times in a second
  for (int i = 0; i < 5; i++) {
    // Read the buttons value
    int button = lcd.button();
    switch (button) {
    // Right button was pushed
    case KEYPAD_RIGHT:
      setting++;
      break;
    // Left button was pushed
    case KEYPAD_LEFT:
      setting--;
      break;
    // Up button was pushed
    case KEYPAD_UP:
      switch (setting) {
```

```
  case DAYS:
    days++;
    break;
  case HOURS:
    hours++;
    break;
  case MINUTES:
    minutes++;
    break;
  case SECONDS:
    seconds++;
  }
  break;
// Down button was pushed
case KEYPAD_DOWN:
  switch (setting) {
  case DAYS:
    days--;
    if (days == -1) days = 99;
    break;
  case HOURS:
    hours--;
    if (hours == -1) hours = 23;
```

```
      break;
    case MINUTES:
      minutes--;
      if (minutes == -1) minutes = 59;
      break;
    case SECONDS:
      seconds--;
      if (seconds == -1) seconds = 59;
    }
  }
  setting %= 4;
  printSetting();
  days %= 100;
  hours %= 24;
  minutes %= 60;
  seconds %= 60;
  printTime();
  // Wait one fifth of a second to complete
  while(millis() % 200 != 0);
 }
}
// Print the current setting
void printSetting() {
```

```
  lcd.setCursor(9,0);
  switch (setting) {
  case DAYS:
    lcd.print("Days   ");
    break;
  case HOURS:
    lcd.print("Hours  ");
    break;
  case MINUTES:
    lcd.print("Minutes");
    break;
  case SECONDS:
    lcd.print("Seconds");
  }
}
// Increase the time model by one second
void incTime() {
  Serial.begin(9600);
  Serial.println(A1);
 int sensorValue = analogRead(A1);
  if(sensorValue<800)
{
  // Increase seconds
```

```
  seconds++;
  if (seconds == 60) {
    // Reset seconds
    seconds = 0;
    // Increase minutes
    minutes++;
    if (minutes == 60) {
      // Reset minutes
      minutes = 0;
      // Increase hours
      hours++;
      if (hours == 24) {
        // Reset hours
        hours = 0;
        // Increase days
        days++;
      }
    }
  }
}
}
// Print the time on the LCD
void printTime() {
```

```
  // Set the cursor at the begining of the second row
  lcd.setCursor(0,1);
  char time[17];
  sprintf(time, "%02i days %02i:%02i:%02i", days, hours, minutes, seconds);
  lcd.print(time);
}
```

B. INTERIOR LIGHTING AND LUBRICATION SYSTEM

The circuit diagram of interior lighting system and lubrication system, which is of the fatigue test machine, is shown in Figure B.1.

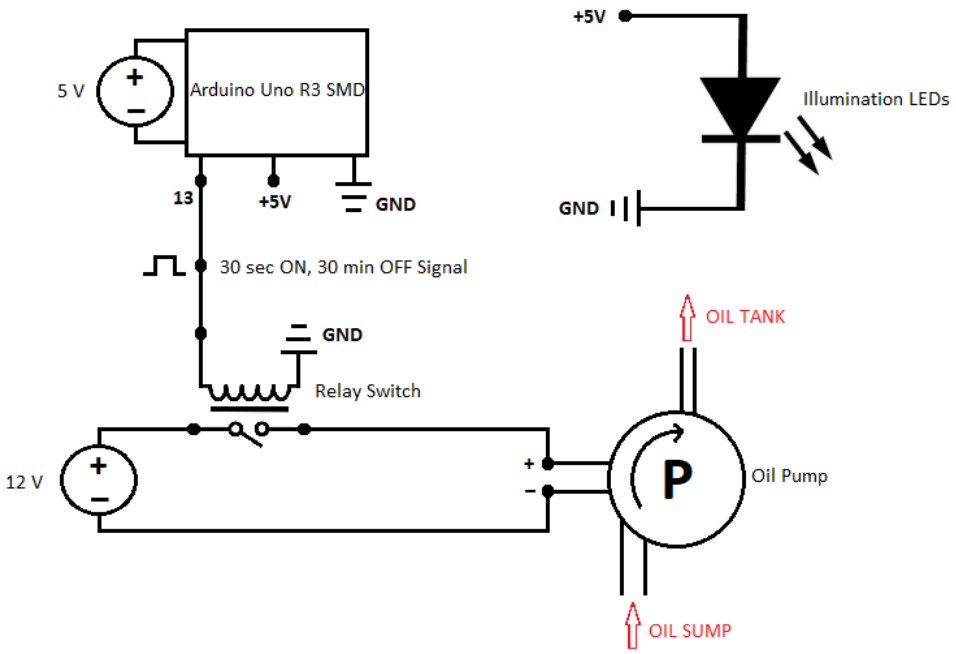

Figure B.1. Circuit Diagram of Interior Lighting and Lubrication System

The software codes in Arduino® Uno R3 SMD of the system are stated below:

```
// the setup function runs once when you press reset or power the board
void setup() {
  // initialize digital pin LED_BUILTIN as an output.
  pinMode(13, OUTPUT);
}
// the loop function runs over and over again forever
void loop() {
  digitalWrite(13, HIGH);   // turn the SWITCH on (HIGH is the voltage level)
  delay(30000);                       // wait for thirty seconds
  digitalWrite(13, LOW);    // turn the SWITCH off by making the voltage LOW
  delay(1800000);                     // wait for thirty minutes
}
```